

N66 37967.

DATA FROM EXPLORER 17 ON COMPOSITION OF THE UPPER ATMOSPHERE*

CARL REBER

INTRODUCTION

The Explorer 17 aeronomy satellite carried two double-focusing magnetic mass spectrometers designed [Meades, 1960; Hall *et al.*, 1960; Spencer and Reber, 1962] to measure the concentrations of the major neutral-particle constituents of the earth's upper atmosphere. The ambient densities

of helium, oxygen, and nitrogen were obtained between north and south latitudes of 58° and from the perigee altitude of 257 km to an altitude in excess of 700 km. Data for various local times, altitudes, and geographic locations have been combined to provide a broader altitude coverage than could have been experienced at any single

TABLE 1.—*Tabulated Mass Spectrometer Data*

The local sun time, angle of attack (α) geographic latitude and longitude are averaged over the 4-minute pass. The stations involved are: BP, Blossom Point, Md.; COL, College, Alaska; FTM, Fort Myers, Fla.; GF, Grand Forks, Minn.; QUI, Quito, Ecuador; MOJ, Mojave, Calif.; NFL, Newfoundland; OOM, Woomera, Australia; JOB, Johannesburg, South Africa.

Pass and Station	Date	Local Time, hours	α	Geog. Lat.	Geog. Long.
15 BP-----	4/ 4/63	21.15	6°	38.5°	-75.0°
50 COL-----	4/ 6/63	0.65	16°	57.0°	-149.0°
80 COL-----	4/ 8/63	0.99	9°	55.0°	-147.0°
80 FTM-----	4/ 8/63	4.89	63°	18.0°	-92.0°
118 BP-----	4/10/63	18.81	70°	37.0°	-72.0°
120 GF-----	4/11/63	20.32	51°	51.0°	-98.5°
138 BP-----	4/12/63	2.51	12°	37.0°	-84.0°
152 BP-----	4/13/63	2.01	14°	39.5°	-68.5°
167 BP-----	4/14/63	1.65	20°	39.5°	-75.0°
182 BP-----	4/15/63	1.54	25°	37.0°	-78.0°
183 QUI-----	4/15/63	3.26	23°	4.5°	-79.0°
197 BP-----	4/16/63	1.43	27°	34.0°	-81.5°
211 BP-----	4/17/63	0.53	45°	41.5°	-71.5°
226 BP-----	4/18/63	0.48	53°	38.5°	-74.0°
241 BP-----	4/19/63	24.19	62°	38.0°	-79.5°
242 MOJ-----	4/19/63	0.64	54°	31.0°	-121.5°
254 NFL-----	4/20/63	22.75	82°	49.0°	-53.0°
270 BP-----	4/21/63	23.30	80°	41.50°	-71.5°
271 GF-----	4/21/63	22.88	85°	45.0°	-101.0°
708 NFL-----	5/20/63	7.18	39°	49.5°	-49.5°
795 OOM-----	5/26/63	15.81	63°	-34.0°	137.5°
800 JOB-----	5/26/63	15.90	65°	-37.5°	19.0°
888 JOB-----	6/ 1/63	13.24	33°	-27.0°	25.0°

*Published in *Journal of Geophysical Research*, 69(21):4681-4685, November 1, 1964.

location. Data are presented for helium, atomic oxygen, and molecular nitrogen; molecular oxygen and atomic nitrogen data will be presented and discussed in a later report along with other data obtained under more varied conditions.

EXPERIMENT

The mass spectrometer measured the number densities of the various species which were in its ionizing, or sampling, region. Before reaching this sampling region, however, some of the neutral particles underwent collisions with various parts of the spectrometer structure; thus the number measured by the spectrometer was generally different from the ambient number density. The relationship between the spectrometer measurements and the ambient number densities was found to be a function of particle species, satellite velocity, and the angle between the spectrometer axis and the satellite velocity vector (angle of attack α). Using satellite velocity and angle of attack, both obtained from the tracking stations and the satellite's optical aspect system, calcula-

tions have been carried out for each species and have been used to convert the measured quantities to the ambient values presented here. The contribution of residual gas has also been taken into account.

The absolute accuracy of the number density data is ± 40 percent, reflecting laboratory vacuum calibration error and the uncertainties in the ambient number density calculations. The relative accuracy of the data obtained for similar angles of attack is about 5 percent; for data obtained when the angles of attack differ by 70° or more, the relative accuracy is about 30 percent. The mean mass data and the concentration ratios are good to ± 10 percent. Since the relative accuracy of the number density varies with the angle of attack, this quantity, the local sun time, and other pertinent information are given in Table 1.

DATA

Figure 1 shows the ambient number densities of the major constituents plotted as a function of

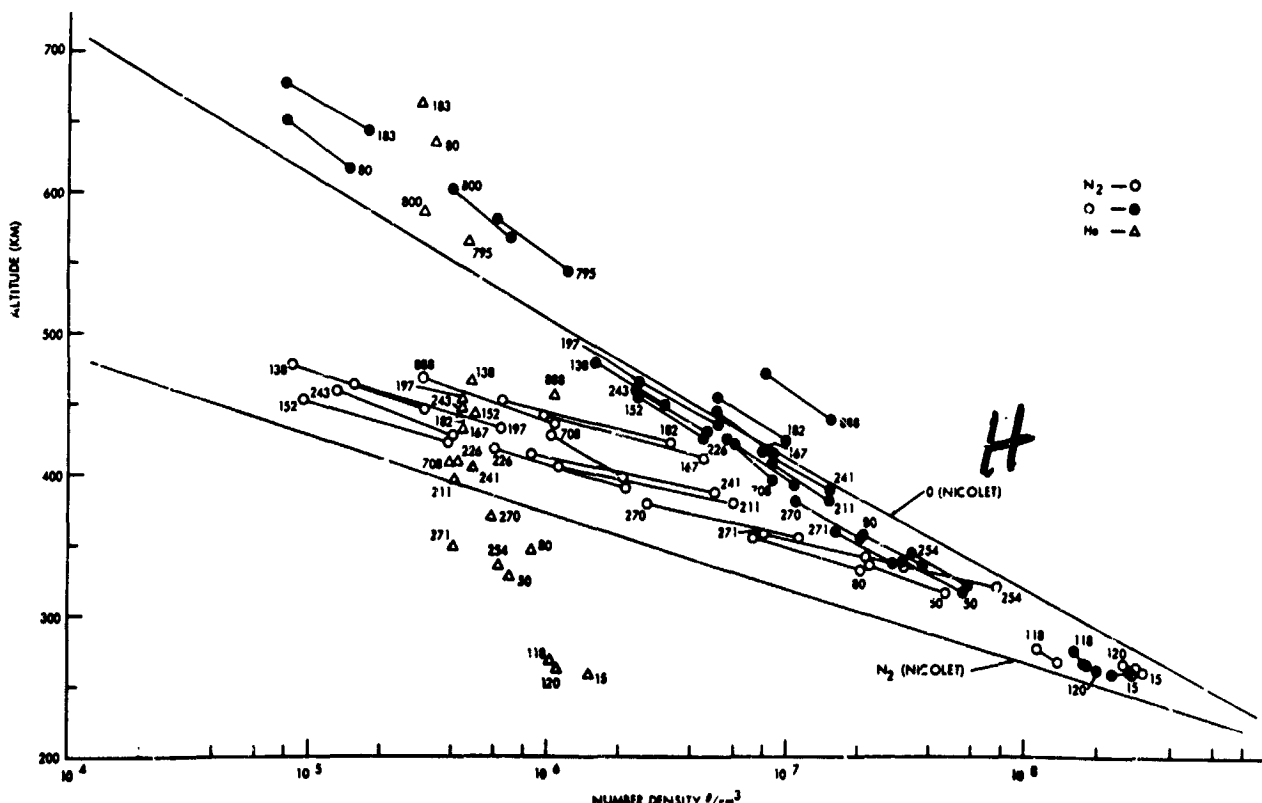


FIGURE 1.—Ambient number densities of the major constituents versus altitude. These data include many local times and geographic locations. The orbit numbers refer to Table 1. Nicolet's model for $T = 700^\circ\text{K}$ is included for reference.

altitude for a number of different local times and locations. A single satellite interrogation (pass) is indicated by two data points joined by a straight line for molecular nitrogen and atomic oxygen and by one point for helium. The Nicolet model (private communication) is included for reference.

For the times concerned, the number densities of helium and atomic oxygen are comparable at about 600 km, with helium predominant at higher

altitudes. Between 300 and about 600 km, atomic oxygen is the major constituent; in the 250- to 300-km region, molecular nitrogen and atomic oxygen have nearly equal concentrations.

There is, at present, insufficient daytime data to determine scale heights for the sunlit atmosphere. However, during the night at higher altitudes the concentration gradients are consistent with the scale heights for temperatures of 700° to 750°K.

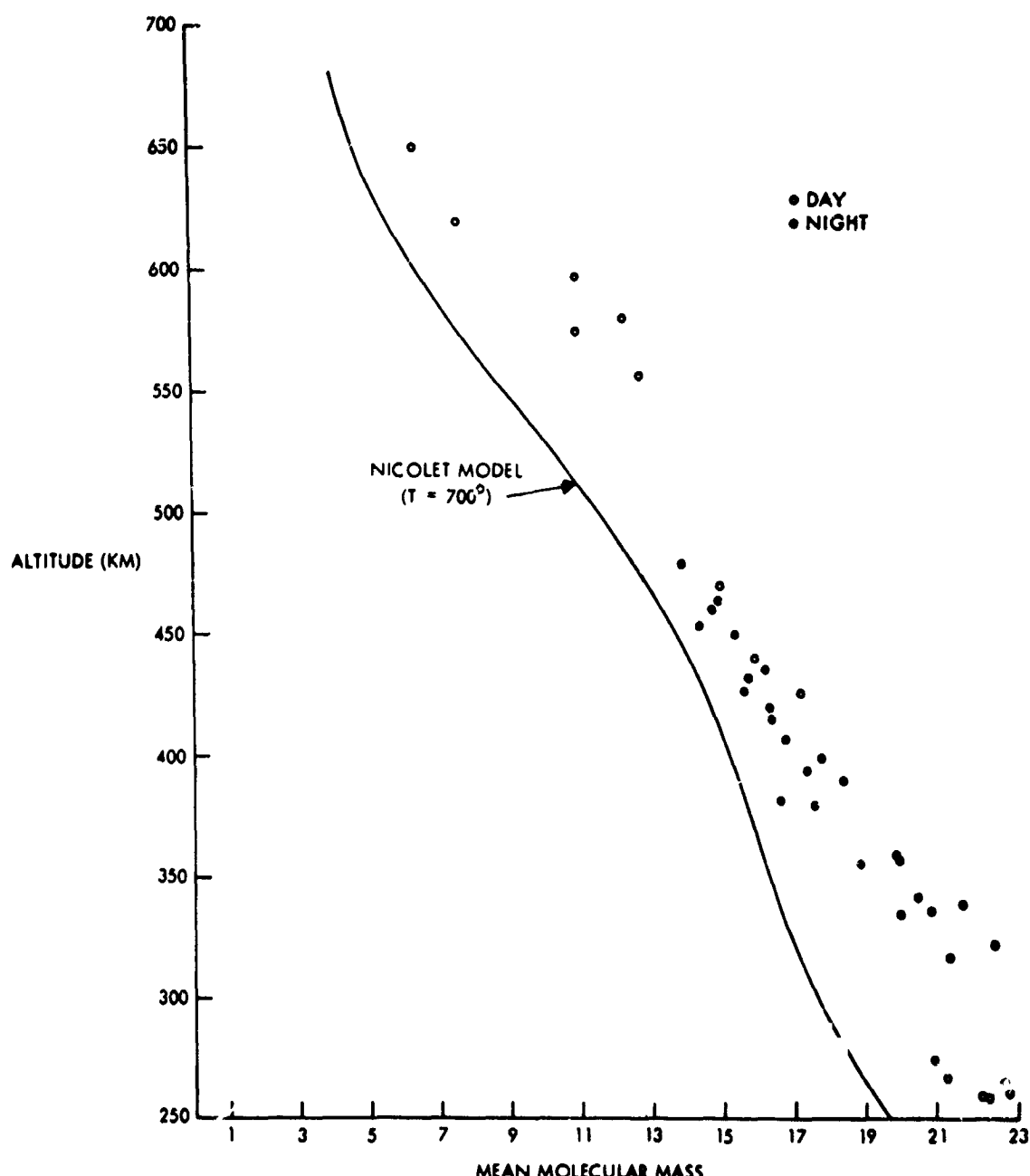


FIGURE 2.—Mean molecular mass versus altitude. The mean mass was calculated using the three major constituents measured, N₂, O, and He. Nicolet's model is included for reference.

There appears to be a deviation from nighttime diffusive equilibrium in the 300- to 350-km altitude range for N_2 . This may be indicative of longer times required for N_2 to diffuse at these altitudes; however, as noted above, the data shown are representative of many time and geographic locations and may not provide an accurate instantaneous vertical distribution. It is interesting to note that the data from passes 167, 182, and

183, for which the densities are higher than for other nighttime passes, were obtained shortly after a minor magnetic disturbance which occurred on April 14. All data shown are measured values and are not averaged or smoothed in any way.

Figure 2 shows the variation of mean molecular mass with altitude. These data were calculated using the measurements of helium, atomic oxygen,

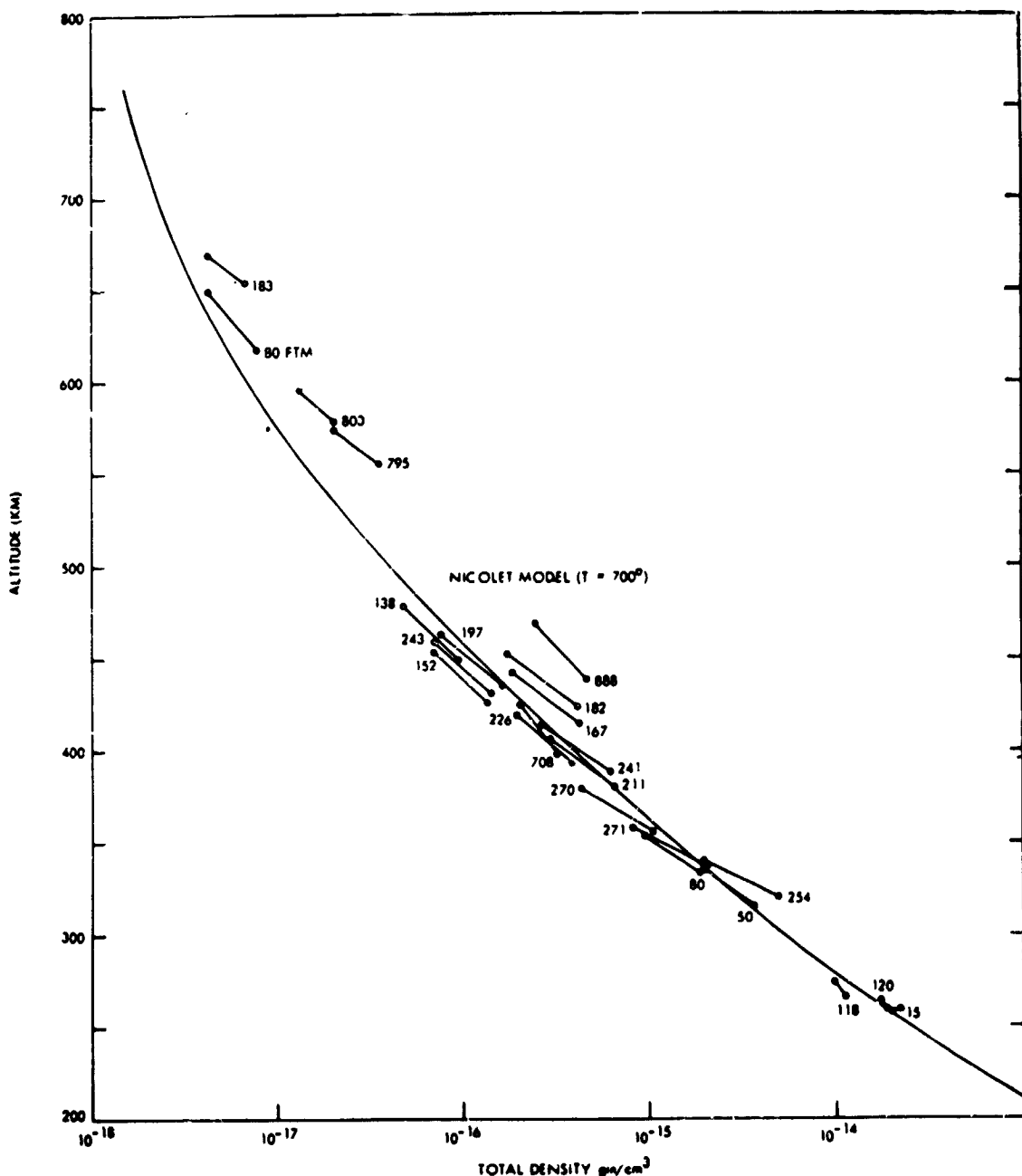


FIGURE 3. Total mass density versus altitude. The total mass density was calculated using the densities for N_2 , O, and He. The orbit numbers refer to Table 1. Nicolet's model is included for reference.

and molecular nitrogen only, other measured gases providing a negligible contribution of the mean mass. The presence of hydrogen, which the instrument was not designed to measure, would reduce the value of the mean mass somewhat at higher altitudes.

The total mass density, shown in Figure 3, was computed by summing the contributions from

molecular nitrogen, atomic oxygen, and helium. The results obtained in this way agree with the densities obtained independently by the pressure gage experiments on Explorer 17. This agreement lends support to the calculations relating the concentrations in the sampling region to the ambient number densities, as the pressure gage kinetics have been studied extensively [Horowitz,

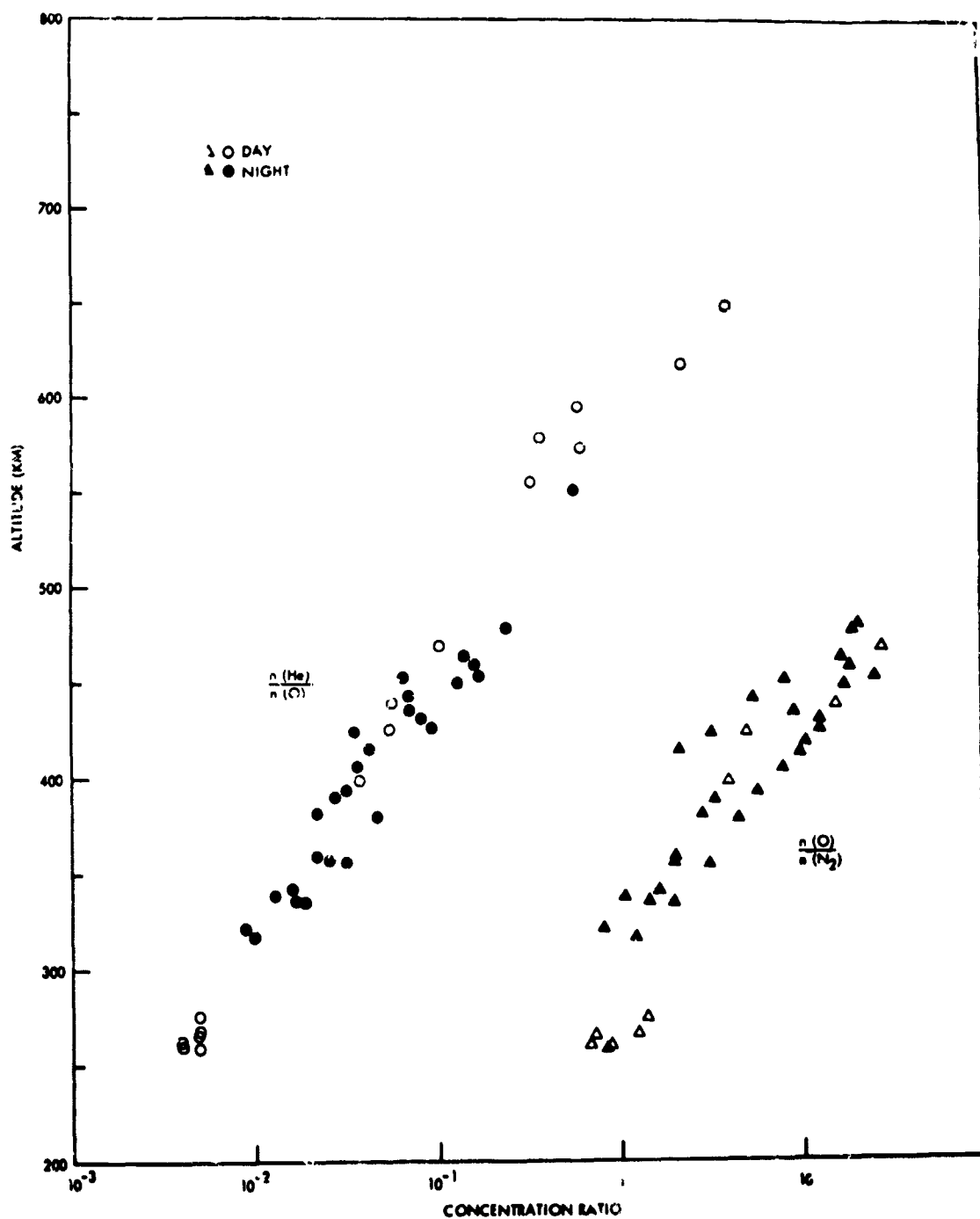


FIGURE 4.—Concentration ratios of the major constituents versus altitude.

1953]. Also, the total density measurements from the mass spectrometers agree in general within a factor of 2 with atmospheric density calculated from satellite drag observations [Bryant, 1964].

Figure 4 shows the variation with altitude of the concentration ratios of helium to atomic oxygen and atomic oxygen to molecular nitrogen.

ACKNOWLEDGMENT

I am indebted to Professor Marcel Nicolet for many hours of stimulating discussions about the data from Explorer 17, particularly with respect to extracting the scientifically interesting from the technically involved.

REFERENCES

- BRYANT, R., Densities obtained from drag on Explorer 17, *J. Geophys. Res.*, **69**, 1423-1425, 1964.
HALL, L. G., P. F. HOWDEN, and T. F. IWASKA, Design of a mass spectrometer for use in a satellite, paper presented at Meeting of ASTM Committee E-14 on Mass Spectroscopy, 8th Annual Meeting, Atlantic City, June 26 through July 1, 1960.
HOROWITZ, R., and D. KLEITMAN, A method for determining density in the upper atmosphere during rocket flight, *Naval Res. Lab. Rept. 4246*, Washington, D. C., 1953.
MEADOWS, E. B., Design requirements of a mass spectrometer for satellite use, paper presented at Meeting of ASTM Committee E-14 on Mass Spectroscopy, 8th Annual Meeting, Atlantic City, June 26 through July 1, 1960.
SPENCER, N. W., and C. A. REBER, A mass spectrometer for an aeronomy satellite, *Space Res.*, **3**, 1151-1155, 1964.

N64 - 33630

A NIGHT-TIME MEASUREMENT OF OZONE ABOVE 40 KM*

EDITH I. REED AND REUBEN SCOLNIK

The ozone distribution between 40 and 70 km was measured near midnight, May 27, 1960, from Wallops Island, Virginia by means of photometers sensitive to the ultraviolet airglow at wavelengths between 2400 and 2900 Å. Below 60 km, the densities are within a factor of two of the daytime photochemical equilibrium, as represented by Johnson's late afternoon measurement of June 14, 1949. Above 60 km, the ozone density increased with altitude, with its maximum increase, a factor of 6 over the day time value, occurring at 63 km.

INTRODUCTION

At high altitudes, above the principal ozone maximum, ozone concentration as a function of altitude should be governed principally by the presence or absence of sunlight, and vary in a predictable manner from day to night and from season to season [Chapman, 1930]^{a,b}. The first direct measurement of the daytime profile was a result of studies of the sun conducted by the Naval Research Laboratory on a V-2 rocket in 1949. Ozone densities up to 70 km were deduced from solar spectra and were consistent with computed photoequilibrium profiles [Johnson, *et al.*, 1952]. Chapman also suggested that at high altitudes, above the ozone maximum and below the atomic oxygen maximum, ozone would increase at night as a result of a reaction between atomic and molecular oxygen. Several have treated this problem numerically, including Nicoll [1957], Barth [1961], Dutsch [1961], Paetzold [1961], Wallace [1962], and Hunt [1964], but with varying results, depending on the set of reactions, reaction rates, and initial concentrations which were chosen. Of particular difficulty is the computation of the effects of minor constituents such as hydrogen, nitrogen oxides, and the hydroxyl radical.

Ground based measurements of ozone content at these altitudes have not been satisfactory. Measurements of total ozone content are not particularly helpful since variations in the ozone

content below 30 km due to air movements are comparable to the expected night time increase at higher altitudes. However, the discovery of the ultraviolet airglow and a general improvement in the techniques of ultraviolet photometry made a night time measurement of ozone feasible.

In 1957, the Naval Research Laboratory flew an ultraviolet photometer with a response from 2600 to 2900 Å, and did observe an ultraviolet airglow layer centered at 101 km [Tousey, 1958]. This had been predicted from laboratory observations which showed that the Herzberg bands of molecular oxygen, the visible end of which had been observed in the airglow [Chamberlain, 1955], extend to 2563 Å in the ultraviolet [Broida and Gaydon, 1954]. But because an unknown amount of the observed airglow could be due to an OI line at 2972 Å, where the filter transmission is still 10 percent of its maximum; the ozone density could not be determined unambiguously.

In May 1960, Goddard Space Flight Center flew a number of ultraviolet photometers, including some whose filters were centered at 2620 Å and narrow enough so that the absorption cross section of ozone varied by only 50 percent over the bandwidth of the filter. These data, when interpreted with the aid of an airglow spectrum obtained by T. Stecher (of GSFA), provide an ozone density profile between 40 and 70 km.

INSTRUMENTATION

NASA Aerobee 4.05, one of a series of payloads designed for stellar photometry [Boggess, 1961],

*Published as Goddard Space Flight Center Document X-613-04-867, September 1964.

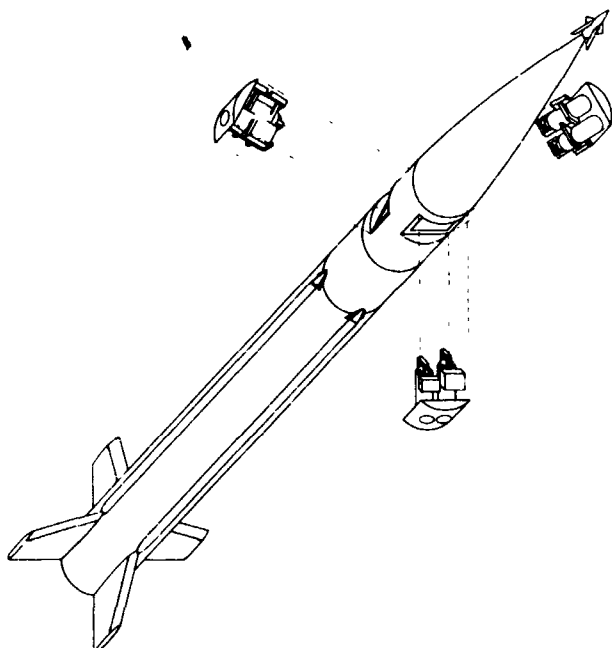


FIGURE 1.—Location of photometers on Aerobee 4.05.

contained three pairs of photoelectric photometers, each pair mounted 120 degrees apart around the rocket axis (See Figure 1) looking out at three different angles to that axis: nominally, 75°, 90°, and 105°. One photometer of each pair was sensitive to light in the spectral region centered near 2620 Å, while the response of the other was centered near 2260 Å, but with their optical axes parallel. Each pair was mounted on a removable door, which, when installed, became an integral part of the rocket skin. Since the principal purpose of this instrumentation was ultraviolet star spectroscopy, 2620 Å photometers were preferred to the 2680 Å ones (to reduce ambiguity in the interpretation of stellar data due to the strong magnesium doublet at 2800 Å). However, to correlate the data from this flight with that of earlier flights, one 2680 Å photometer was included. This was mounted on the door containing the 90° photometers, and also looked at 90° with respect to the rocket axis.

The optical system of each photometer was similar and is shown in Figure 2. Calcium fluoride was used for all lenses in the 2260 Å units; quartz for those in the 2620 and 2680 Å photometers. The field of view had a total width of between 4 to 5°.

Isolation of the 2600 Å region was achieved by combining two millimeters of 0.05 percent lead-

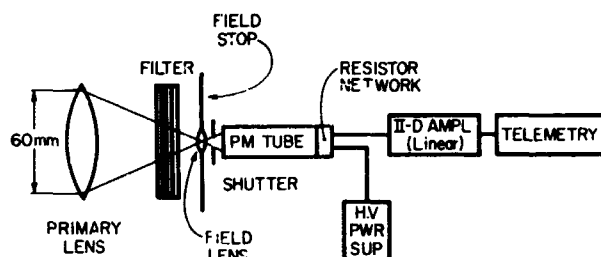


FIGURE 2.—Optical-electrical schematic of a photometer.

doped KC1:KBr (1:1) crystal with Cation-X in thin sheets of polyvinyl alcohol [Childs, 1961]. Three millimeters of nickel sulfate hexahydrate provided a sharp cutoff for longer wavelengths; one Corning No. 7-54 and one Corning 9-54 filter sharpened the shorter wavelength cutoff. A typical filter had a transmittance of 0.18, an effective wavelength of 2620 Å and a 200 Å bandwidth.

The 2700 Å filter consisted of three Corning 7-54 filters, one sheet of Cation-X and 5 millimeters of nickel sulfate hexahydrate. It has an effective wavelength of 2680 Å, a transmittance of 0.16, and a bandwidth of 320 Å.

The relative spectral response of the filters (see Figure 4) was measured by C. Childs, formerly of this laboratory, with a recording spectrophotometer, Cary Model No. 14, with an analytical accuracy of $\frac{1}{2}$ of 1 percent for relative spectral transmission, a wavelength calibration of 4 Å, and a resolving power of 1 Å. Over the wavelength regions covered by each filter, the photomultiplier was assumed to have a constant sensitivity and the lenses a constant transmissivity. The rela-

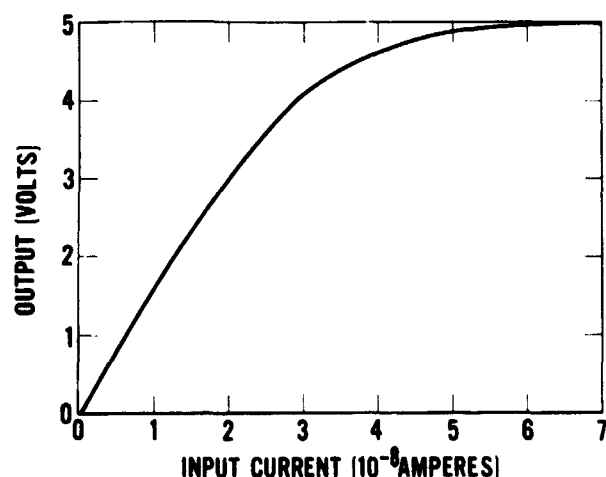


FIGURE 4.—Calibration curve for converter-amplifier.

tive response of the photometers was determined by use of the 2537 Å line, to which all three types of photometers respond with an easily measured signal.

The 2680 Å photometer used RCA's well-known 1P28 as a detector; all others used EMI's No. 6256B, an end-on fused silica window multiplier with cesium antimonide photocathode. A solenoid-operated shutter between the field stop and multiplier gave optical zero signals several times during the flight. The 1P28 and 6256B's were operated at 1000 and 1200 volts respectively; each detector had its own solid state DC to DC inverter power source with a resistor divider network at the base of each multiplier.

Each photomultiplier output was amplified to the zero to five volt range required by the telemetry system with what was essentially an impedance converter. Designed by G. Baker of the laboratory, the converter-amplifier had an electron tube (5886) input stage and ended with an emitter follower, with an overall voltage gain of 2.5 for small signals. It was purposely nonlinear in order to extend the dynamic range. A typical calibration curve is shown in Figure 3. The output voltage went directly to a pulse position modulation telemetry transmitter which relayed the data to the ground receiving equipment.

BASIC DATA

Aerobee-Hi NASA 4.05 was launched at 0030 EST on May 27, 1960 from Wallops Island, Virginia ($37^{\circ}50' N$, $75^{\circ}29' W$). The vehicle performance was normal: propulsion ended at 52.4

sec after launch at an altitude of 36.6 km with a vertical velocity of 1.84 km/sec and a horizontal velocity of .260 km/sec at an azimuth of 111° . The rocket spun about its longitudinal axis at a rate of 2.16 rps and soon entered a precession cone of 5.7° half angle, whose axis was 15.6° from zenith at an azimuth of 96° , with a period of 75 sec. Aspect during the ascent and free-fall portions of the flight was determined from a combination of data from magnetometers, trajectory information, and horizon and star data from the photometers. Down-leg aspect could not be determined with useful accuracy below the free-fall region. A peak altitude of 215.3 ± 0.2 km was reached 249.4 seconds after launch. Telemetry ceased at 468 sec; no recovery of instrumentation was attempted.

In Figure 5 is a sample of the telemetry record from two of the photometers for a period corresponding to three revolutions of the vehicle, while the airglow layer is still above the rocket. Since these photometers are nearly perpendicular to the rocket axis, the zenith angle of the photometer axis changes from a minimum (76° for the time in Figure 5) as the photometer points skywards, through 90° as it scans the horizon, and to a maximum of 100° as it points earthward. Ozone is relatively opaque around 2600 Å, and the airglow in Figure 5 can be seen only when the zenith angle of the photometer is near a minimum. The ozone is relatively transparent to the light passed by the 2260 Å filter, and the brightening of the airglow at the horizons can be clearly seen. (The light is probably of wavelengths longer than 2700 Å, passed through the long wavelength tail of the 2260 Å filter.) The southern horizon appears wider because it is merged with several bright stars in the Milky Way. As the vehicle increased in altitude, the signal from the 2620 Å photometer resembled that from the 2260 Å photometer, with bright horizons, a less bright sky toward zenith, and a dark earth. Above the airglow layer, the sky was dark (except for the brighter stars) and the earth appeared light. The noise in the record is due partly to the photomultiplier and partly to stars. The records were read at the midpoint between horizons, and analyzed to yield both a distribution of ozone with altitude and the volume emission of the airglow versus altitude.

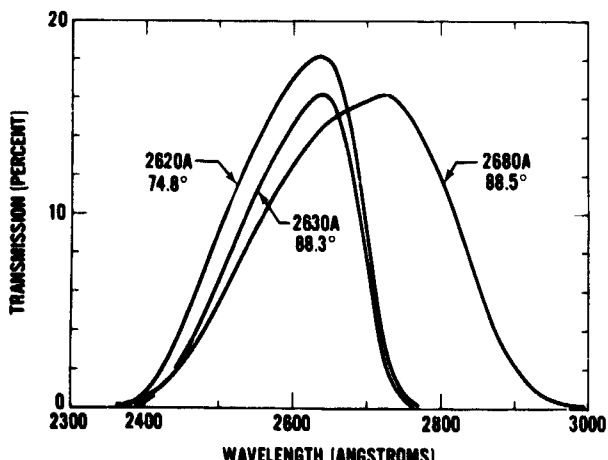


FIGURE 3.—Spectral characteristics of flight filters.

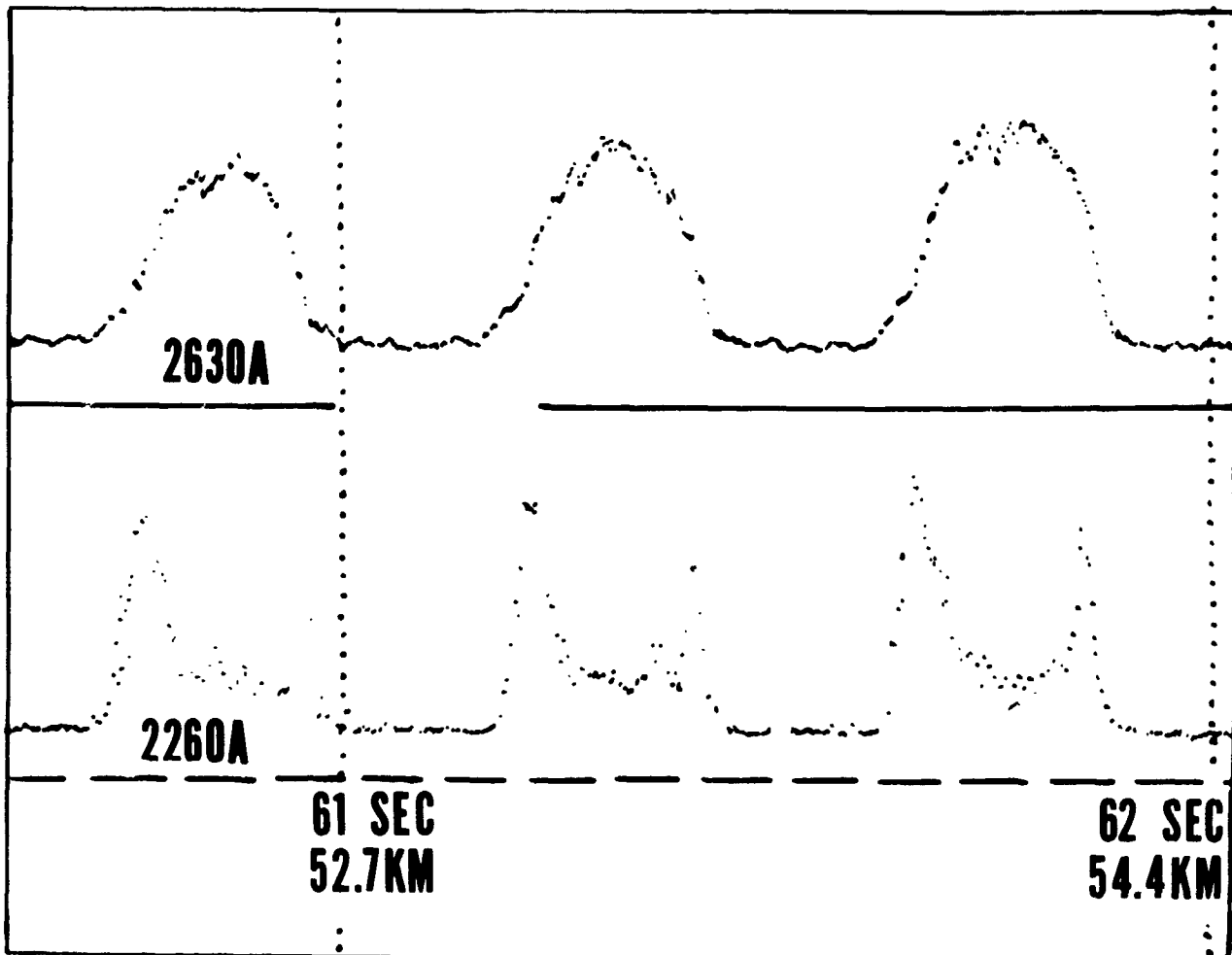


FIGURE 5.—Sample of telemetry record showing roll modulation of the airglow signal. Increasing signal represents increasing light.

The data obtained in the region of interest is shown in Figure 6. Data from 3 of the 7 photometers proved to be useful for ozone measurements. The pass band of the three 2260 Å photometers was too wide to permit an accurate determination of an effective cross section for ozone; the down looking 2620 Å photometer could not see the airglow while the vehicle was below the airglow layer. Data points for the photometers are shown to indicate the scatter in the raw data. As would be expected, the scatter increased rapidly as the signal rose into the non-linear portion of the amplifier response curve. In addition to the data, the angle of the rocket's longitudinal axis with respect to local zenith is given. The rocket took a spiral path with a zenith angle of 8° at thrust termination (52.4 sec) until it entered

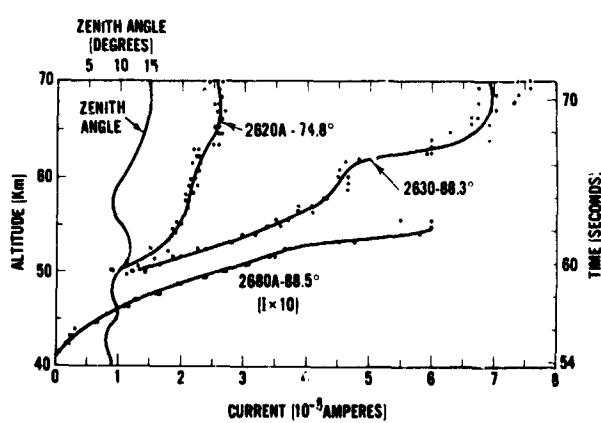


FIGURE 6.—Data from three photometers during the ascent of the rocket. The zenith angle is the angle between the longitudinal axis of the rocket and local zenith; the angle stated for each photometer is the angle between the photometer's optical axis and the rocket's longitudinal axis.

its regular precession cone of motion at about 75 seconds.

OZONE

The ozone content of the atmosphere is obtained from the rate of increase of the airglow signal as the vehicle rose. The energy observed is related to the ozone density in the following manner:

$$n(O_3) = \frac{(\log E_2 - \log E_1)n \cos \gamma}{a(h_2 - h_1)}$$

where $n(O_3)$ is the number of ozone molecules per cm^3

h_1 and h_2 are the lower and upper ends of the altitude interval,

E_1 and E_2 are energies observed at the corresponding altitudes,

n is Loschmidt's number, $2.687 \times 10^{19} \text{ cm}^{-3}$,

γ is the angle between the photometer axis and zenith, and

a is the absorption coefficient, cm^{-1} , base 10.

This was applied to the smooth curves in Figure 6 at one-second intervals.

Since the cross section of ozone varies appreciably over the wavelength interval passed by each filter, some assumption must be made concerning the spectrum of the airglow. For this purpose, the spectrum observed by T. Stecher (private communication) was used, and the absorption coefficient, a , computed for each photometer where

$$a = \frac{\sum E_i R_i a_i}{\sum E_i R_i}$$

where E_i is the energy in a particular wavelength interval, i ,

R_i is the corresponding relative transmission of the filter, and

a_i is the corresponding absorption coefficient.

The absorption coefficients used were from the tabulation of Inn and Tanaka [1953, 1959] which in the region of interest here are about 10 percent higher than those of Vigroux [1953] and 1 or 2

percent lower than those of DeMore and Raper [1964]. The effective absorption coefficients calculated on this basis are: 2620 A (88.3°), 114.4 cm^{-1} ; 2620 A (74.8°), 113.8 cm^{-1} ; and 2680 A (88.5°), 79.48 cm^{-1} .

The resulting ozone density is shown in Figure 7 as a function of altitude. It is felt that the spectral characteristics of the photometers, the airglow and the ozone absorption coefficient are sufficiently well known such that they contribute no more than a total of about 20 percent uncertainty to the number density of ozone. This would be a systematic error which would not affect the shape of the curve.

The angle of the photometers with respect to zenith could easily contribute an uncertainty of 20 percent to both the absolute and relative values of the ozone densities. It is based upon magnetometer data and the assumption that at the end of thrust the rocket axis was aligned with the velocity vector.

The largest source of error is in the character of the data, which contains noise from the photo-multiplier dark current, stray pulses, and stars. It is difficult to separate this from the possible temporal and spatial variations of the airglow itself. A temporal variation could be responsible for some of the shape of the curve, but it is unlikely that the airglow would vary sufficiently in the 16 seconds of time that the ozone curve represents, to be responsible for its major features. Spatial variation is not thought to be a major

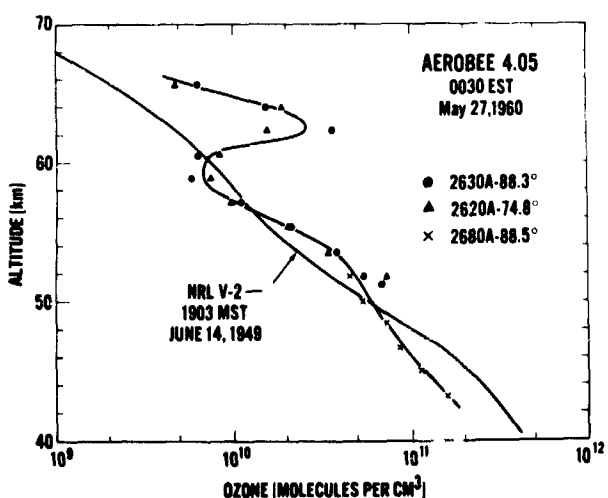


FIGURE 7.—Altitude distribution of ozone.

source of uncertainty in the data since the numbers derived from the two photometers which were looking at different portions of the sky agree reasonably well. The magnitude of the noise-like errors is apparent from the scatter of points about the curve and is on the order of 50 percent.

For comparison the daytime ozone distribution as measured by absorption of the solar spectra between 2500 and 3400 Å [Johnson, et al, 1952] is shown. The daytime profile was computed using the ozone absorption coefficients of $N\gamma$ and Choong [1933], which in the spectral region of interest are 10 to 15 percent higher than those of Inn and Tanaka used for the night time profile.

The most important feature of the profile is the factor of 6 increase in ozone density over the daytime profile above 60 km. While this may be in error by 50 percent or more, it is believed that the shape of the curve does indicate an increase of ozone density at night in this region, and that it is on the order of a half of a magnitude.

Techniques are being developed by various workers to use satellites for the measurement of ozone in this region. Venkateswaran [1961], observed the sunlight reflected from Echo I as it emerged from the earth's shadow, using various wavelength pairs between 4700 and 7000 Å. His results above 55 km are about a factor of 15 higher than the measurements by Johnson, et al. However Venkateswaran [1963] states that this method probably gives too high values at levels above the principal ozone maximum.

The second type of observation was made at sunrise and sunset by a satellite borne radiometer with a response center at about 2630 Å [Rawcliffe, et al, 1963]. At 60 km his data are about 20 percent lower than Johnson's, but approach Johnson's data, and above 80 km are somewhat higher than the trend of Johnson's data.

It is expected that the night time values would be higher. The magnitude of the effect, besides depending on reactions among the various oxygen species and third bodies, depends critically on such things as the initial hydrogen concentrations chosen [Bates and Nicolet, 1950, and Wallace, 1962] and possible reactions involving atomic nitrogen [Barth, 1961]. Perhaps the most recent computation of ozone densities has been done by B. G. Hunt [1964] using an atmosphere in which he assumes the only reactive constituent is oxy-

gen. (The effects of atomic nitrogen and hydrogen would be to lower the calculated O and O₃ concentrations.) Between 40 and 50 km, Hunt's curve for just before sunrise conditions is as much as 30 percent lower than Johnson's daytime profile, crosses it at 53 km, and reaches a maximum value of 5×10^{10} molecules of O₃ per cm at 69 km.

AIRGLOW

The other principal result from the analysis of data from these photometers is information concerning the distribution of the airglow. Volume emission can be deduced from the data obtained as the vehicle passes through the emitting region. The energy calibration of the photometers has been used in preparing these curves, (Figure 8) so that they do rightly represent the relative energy in the portion of the spectrum passed by the different filters. Ten arbitrary units represent on the order of one photon cm⁻³ sec⁻¹ per Å. The airglow as measured by the 2680 Å photometer is 2.3 times that sensed by the 2620 Å photometers. The airglow measured by the 2260 Å photometers is 0.15 times that of the 2620 Å photometers; nearly all the energy measured by the 2260 Å photometers has come through a long wavelength tail of the filters. This pattern is completely consistent with a spectrum of the airglow horizon obtained by T. Stecher with a spectrograph flown at 0030 local time on July 19, 1963.

The 2680 Å filter was similar in construction and characteristics to those flown in March 1957 [Tousey, 1958] and November 1959 [Friedman, 1961, Packer, 1961]. The altitude of maximum

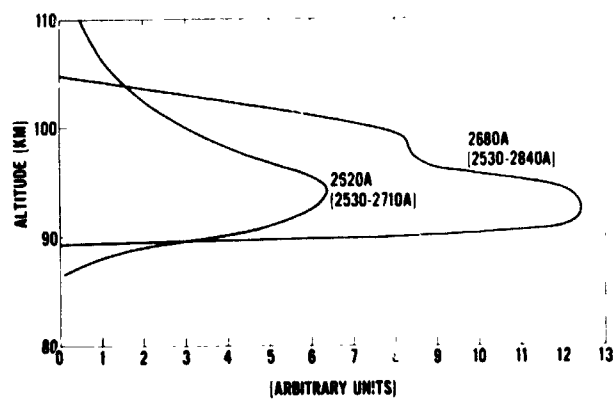


FIGURE 8.—Altitude distribution of the ultraviolet emission.

emission were 101 and 96 km respectively, compared to 92 km for this flight. The zenith intensity for the 1957 flight was 3.4 rayleighs per Angstrom (Dunkelman, private communication) and for the 1959 flight was 1.94 rayleigh per Angstrom. The airglow during the flight of Aerobee 4.05 was somewhat brighter, but within a factor of 10 of these values.

The brighter stars and the Milky Way were readily noted in the records as the photometer scanned across the sky. The signal in the absence of obvious stars indicated that less than 15 percent of the light from extended sources originated above the emission layer indicated in Figure 8.

ACKNOWLEDGMENTS

We thank the following colleagues at Goddard Space Flight Center for their help: Dr. A. Boggess III for making the data from this rocket payload available to us for this purpose; G. Baker and R. M. Windsor for the electronic instrumentation; E. Serra for engineering assistance in the payload preparation; T. Stecher for an advance copy of his airglow spectrum, without which the effective absorption cross section could not have been determined with significant accuracy; L. Dunkelman for the absolute values of the night airglow measurement in March 1957; and Dr. J. E. Kupperian, Jr. for his encouragement and suggestion of analysis of this data.

REFERENCES

- BARTH, C. A., Nitrogen and oxygen atomic reactions in the chemosphere, *Chemical Reactions in the Lower and Upper Atmosphere*, Stanford Research Institute, Interscience Publ., 303-326, 1961.
- BATES, D. R., and M. NICOLET, The photochemistry of atmospheric water vapor, *J. Geophys. Res.*, 55, 301-327, 1950.
- BOGGESS III, A., Ultraviolet astronomical photometry from rockets, *Space Astrophysics*, W. Liller, ed., McGraw-Hill Book Co., 121-132, 1961.
- BRODIA, H. P., and A. G. GAYDON, The Herzberg bands of O₂ in an oxygen afterglow and in the night-sky spectrum, *Proc. Roy. Soc., London U222*, 181-195, 1954.
- CHAMBERLAIN, J. W., The ultraviolet airglow spectrum, *Astrophys. J.* 121, 277-286, 1955.
- CHAPMAN, S., On ozone and atomic oxygen in the upper atmosphere, *Phil. Mag.*, 10, 369-383, 1930.
- CHAPMAN, S., A theory of upper-atmospheric ozone, *Mem. R. Met. Soc.*, 3, 103-125, 1930.
- CHILDS, C. B., Broad-band ultraviolet filters, *J. Opt. Soc. Am.*, 51, 895-897, 1961.
- DEMORE, W. and O. RAPER, Hartley band extinction coefficients of ozone in the gas phase and in liquid nitrogen, carbon monoxide, and argon, *J. Phys. Chem.*, 68, 412-414, Feb. 1964.
- DÜTSCH, H. U., Current problems of the photochemical theory of atmospheric ozone, *Chemical Reactions in the Lower and Upper Atmosphere*, Stanford Research Institute, Interscience Publ., 167-180, 1961.
- FRIEDMAN, H., A survey of NRL rocket research results obtained since the last COSPAR meeting, *Space Research II*, H. C. van de Hulst, ed., Interscience, N.Y. 1021-1035, 1961.
- HUNT, B. G., A non-equilibrium investigation into the diurnal photochemical atomic oxygen and ozone variations in the mesosphere, *W. R. W. Report, Tech. Note PAD 82*, Feb. 1964 (Box 1424H, C. P. O. Adelaide, South Australia).
- INN, E. C. Y. and Y. TANAKA, Absorption coefficient of ozone in the ultraviolet and visible regions, *J. Opt. Soc. Am.*, 43, 870-873, 1953.
- INN, E. C. Y., and Y. TANAKA, Ozone absorption coefficients in the visible and ultraviolet regions, *Advan. Chem. Ser.*, No. 21, American Chemical Society, Washington, D.C., 263-268, 1959.
- JOHNSON, F. S., J. D. PURCELL, R. TOUSEY, and K. WATANABE, Direct measurements of the vertical distribution of atmospheric ozone to 70 kilometers altitude, *J. Geophys. Res.*, 57, 157-176, 1952.
- NICOLET, M. Nitrogen oxides and the airflow, *The Threshold of Space*, M. Zelikoff, ed., Pergamon Press, 40-57, 1957, Ny. T.-Z., and S.-P. CHOONG, *Chinese J. Phys.*, 1, 38, 1933.
- PACKER, D. M., Altitudes of the night airglow radiations, *Ann. Geophys.*, 17, 67-75, 1961.
- PAETZOLD, H. K., The photochemistry of the atmospheric ozone layer, *Chemical Reactions in the Lower and Upper Atmosphere*, Sanford Research Institute, Interscience Publ., 181-195, 1961.
- RAWCLIFFE, R. D., G. E. MELOY, R. M. FRIEDMAN, and E. H. ROGERS, Measurement of vertical distribution of ozone from a polar orbiting satellite, *J. Geophys. Res.*, 68, 6425-6429, Dec. 15, 1963.
- TOUSEY, R., Rocket Measurements of the Night Airglow, *Ann. Geophys.*, 14, 186-195, April-June 1958.
- VENKATESWARAN, S. V., J. G. MOORE, and A. J. KRUEGER, Determination of the vertical distribution of ozone by satellite photometry, *J. Geophys. Res.*, 66, 1751-1771, 1961.
- VENKATESWARAN, S. V., On some problems of exploration of the upper atmosphere between 50 and 100 km by means of rockets and satellites, *Rocket and Satellite Meteorology: Proc. 1st Int'l. Symp. Rocket and Satellite Meteorology*, H. Wexler and J. E. Caskey, Jr., eds., John Wiley and Sons, 199-209, 1963.
- VIGROUX, E., Contribution à l'étude expérimentale de l'absorption de l'ozone, *Ann. de Phys.*, 8, 709-762, 1953.
- WALLACE, L., The OH nightglow emission, *J. Atmos. Sci.*, 19, 1-16, 1962.

SOME ASPECTS OF WIND SHEAR IN THE UPPER ATMOSPHERE*

R. G. ROPER

The wind motions responsible for the shearing of sodium vapor trails ejected from rockets in the 70 to 140 km region of the upper atmosphere are subjected to an analysis based on generally accepted theories of hydrodynamic turbulence. The region from 80 to 100 km is of particular interest in that here the predictions of shear turbulence theory are well substantiated. The energy spectrum of the height shear is found to follow the 4/3 power law proposed by Tchen, and is associated with a vertical correlation distance of approximately 6 km. The existence of an isotropic inertial region of maximum scale 3 km, previously indicated by analysis of meteor data, is confirmed. The vertical scale of the turbulent eddies is found to be the atmospheric pressure scale height, a phenomenon which has been observed by others, but which, as yet, has no satisfactory explanation.

1. TURBULENCE THEORY

The complete development of the relationships used in the analysis of wind shear is beyond the scope of this work; the following, used in conjunction with the references quoted, should provide an adequate background for consideration of the subsequent analysis.

1.1 Energy Spectrum Analysis

If there exists in a turbulent flow field a range of scales which receive energy from larger scale motions and pass it on undiminished to smaller scale motions, then, for this so-called inertial (non-dissipative) range of scales, the only form of energy spectrum function dimensionally possible is

$$E(k) = \alpha \epsilon^{2/3} k^{-5/3} \quad (\text{Kolmogoroff, 1941})$$

where ϵ is the rate at which the turbulent energy is received by (and leaves) the inertial range of scales, k is the wavenumber vector corresponding to the real space scale r , and α is an absolute constant of order unity.

Batchelor (1953) has shown that, for such an inertial region which also possesses the property of isotropy, the fluid velocity differences measured as a function of the separation r follow the relation

$$[u(x) - u(x+r)]^2 = 4.82\alpha(\epsilon r)^{2/3} \quad (1)$$

In real space, the energy spectrum function $E(r)$ is defined by

$$E(r) = [u(x) - u(x+r)]^2 \quad (2)$$

Tchen (1954) has considered an otherwise isotropic region subjected to a mean shear, and finds that equation 1 is modified, becoming

$$[u(x) - u(x+r)]^2 = a r^{4/3} \quad (3)$$

where a involves α , ϵ , and the mean gradient. Thus, for what may be termed shear turbulence, in real space

$$E(r) \sim r^{4/3} \quad (4)$$

1.2 Correlation Analysis

An energy spectrum function equivalent to that based on velocity differences can be formulated from the lateral or longitudinal velocity correlations defined as

$$f(r) = \frac{u_f(x)u_f(x+r)}{u_f^2}$$

and

$$g(r) = \frac{u_n(x)u_n(x+r)}{u_n^2} \quad (5)$$

where $u_f(x)$, $u_f(x+r)$, $u_n(x)$, $u_n(x+r)$ are the turbulent components of the velocity at two points x and $x+r$ respectively, measured parallel (suffix f) and normal (suffix n) to the vector separation r .

*Published as Goddard Space Flight Center Document X-651-64-337, November 1964.

In isotropic turbulence, $u_r^2 = u_n^2 = u_0^2$, the velocity characteristic of the energy bearing eddies of the Kolmogoroff spectrum.

Introduction to the equation of continuity for incompressible fluids leads to the relation

$$g(r) = f(r) + \frac{1}{2}r \frac{\partial f}{\partial r} \quad (6)$$

(von Karman and Howarth, 1938)

between the functions f and g , or, if the turbulence is isotropic in two dimensions only,

$$g(r) = f(r) + r \frac{\partial f}{\partial r} \quad (7)$$

These functions, f and g , may be called Eulerian space correlation functions, and either may be denoted by $R(r)$. If the range of scales under observation is inertial, then $R(r)$ must depend only on ϵ , and the only form dimensionally possible is

$$u_0^2[1 - R(r)] \sim \epsilon^{2/3} r^{2/3}$$

$$\text{i.e.} \quad 1 - R(r) \sim r^{2/3}$$

(for any given flow field, u_0 and ϵ are constant).

Introduction of the relations 6 and 7 above gives, with c a constant

$$f = 1 - cr^{2/3} \quad (8)$$

$$\text{and} \quad g = 1 - 4/3 cr^{2/3} \quad (9)$$

for three dimensional isotropy

$$\text{or} \quad g = 1 - 5/3 cr^{2/3} \quad (10)$$

for isotropy in two dimensions only.

Since the variations of the correlation difference function $[1 - R(r)]$ with r is the same as that of $E(r)$ in equation 1, we may suppose that the dependence of $[1 - R(r)]$ on r will be similarly modified in the presence of a mean shear

$$\text{i.e.} \quad [1 - R(r)] \sim r^{4/3} \quad (11)$$

If, in fact, equation 11 is pertinent, then the relationships between f , g , and r (equations 8, 9, 10) will now become

$$f = 1 - ar^{4/3}$$

$$\text{and} \quad g = 1 - 5/3 ar^{4/3}$$

$$\text{or} \quad g = 1 - 7/3 ar^{4/3}$$

An indication of the degree of isotropy can be obtained by considering the ratio

$$S = \frac{1-f}{1-g}$$

For two dimensional isotropy

$$S = 0.60 \text{ without mean shear}$$

$$\text{and} \quad S = 0.43 \text{ with mean shear}$$

For three dimensional isotropy

$$S = 0.75 \text{ without mean shear}$$

$$\text{and} \quad S = 0.60 \text{ with mean shear}$$

The relative importance of mean shear will be indicated by the form of either the energy spectrum function $E(r)$, or the correlation difference function $[1 - R(r)]$.

2. THE PRACTICAL APPLICATION OF TURBULENCE THEORY

2.1 The Mean Wind Profile

In applying the relations developed above to the wind vectors measured by means of sodium vapor trails ejected as a tracer into the upper atmosphere, the relative importance of the mean motion must not be overlooked. The velocities used in the energy spectrum and correlation analyses of the previous section must be the turbulent velocities, or departures from the mean motion. In normal correlation analysis, the mean value of a set of observations is usually taken as the mean value of the measured data, which, when applied to wind height shear data, would be tantamount to the assumption of a mean wind profile which is constant with height. Such a profile is the exception rather than the rule in meteorological phenomena.

Practically any attempt to prescribe a mean wind profile to the measured winds will be subjective to a certain extent. If one uses a polynomial fit, for example, it must be truncated before it can assume any of the features of the measured profile which are due to the turbulent motions present. From experience based on the measurement of winds in the 75 to 105 km region by means of radio reflections from meteor trails (Elford, 1958, 1964), a quadratic change with height of the mean wind over any given 20 km interval should best

describe the contribution of the mean motion without destroying any of the characteristics of the turbulent flow field. In the present analysis, the windspeed/azimuth data are converted to zonal and meridional components, and a polynomial profile of order $Z+1$, where

$$Z = \frac{\text{Total height range covered by data (km)}}{20},$$

is fitted to each. The profiles thus determined are subtracted from the relevant measured profiles to give zonal and meridional turbulent velocities.

2.2 The Determination of $E[\Delta h]$

The available sodium trail data lists wind speed and azimuth against height, and usually involves irregularly spaced height intervals. The sampling irregularity exists for two reasons:

- a) there is an occasional difficulty in absolutely identifying the same point on the trail in consecutive photographs;
- b) the wind profile between consecutive observational heights is linear. This is usually obvious from the photographs, and can easily be allowed for in subsequent analysis.

Whereas equal height interval sampling is not absolutely necessary for subsequent reduction, it does simplify the analysis, and so linear interpolation between the listed data points is used to provide a profile with data points spaced 0.2 km in height.

The energy spectrum function is computed as

$$E(\Delta h_i) = \frac{1}{N} \sum_{k=1}^N (u_{k+i} - u_k)^2 \quad (12)$$

in which

$$N = 5(H_2 - H_1) - i$$

where $i = 1, 2, 3, \dots, N$

such that $\Delta h_i = 0.2$ km.

$$\Delta h_2 = 0.4 \text{ km}$$

etc.

and H_1, H_2 (in km) are the lower and upper bounds respectively of the region for which $E(\Delta h)$ is being determined. Such partitioning of the height range is necessary since there is considerable variation in the characteristics of the flow

over the total height range sampled (usually some 70 to 200 km).

Energy spectrum functions may be calculated using

- a) zonal turbulent velocities
- b) meridional turbulent velocities

and c) turbulent windspeed.

The turbulent windspeed w is defined here as

$$w = \text{measured windspeed} - \\ ((\text{mean zonal wind})^2 + (\text{mean meridional wind})^2)^{1/2}$$

2.3 Correlation Analysis

The two correlation functions f and g defined in 1.2 refer to turbulent velocity components measured parallel and normal to the separation vector. Since vertical velocities in this region of the upper atmosphere are so much less than the associated horizontal components, the magnitude of the vertical component cannot be determined from sodium trail photographs. (Most workers in this field consider the upper limit for mean plus random vertical motions to be some 10 metres/sec). However, we may redefine f and g in terms of the orthogonal zonal and meridional flow fields, with a view to investigating possible isotropy. This has been done by meteorologists in the past, with at least partial success (see, for example, Hutchings (1955)).

The normalizing factors \bar{u}_z^2 and \bar{u}_n^2 are best estimated by the standard correlation function definition. The correlation functions f and g then become

$$f(\Delta h_i) = \frac{\sum_{k=1}^N u_{k+i} u_k}{\left[\sum_{k=1}^N u_{k+1}^2 \sum_{k=1}^N u_k^2 \right]^{1/2}} \quad (14)$$

where u are the zonal turbulent wind velocities and

$$g(\Delta h_i) = \frac{\sum_{k=1}^N v_{k+i} v_k}{\left[\sum_{k=1}^N v_{k+1}^2 \sum_{k=1}^N v_k^2 \right]^{1/2}}, \quad (15)$$

where v are meridional turbulent wind velocities, and N and i are as previously defined for equation 12.

3. PRELIMINARY RESULTS

The analysis of Section 2 has been applied to data obtained from a sodium trail release over the Eglin Air Force Base, Florida (29.6° N, 86.6° W) at 1910 CST on May 21, 1963 (Edwards et al., 1963). In this experiment, wind speed and azimuth were obtained over a height range of 69 to 140 km.

3.1 The Mean Wind Profile

Since the data covers the height range from 69 to 140 km, polynomials of order 4 are fitted to the zonal and meridional measured profiles. These yield mean zonal and meridional profiles

$$u_{\text{mean}} = 38.6 - 126h - 244h^2 + 174h^3 + 205h^4$$

$$v_{\text{mean}} = -30.4 + 19.8h + 148h^2 - 16.8h^3 - 125h^4$$

where u, v are in metres/sec and h is the normalized height given by

$$h = (2z - z_{\min} - z_{\max}) / (z_{\max} - z_{\min})$$

where z is the height variable

z_{\max} the maximum and

z_{\min} the minimum heights of the available data, all heights being in kilometers.

Normalization of the height range stabilizes the least squares fitting process, and makes the relative importance of the individual terms of the fitted polynomials more obvious than is the case when the mean velocities are expressed as power series in the actual height z . Results are plotted in Figs. 1 and 2.

The meteorological significance of these profiles, in particular the reversal of both the zonal and meridional components above 110 km, cannot be evaluated from consideration of this single firing.

3.2 The Turbulent Wind Profile

As mentioned in Section 2, the 70 to 200 km height range covers a number of characteristically different regions. The wind motions observed below approximately 105 km indicate the presence of small-scale structure, while those above 110 km do not appear to be at all turbulent, even though vertical shear is present. In the results presented here, discussion is confined to the consideration of

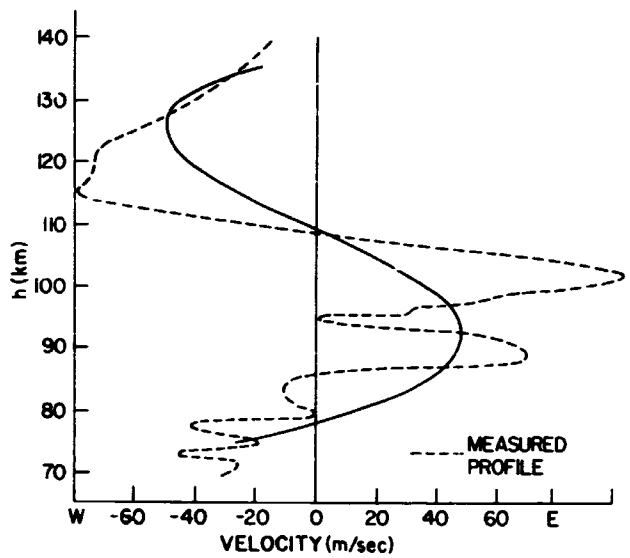


FIGURE 1.—Mean zonal profile.

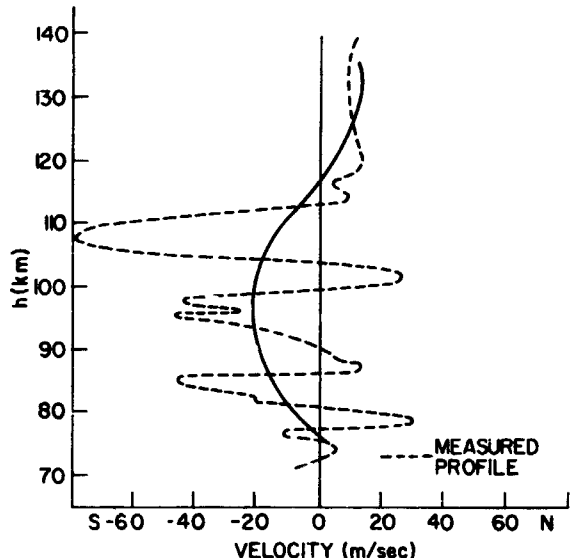


FIGURE 2.—Mean meridional profile.

the region from 80 to 100 km, which has been found to be representative of a turbulent region which can be adequately described by available statistical theories of hydrodynamic turbulence (Plamont and Jager, 1961; Zimmerman, 1962; Roper, 1962).

The measured zonal and meridional profiles, and the deviations from the mean wind for the height range 80 to 100 km are plotted in Figures 3 to 6. Whereas the immediately obvious wave-like nature of the turbulent profile would suggest a wave theory approach as likely to be the most profitable for consideration of the wind motions

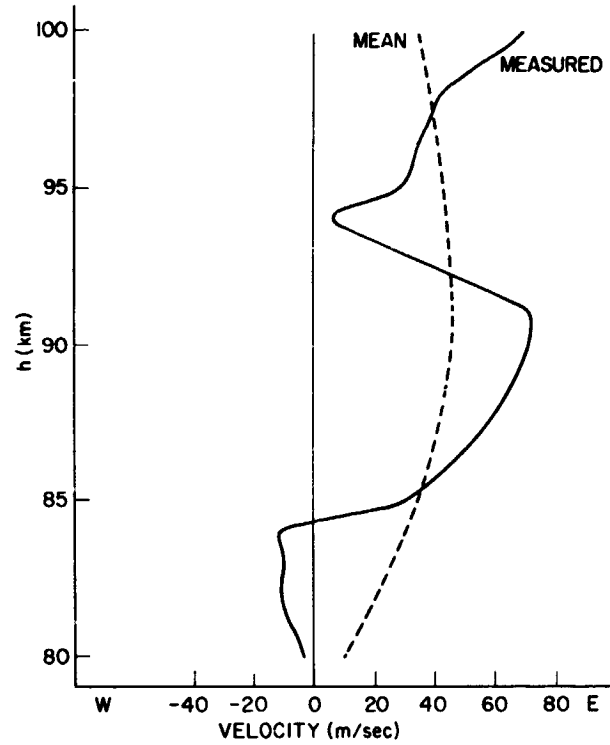


FIGURE 3.—Zonal profile, 80-100 km.

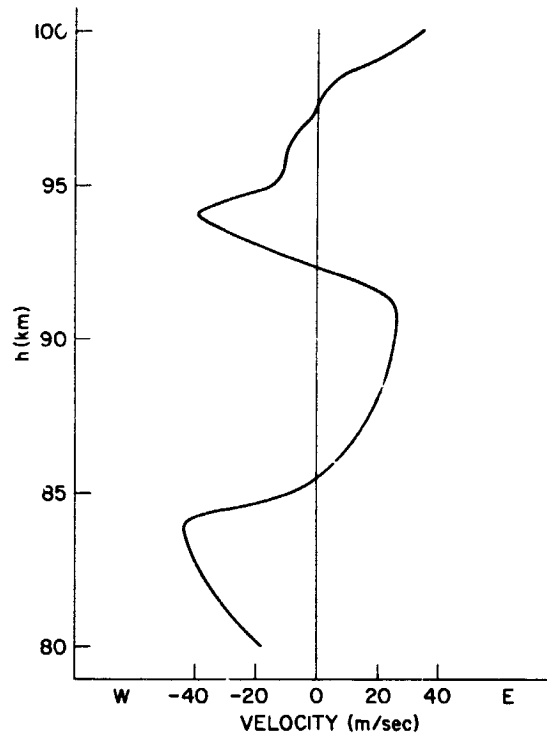


FIGURE 5.—Turbulent zonal profile.

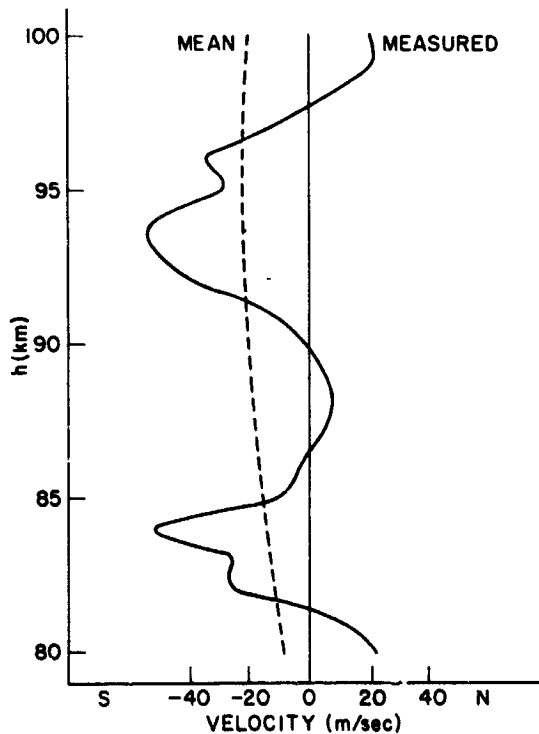


FIGURE 4.—Meridional profile, 80-100 km.

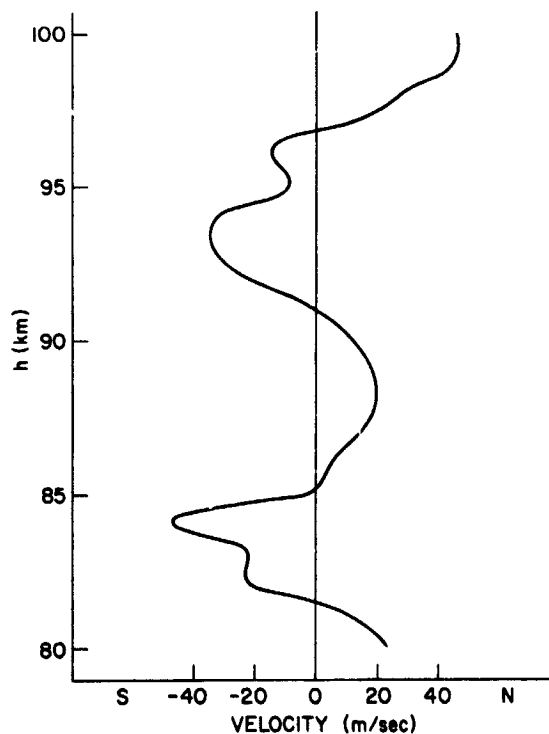


FIGURE 6.—Turbulent meridional profile.

in this region, applications of available wave theories (e.g., Hines, 1959) have not produced consistent results. The possibility of generation of turbulence in the 80 to 100 km region by vertically propagating gravity waves has been proposed by Hines (1963). The purpose of the present work, however, is not to determine the source of the turbulent energy, but rather to substantiate the evidence that the observed shears characterize a region of hydrodynamic turbulence.

3.3 The Energy Spectrum Functions

The energy spectrum functions for the zonal and meridional turbulent wind profiles for the 80 to 100 km region have been computed using the methods described in Sections 2.2 and 2.3. As can be seen from Figures 7 and 8, the velocity difference spectrum $E(\Delta h)$ and the correlation difference function $[1 - f(\Delta h)]$ for the zonal turbulent velocities are completely equivalent. This is not surprising, since both functions are solutions of the same equation

$$F = a\Delta h^m$$

(see Sections 1.1 and 1.2).

Similarly for the meridional spectra of Figures 9 and 10. The slope m of the log log plots of both the zonal and meridional $E(\Delta h)$ (or $[1 - R(\Delta h)]$) spectrum functions against height difference Δh is constant at $4/3$ for separations Δh up to 3 km, indicative of an isotropic region subject to a mean wind shear (Tchen, 1954).

3.4 Isotropy

Since the energy spectrum functions and the correlation difference functions all follow an established (shear) law at small scales in the height range from 80 to 100 km, it is possible to determine the nature of the isotropy at these scales in this region.

Figure 13, curve A, is a plot of the variation of

$$S = \frac{1-f}{1-g}$$

against Δh .

In the region up to a scale of 3.5 km, S has a value of approximately 0.7, indicating an isotropy lying somewhere between two and three dimensional. The increase in S at scales greater than approximately 3 km is due to the breakdown

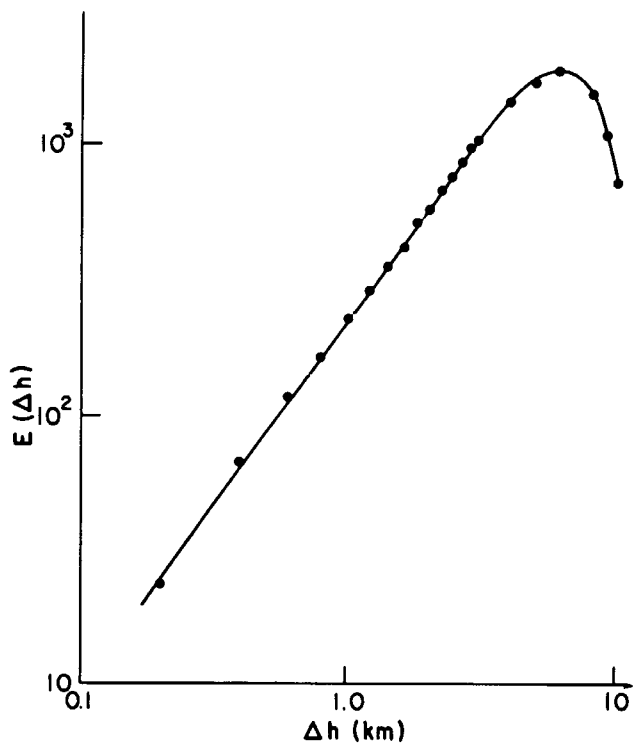


FIGURE 7.—The zonal energy spectrum function.

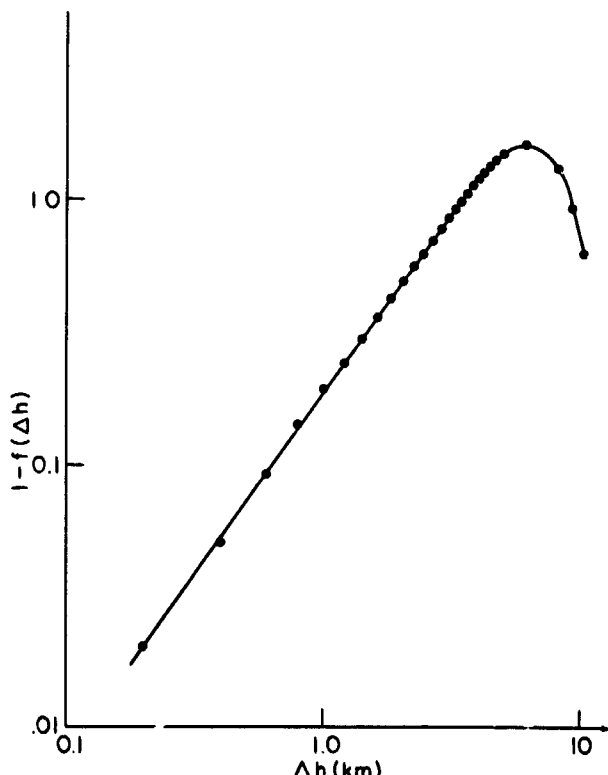


FIGURE 8.—The zonal correlation difference function.

at this scale of the $4/3$ power law in both zonal and meridional spectrum functions.

The function S has been found to be quite sensitive to variation in the parameters specifying the mean wind profiles. For example, if, instead of the fourth order polynomial fits to the total height range of the zonal and meridional data, linear mean wind profiles are fitted over the height range 80 to 100 km only, subsequent spectrum analysis yields the S function of curve *B* of Figure 13. This curve would indicate the existence of three dimensional isotropy for scales up to 3 km. It is possible that the 4th order polynomial fits are, in fact, attributing a small fraction of the random wind variations to the mean motion. However, in order to correlate spectra obtained for different height strata (as is done in the next section), a continuous mean profile is required, and has therefore been used throughout the analysis.

3.5 Vertical Scale

The vertical scale associated with the turbulent wind structure is conveniently defined by the Δh corresponding to the maximum value of either $E(\Delta h)$ or $[1 - R(\Delta h)]$. As can be seen from

Figures 7, 9 and 11, which are plotted using zonal, meridional and windspeed turbulent velocities respectively, the vertical correlation distance as defined above is not the same for each component, i.e., the wind motions are not isotropic at the maximum of $E(\Delta h)$. However, for the purpose of comparison with stratospheric and lower mesospheric data, where meridional winds are, for the most part, negligible, consideration need only be given to the zonal energy spectrum.

The variation of vertical scale with height in the stratosphere has been determined by Webb (1964) from a series of Robin soundings at Eglin. His results indicate an exponential increase of the vertical scale with height, from approximately 800 metres at 35 km to 2 km at 55 km. He has extrapolated this exponential to a height of 90 km, and finds a vertical scale of 6 km which is the value determined for this height by Greenhow (1959) from a correlation analysis of wind shears determined by means of radio reflections from meteor trails at Jodrell Bank (53°N).

In order to investigate the change with height of the vertical correlation distance in the 80 to 130 km region, the sodium trail data was sub-

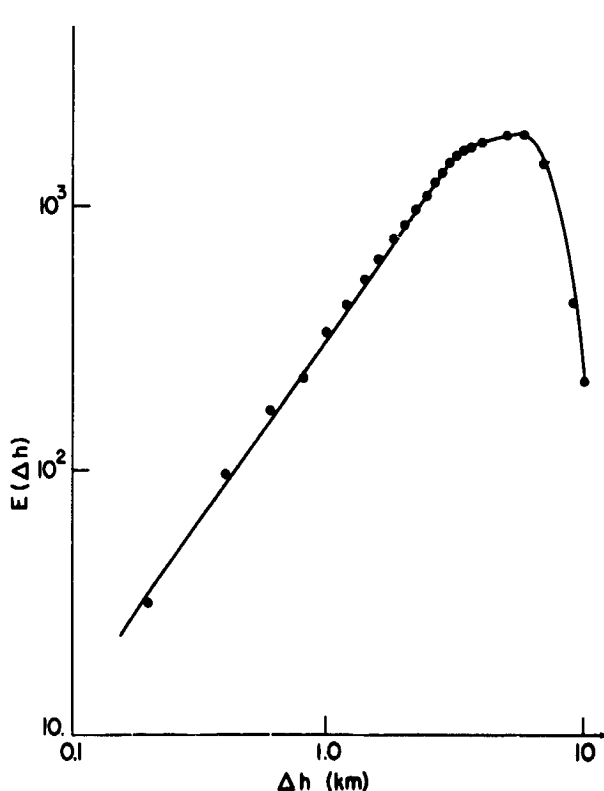


FIGURE 9.—The meridional energy spectrum function.

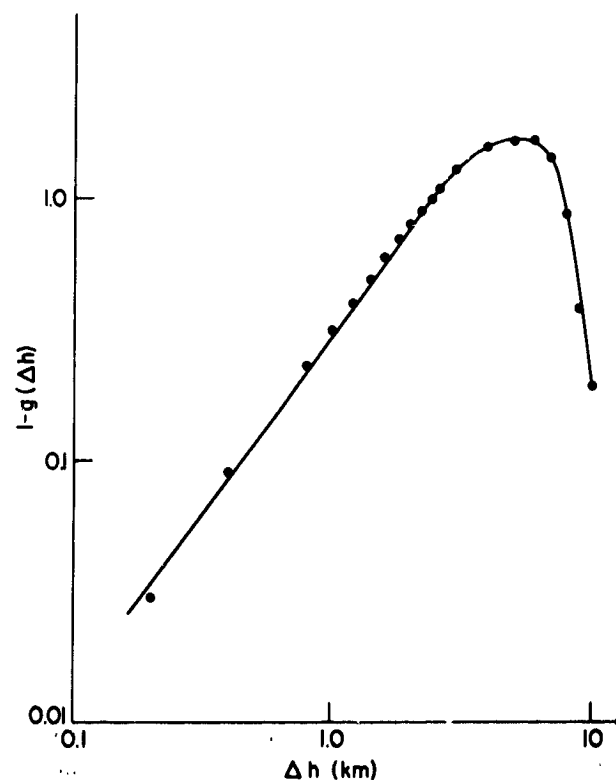


FIGURE 10.—The meridional correlation difference function.

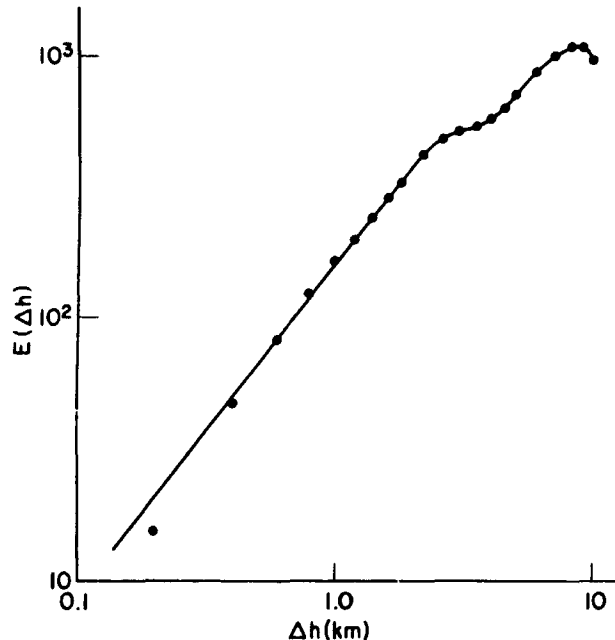


FIGURE 11.—The windspeed energy spectrum function.

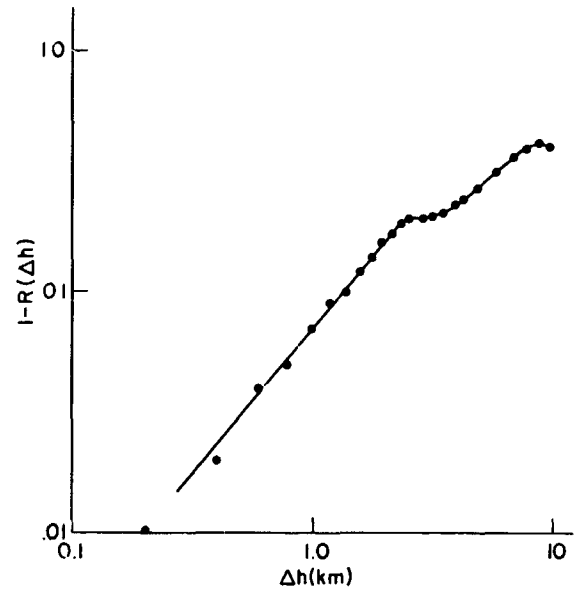


FIGURE 12.—The windspeed correlation difference function

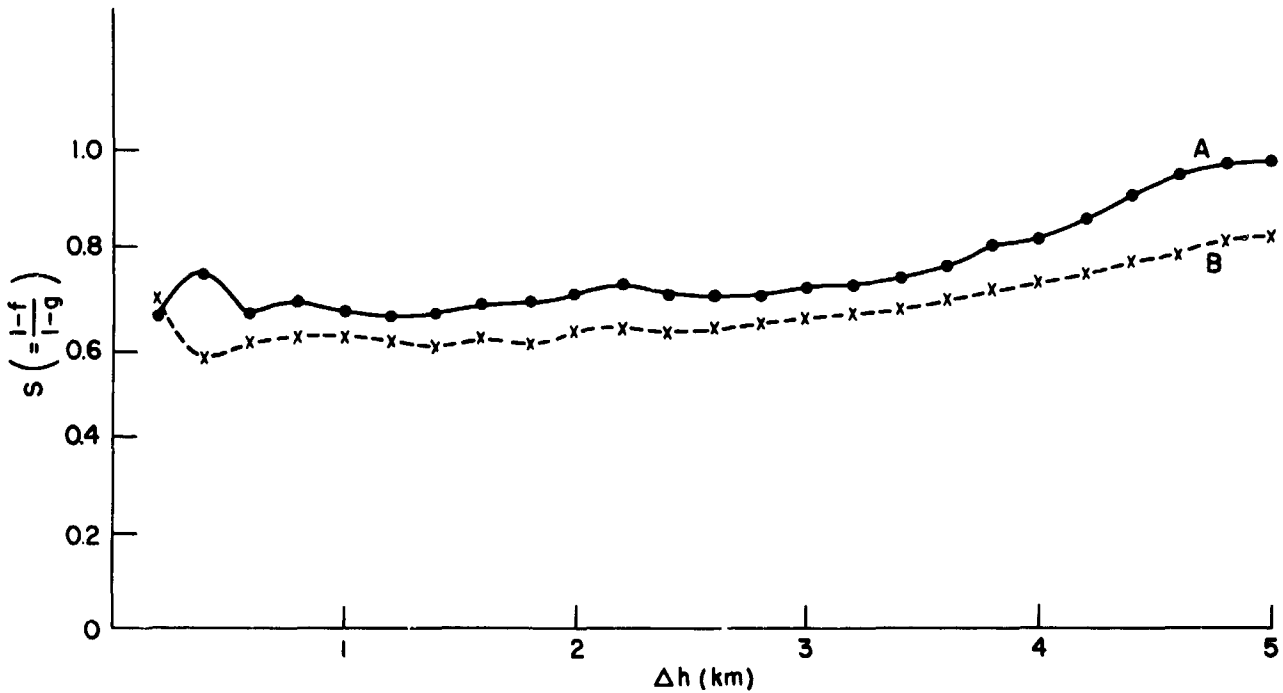


FIGURE 13.—Variation of the isotropy parameter "S" with scale.

jected to a stepwide analysis, starting with the 75 to 95 km height range, and proceeding via the 80 to 100, 85 to 105, etc. ranges to 115 to 135 km. The maxima of the resultant $E(\Delta h)$ curves were then plotted as the vertical scales at the midpoints of the respective height ranges. The results are shown in Figure 14, together with Green-

how's determination, and the 7.8 km at 94 km (October, 1961) determined from radio meteor trail shears at Adelaid's (35° S) (Roper, 1962). The dashed line is Webb's extrapolated variation. While there is excellent agreement with Webb's proposed exponential increase, there is also good agreement between the vertical scales measured

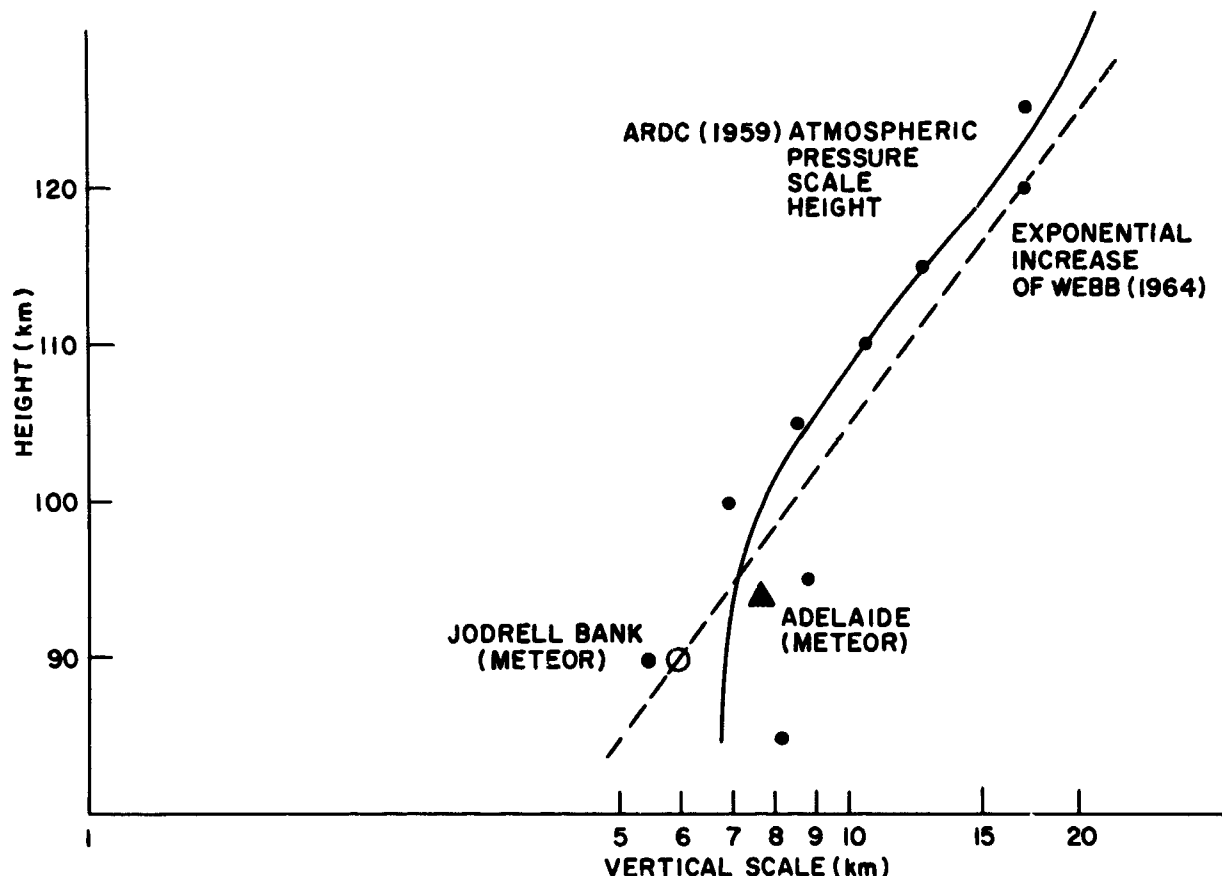


FIGURE 14.—Variation of the vertical scale of the zonal turbulent wind component with height.

at various altitudes for the Eglin firing, and the atmospheric pressure scale height (also shown in Figure 14). This phenomenon has also been observed by others (e.g., Zimmerman (1964)). As yet, no satisfactory explanation for such a dependence has been proposed.

Above 125 km, the magnitudes of the deviations of the measured winds from the mean wind values becomes insignificant. Wind motions at these heights for this particular firing are characteristically nonturbulent.

CONCLUSIONS

The techniques of spectrum analysis based on hydrodynamic turbulence theory can be profitably applied to wind data obtained from sodium trail rocket firings, at least in the height range from 80 to 100 km. The analysis of further firings should indicate whether or not the mean profiles determined as a prelude to spectrum analysis have any meteorological significance.

REFERENCES

GENERAL

- KOLMOGOROFF, A., C. R. AKAD. SCI. U.R.S.S., *30*, 301, 1941.
- BATCHELOR, G. K., *The Theory of Homogeneous Turbulence*, Cambridge University Press, 1953
- CORRSIN, S., *Jour. Geophys. Res.*, *64*, 2134, 1959
- TCHEN, C. M., *Phys. Rev.*, *94*, 4, 1954
- KARMAN, T., von and HOWARTH, L., *Proc. Roy. Soc., London* *184*, 192, 1938
- ELFORD, W. G., *Plan. and Space Sci.*, *1*, 94, 1958
- ELFORD, W. G., 1964 (unpublished)
- HUTCHINGS, J. W., *Jour. Met.*, *12*, 263, 1955
- EDWARDS, H. D. et al., *Jour. Geophys. Res.* *68*, 6062, 1963
- BLAMONT, J. E., and DE JAGAR, C., *Ann. de Geophys.*, *17*, 134, 1961
- ZIMMERMAN, S. P., *Ann de Geophys.* *18*, 116, 1962.
- ROPER, R. G., Ph.D. Thesis, University of Adelaide, 1962
- HINES, C. O., *Jour. Geophys. Res.*, *64*, 2210, 1959
- HINES, C. O., *Quart. Jour. Roy. Met. Soc.*, *89*, 1, 1963
- WEBB, W. L., U.S. Army E.R.D.A.—130, White Sands, New Mexico. April 1964
- GREENHOW, J. S., and NEUFELD, E. L., *Jour. Geophys. Res.*, *64*, 2129, 1959
- ZIMMERMAN, S. P., *Jour. Geophys. Res.*, *65*, 784, 1964.

APPENDIX I

RESUME OF THE COMPUTER PROGRAM

The computer program has been written in FORTRAN IV for execution on an IBM 7094, and consists of the following routines:

1. The main program SHEAR which reads and does some processing of the input data (which is punched on cards).

SHEAR calls subroutines

a) FIT, which fits polynomial profiles to the zonal and meridional wind velocity/height profiles by the method of least squares, utilizing

b) MATS, to solve the set of independent linear equations

c) The total wind speed profile is calculated by TRADE.

d) OUTPUT performs the energy spectrum and correlation analyses, and printout of same.

e) PAGE is a utility routine which turns and numbers the output pages, and prints an appropriate heading on each.

Input Data

The input data is on punched cards, and is read as follows:

1. Header Card; the information punched on this card is printed at the top of each page of output. The full 72 columns can be used for any type of alphanumeric heading.

2. The parameters specifying the mean zonal and meridional profiles. These determine the order of the polynomial fitted to

a) the zonal (punched in columns 2, 3) and

YR	MO	DAY	HOUR	HEIGHT	WINDSPEED	AZIMUTH
3	3	9	14	19	24	29

all integer

must be right adjusted if integer; anywhere in appropriate field if decimal punch is included.

5. After all data of 4. a blank card to flag "end of data."

6. Further height ranges as for 3 as required.

7. a) If a change in the mean wind profile is required a card with a 2 punched in column 1 may be substituted for any of the cards 6, and followed by a card of format 2 above which specified the

b) the meridional (punched in columns 5, 6) measured data to determine the mean profile. e.g., a 5 punched in column 3 will fit a polynomial of the form

$$a_1 + a_2 h + a_3 h^2 + a_4 h^3 + a_5 h^4$$

to the zonal wind data.

The maximum allowable value of the subscript i in the a_i above is 10.

3. The height range (must be integral, and in km) over which the energy spectrum and correlation analyses are to be performed. This can be any fraction of the height interval covered by the input data, but must not be less than 10 km unless an appropriate spectral range is punched in column 13. The minimum of the height range interval is punched in columns 2 to 5, the maximum in columns 6 to 9. If OUTPUT is required to produce spectra over height differences to other than a maximum of 10 km, the required maximum height difference can be punched in columns 10 to 13. This entry must not exceed the height range specified in columns 2 to 9. If this last field is left blank, spectra to 10 km are output.

4. The trial data, which must not exceed a maximum to minimum height range of 150 km. The data is punched as year, month, day, hour (local time, 24 hour clock), height (km), wind-speed (metres/sec), and azimuth (degrees) as follows

new profile. This card is then followed by further height ranges (as for 6.) as required.

7. b) If a completely new set of header plus data cards is to be processed after either stages 5, 6, or 7a, a card with a 1 punched in column 1 will return control to the start of the program, which will then read in the new set of data cards sequenced as from 1 above.

APPENDIX II
Listing of the FORTRAN IV Program

08/

SHEAR
 EXTERNAL FORMULA NUMBER — SOURCE STATEMENT — INTERNAL
 C SODIUM TRAIL HEIGHT SHEAR ANALYSIS PROGRAM
 C CALCULATES THE ENERGY SPECTRUM FOR TOTAL SHEAR, AND FOR ZONAL AND
 C MERIDIONAL SHEAR COMPONENTS
 C READS INPUT DATA AS FOLLOWS
 C A HEADER CARD, PUNCHED WITH DETAILS OF FIRING TIME, ETC.
 C FORMAT 12A6
 C THE PARAMETERS SPECIFYING THE MEAN ZONAL AND MERIDIONAL PROFILES,
 C FORMAT 213
 C THE HEIGHT RANGE OVER WHICH ANALYSIS IS TO BE PERFORMED, ZMIN,
 C ZMAX, AND THE MAXIMUM OF THE OUTPUT SPECTRAL RANGE DESIRED.
 C FORMAT 1X2F4.0, 14.
 C SPECTRAL RANGE MUST NOT EXCEED ZMAX-ZMIN.
 C IF NO SPECTRAL RANGE IS SPECIFIED, ZMAX-ZMIN MUST BE GREATER THAN
 C 10KM, AND SPECTRA WILL BE OUTPUT TO 10KM.
 C THE TRAIL DATA, YEAR MONTH DAY LOCAL TIME (HOURS AND MINUTES,
 C 24 HOUR CLOCK) HEIGHT(KM) WIND SPEED(METRES/SEC) WIND AZIMUTH
 C (DEGREES).
 C FORMAT 313, 15, F5.1, 2F5.0
 C A BLANK CARD
 C FURTHER ZMIN, ZMAX AS REQUIRED. IF A 2 APPEARS IN COLUMN 1,
 C PROGRAM WILL READ NEXT CARD AS NEW PROFILE SPECIFICATION, FOLLOWED
 C BY FURTHER ZMIN, ZMAX CARDS. IF A 1 APPEARS IN COLUMN 1, THE
 C PROGRAM WILL READ NEXT CARD AS HEADER CARD OF A COMPLETELY NEW SET
 C OF DATA.
 C
 DIMENSION BZ(10), BM(10)
 DIMENSION RESULT(12), ZI(750), WINDI(750), AZRADI(750), ZONAL(750),
 1ERID(750), TZONAL(750), TMERID(750)
 DIMENSION TSPEED(750), AW(5)
 COMMON ZI, WINDI, AZRADI, ZONAL, ERID, TZONAL, TMERID, TSPEED
 C = 0.05
 CS = 0.000001
 PI = 3.1415926
 TWOPI = 2.0*PI
 999 NGO=0
 NI=0
 I=0
 NSUM=0
 ZERO=0.0
 READ (2,1)RESULT
 1 FORMAT(12AC)
 17 READ (2,4)NP,NQ
 4 FORMAT (213)
 NFIT=-1
 2 READ(2,3)NGO, ZMIN, ZMAX, NDIFF
 3 FORMAT(II,2F4.0,I4)
 IF(NGO)19, 19, 18
 18 IF(NGO-2)999, 17, 17
 19 CONTINUE
 IF(NDIFF)20, 20, 21
 20 NDIFF=10
 21 MIN=ZMIN+C
 MAX=ZMAX+C

SHEAR
 EXTERNAL FORMULA NUMBER — SOURCE STATEMENT — INTERNAL
 08/

C IF(NI)5, 5, 101
 TRAIL DATA INPUT
 5 READ (2,6)MYEAR, MONTH, JOUR, LTIME, Z, WIND, AZDEG
 6 FORMAT(3I3, I5, F5.1, 2F5.C)
 IF(MYEAR>100,100, 7
 7 I=I+1
 IF(I-1)11, 11, 8
 8 ZDIFF=Z-ZI(I-1)
 MZ=10.0 * Z+C
 LZ=10.0 * ZI(I-1)+C
 LDIFF=MZ-LZ
 IF(LDIFF>2)12, 11, 9
 12 WRITE (3,6)MYEAR, MONTH, JOUR, LTIME, Z, WIND, AZDEG
 WRITE(3,13)
 13 FORMAT(1X////1X26HDATA CARDS OUT OF SEQUENCE////1X20HEXECUTION
 1TERMINATED////1X)
 PRINT 13
 CALL EXIT
 C INTERPOLATION ROUTINE
 9 NPOINT=LDIFF/2-1
 NSUM=NSUM+NPOINT
 GRAD=(WIND - WINDI(I-1))/ZDIFF
 AZDIFF=AZDEG/57.3-AZRADI(I-1)
 IF(ABS(AZDIFF)-PI)>94,94,91
 91 IF(AZDIFF)<92,94,93
 92 AZDIFF=AZDIFF+TWOPI
 GOTO94
 93 AZDIFF=AZDIFF-TWOPI
 94 AZGRAD=AZDIFF/ZDIFF
 DO10J=1,NPOINT
 ZI(I)=ZI(I-1)+0.2
 WINDI(I)=WINDI(I-1)+C.2 * GRAD
 AZRADI(I)=AZRADI(I-1)+C.2 * AZGRAD
 IF(AZRADI(I))>95,96,96
 95 AZRADI(I)=AZRADI(I)+TWOPI
 96 IF(AZRADI(I)-TWOPI)>98,98,97
 97 AZRADI(I)=AZRADI(I)-TWOPI
 98 CONTINUE
 I=I+1
 10 CONTINUE
 11 ZI(I)=Z
 WINDI(I)=WIND
 AZRADI(I)=AZDEG/57.3
 GO TO 5
 100 NI=I
 C ALL DATA IN. COMMENCE COMPUTATION
 HDIFF=ZI(NI)-ZI(1)
 HPLUS=ZI(NI)+ZI(1)
 C CALCULATE ZONAL AND MERIDIONAL WIND COMPONENTS
 DO201J=1,NI
 ZONAL(J)=WINDI(J) * SIN(AZRADI(J))
 201 ERID(J)=WINDI(J) * COS(AZRADI(J))
 101 NZ=0
 LMIN=10 * MIN
 LMAX=10 * MAX

SHEAR
EXTERNAL FORMULA NUMBER — SOURCE STATEMENT — INTERNAL

08/

```

CALL PAGE (RESULT, ZERO)
DO104J = 1,NI
LZ = ZI(J) * 10.0+C
IF(LZ-LMIN)104,102,102
102 IF(LZ-LMAX)103,103,104
103 NZ = NZ+1
104 CONTINUE
      WRITE (3,105)NI, NSUM, ZMIN, ZMAX, NZ, NP, NQ
105 FORMAT(1X////1X33HTOTAL NUMBER OF INPUT DATA POINTS I8///1X26HINC
1LUDING INTERPOLATION OF 15,7H POINTS ////1X45HNUMBER OF DATA POINT
2S WITHIN THE HEIGHT RANGE F5.0,6H KM TO,F5.0,3H KM I8///1X31HEAST
3 WEST PROFILE SPECIFICATION I5 //1X33HNORTH SOUTH PROFILE SPECIFI
4CATION I3 //1X)
START = 1
CALL PAGE (RESULT, START)
WRITE (3,106)ZMIN, ZMAX
106 FORMAT(1X50HCALCULATED ZONAL AND MERIDIONAL MEAN WIND PROFILES
110X12HHEIGHT RANGE F5.0,6H KM TO F5.0,3H KM/1HO
2/10X 6HHEIGHT 10X5HZONAL 12X10HMERIDIONAL 10X10HWIND SPEED /1X/
31X,18X,3(4X12HDATA MEAN,4X)/1X,/)
NHITE = (ZMAX-ZMIN)/20 0-C
NHITE = NHITE+1
INK = 5 * NHITE-1
NFIT = NFIT+1
IF(NFIT)202,202,203
C CALCULATE COEFFICIENTS OF MEAN PROFILE POLYNOMIALS
202 CALL NORMAL (ZONAL, ERID, ZI, NI, BZ, BM, NP, NQ)
203 CONTINUE
C DETERMINE AND PRINT CUT MEAN WIND PROFILES
SUBS = (ZMAX+ZMIN-ZI(1)) * 5.0+1.0+C
DO108L = MIN, MAX, NHITE
IZ = SUBS-FLOAT(L * 5)
J = MAX+MIN-L
H = J
S = (2.0 * H-HFLUS)/HDIFF+CS
AZONAL = 0.0
AMERID = 0.0
DO204M = 1,10
AZONAL = AZONAL+BZ(M) * S * * (M-1)
AMERID = AMERID+BM(M) * S * * (M-1)
204 CONTINUE
MZONAL = AZONAL
MMERID = AMERID
MSPEED = SQRT(AZONAL * * 2+AMERID * * 2)
WRITE(3,107)J, ZONAL(IZ), MZONAL, ERID(IZ), MMERID, WINDI(IZ), MSPEED
107 FORMAT(1XI13,4X,3( F8.0,4XI14,4X),/1X)
108 CONTINUE
CALL PAGE (RESULT, START)
WRITE(3,109)ZMIN, ZMAX
109 FORMAT(1X,22HTURBULENT WIND PROFILE, 10X12HHEIGHT RANGE F5.0,
16HKM TO F5.0, 3H KM/1X/1X, 10X6HHEIGHT, 10X6HTZONAL, 10X11HTMERIDIONA
2L, 10X6HTSPEED/1X)
C DETERMINE AND PRINT CUT TURBULENT WIND PROFILES
NH = (MAX-MIN) * 5+1
K = (ZMAX-ZI(1)) * 5.0+2.0+C
NK = INK

```

SHEAR
 EXTERNAL FORMULA NUMBER — SOURCE STATEMENT — INTERNAL

08/

RMSZ = 0.0
 RMSM = 0.0
 RMST = 0.0
 SUMSQT = 0.0
 DO112J = 1, NP
 TZONAL(J) = 0.0
 TMERID(J) = 0.0
 K = K-1
 $H = ZMAX - 0.2 * \text{FLOAT}(J-1)$
 $IH = H + 0$
 $S = (^0 * H - HPLUS) / HDIFF + CS$
 NK = NK + 1
 DO205M = 1, 10
 $TZONAL(J) = TZONAL(J) + BZ(M) * S * * (M-1)$
 $TMERID(J) = TMERID(J) + BM(M) * S * * (M-1)$

205 CONTINUE
 $TZONAL(J) = ZONAL(K) - TZONAL(J)$
 $TMERID(J) = ERID(K) - TMERID(J)$
 CALL TRADE(J, K)

C CALCULATE RMS TURBULENT VELOCITIES FOR THE HEIGHT RANGE ZMIN/ZMAX
 RMSZ = TZONAL(J) * * 2 + RMSZ
 RMSM = TMERID(J) * * 2 + RMSM
 RMST = TSPEED(J) * * 2 + RMST
 SUMSQT = SUMSQT + 1.0
 IF(NK-INK)112,112,110

110 WRITE(3,111)IH, TZONAL(J), TMERID(J), TSPEED(J)
 111 FORMAT(1X, 10X14, 12XF5.0, 11XF8.0, 13XF5.0/1X)
 NK = 0

112 CONTINUE
 CALL PAGE(RESULT, START)
 RMSZ = SQRT(RMSZ/SUMSQT)
 RMSM = SQRT(RMSM/SUMSQT)
 RMST = SQRT(RMST/SUMSQT)
 WRITE (3,206)ZMIN, ZMAX, (BZ(I), I=1, NP)

206 FORMAT(1X!0HNORMALIZED
 1 1X12HHEIGHT RANGE 10XF7.0,7H KM. TO F7.0, 4H KM./1H0/
 2 , X42HCOEFFICIENTS GIVING BEST FIT TO ZONAL DATA/1X/10E11.3)
 WRITE(3,207)(BM(I), I=1, NQ)

207 FORMAT(1X/1X/
 11X/1X47HCOEFFICIENTS GIVING BEST FIT TO MERIDIONAL DATA/1X/1X10E11
 2.3/1X/)
 WRITE(3,208)RMSZ, RMSM, RMST

208 FORMAT(1X/1X
 1 1X22HRMS TURBULENT VELOCITY/1X/1X10X5HZONALF11.0,11HMETRES/S
 2E0./1X/1X10X10HMERIDIONAL F6.0,11HMETRES/SEC./1X/1X10X10HWIND SPEE
 3D F6.0,11HMETRES/SEC.)
 CALL PACE(RESULT, START)
 WRITE (3,113)ZMIN, ZMAX

113 FORMAT(1X46HENERGY SPECTRUM OF ZONAL WIND HEIGHT VARIATION,
 110X12HHEIGHT RANGE F5.0,6H KM TO F5.0,3H KM./1X)
 C CALCULATE AND OUTPUT ENERGY SPECTRUM FUNCTIONS
 CALL OUTPUT(TZONAL, NH, NDIFF)
 CALL PAGE (RESULT, START)
 WRITE (3,114) ZMIN, ZMAX

114 FORMAT(1X51HENERGY SPECTRUM OF MERIDIONAL WIND HEIGHT VARIATION,

SHEAR
EXTERNAL FORMULA NUMBER -- SOURCE STATEMENT -- INTERNAL

```

CALL PAGE(RESULT, ZERO)
DO104J=1,NI
LZ=ZI(J) * 10.0+C
IF(LZ-LMIN)104,102,102
102 IF(LZ-LMAX)103,103,104
103 NZ=NZ+1
104 CONTINUE
      WRITE (3,105)NI, NSUM, ZMIN, ZMAX, NZ, NP, NQ
105 FORMAT(1X////1X33HTOTAL NUMBER OF INPUT DATA POINTS I8///1X26HINC
1LUDING INTERPOLATION OF 15,7H POINTS ////1X45HNUMBER OF DATA POINT
2S WITHIN TLE HEIGHT RANGE F5.0,6H KM TO,F5.0,3H KM I8///1X31HEAST
3 WEST PROFILE SPECIFICATION I5 //1X33HNORTH SOUTH PROFILE SPECIFI
4CATION 13 //1X)
      START=1
      CALL PAGE(RESULT,START)
      WRITE (3,106)ZMIN, ZMAX
106 FORMAT(1X50HCALCULATED ZONAL AND MERIDIONAL MEAN WIND PROFILES
110X12HHEIGHT RANGE F5.0,6H KM TO F5.0,3H KM/1HO
2/10X 6HHEIGHT 10X5HZONAL 13X10HMERIDIONAL 10X10HWIND SPEED /1X/
31X,18X,3(4X12HDATA MEAN,4X),/1X/)
      NHITE=(ZMAX-ZMIN)/20.0-C
      NHITE=NHITE+1
      INK=5 * NHITE-1
      NFIT=NFIT+1
      IF(NFIT)202,202,203
C   CALCULATE COEFFICIENTS OF MEAN PROFILE POLYNOMIALS
202 CALL NORMAL (ZONAL, ERID, ZI, NI, BZ, BM, NP, NQ)
203 CONTINUE
C   DETERMINE AND PRINT CUT MEAN WIND PROFILES
SUBS=(ZMAX+ZMIN-ZI(1)) * 5.0+1.0+C
DO108L=MIN, MAX, NHITE
IZ=SUBS-FLOAT(L * 5)
J=MAX+MIN-L
H=J
S=(2.0 * H-HPLUS)/HDIFF+CS
AZONAL=0.0
AMERID=0.0
DO204M=1,10
AZONAL=AZONAL+BZ(M) * S * * (M-1)
AMERID=AMERID+BM(M) * S * * (M-1)
204 CONTINUE
      MZONAL=AZONAL
      MMERID=AMERID
      MSPEED=SQRT(AZONAL * * 2+AMERID * * 2)
      WRITE(3,107)J, ZONAL(IZ), MZONAL, ERID(IZ), MMERID, WINDI(IZ),MSPEED
107 FORMAT(1XI13,4X,3( F8.C,4XI4,4X),/1X)
108 CONTINUE
      CALL PAGE (RESULT, START)
      WRITE(3,109)ZMIN, ZMAX
109 FORMAT(1X,22HTURBULENT WIND PROFILE, 10X12HHEIGHT RANGE F5.0,
1 6HKM TO F5.0,3H KM/1X/1X,10X6HHEIGHT, 10X6HTZONAL, 10X11HTMERIDIONA
2L,10X6HTSPEED/1X)
C   DETERMINE AND PRINT CUT TURBULENT WIND PROFILES
NH=(MAX-MIN) * 5+1
K=(ZMAX-ZI(1)) * 5.0+2.0+C
NK=INK

```

SHEAR
 EXTERNAL FORMULA NUMBER — SOURCE STATEMENT — INTERNAL

08/

```

RMSZ=0.0
RMSM=0.0
RMST=0.0
SUMSQT=0.0
DO112J=1,NH
TZONAL(J)=0.0
TMERID(J)=0.0
K=K-1
H=ZMAX-0.2 * FLOAT(J-1)
IH=H+C
S=(2.0 * H-HPLUS)/HDIFF+CS
NK=NK+1
DO205M=1,10
TZONAL(J)=TZONAL(J)+BZ(M) * S * * (M-1)
TMERID(J)=TMERID(J)+BM(M) * S * * (M-1)

205 CONTINUE
TZONAL(J)=ZONAL(K)-TZONAL(J)
TMERID(J)=ERID(K)-TMERID(J)
CALL TRADE(J,K)

C CALCULATE RMS TURBULENT VELOCITIES FOR THE HEIGHT RANGE ZMIN/ZMAX
RMSZ=TZONAL(J) * * 2+RMSZ
RMSM=TMERID(J) * * 2+RMSM
RMST=TSPEED(J) * * 2+RMST
SUMSQT=SUMSQT+1.0
IF(NK-INK)112,112,110
110 WRITE(3,111)IH,TZONAL(J),TMERID(J),TSPEED(J)
111 FORMAT(1X,10XI4,12XF5.0,11XF8.0,13XF5.0/1X)
NK=0
112 CONTINUE
CALL PAGE (RESULT, START)
RMSZ=SQRT(RMSZ/SUMSQT)
RMSM=SQRT(RMSM/SUMSQT)
RMST=SQRT(RMST/SUMSQT)
WRITE(3,206)ZMIN,ZMAX,(BZ(I),I=1,NP)

206 FORMAT(1X10HNORMALIZED,
1      1X12HHEIGHT RANGE 10XF7.0,7H KM. TO F7.0,4H KM./1H0/
2      1X42HCOEFFICIENTS GIVING BEST FIT TO ZONAL DATA/1X/10E11.3)
WRITE(3,207)(BM(I),I=1,NQ)

207 FORMAT(1X/1X/
11X/1X47HCOEFFICIENTS GIVING BEST FIT TO MERIDIONAL DATA/1X/1X10E11
2.3/1X/)
WRITE(3,208)RMSZ, RMSM, RMST

208 FORMAT(1X/1X
1      1X22HRMS TURBULENT VELOCITY/1X/1X10X5HZONALF11.0,11HMETRES/S
2EC./1X/1X10X10HMERIDIONAL F6.0,11HMETRES/SEC./1X/1X10X10HWIND SPEE
3D F6.0,11HMETRES/SEC.)
CALL PAGE (RESULT, START)
WRITE    (3,113)ZMIN, ZMAX

113 FORMAT(1X46HENERGY SPECTRUM OF ZONAL WIND HEIGHT VARIATION,
110X12HHEIGHT RANGE F5.0,6H KM TO F5.0,3H KM/1X)
C CALCULATE AND OUTPUT ENERGY SPECTRUM FUNCTIONS
CALL OUTPUT(TZONAL, NH, NDIFF)
CALL PAGE (RESULT, START)
WRITE    (3,114) ZMIN, ZMAX

114 FORMAT(1X51HENERGY SPECTRUM OF MERIDIONAL WIND HEIGHT VARIATION,
```

SHEAR 08/
EXTERNAL FORMULA NUMBER — SOURCE STATEMENT — INTERNAL
110X12HHEIGHT RANGE F5.0,6H KM TO F5.0, 3H KM/1X)
CALL OUTPUT(TMERID, NH, NDIFF)
CALL PAGE (RESULT, START)
WRITE (3,115)ZMIN,ZMAX
115 FORMAT(1X46HENERGY SPECTRUM OF WIND SPEED HEIGHT VARIATION,
110X12HHEIGHT RANGE F5.0,6H KM TO F5.0,3H KM/1X)
CALL OUTPUT(TSPEED, NH, NDIFF)
GOTO2
END

```

/$ID JO2T      RGR     BLDG 11
$PAUSE
$EXECUTE      IBJOB
IBJOB VERSION 2, 7090 - PP - 929
1

0
$IBJOB        GO
$IBFTC OUT    M94,XR7
1          OUT
          EXTERNAL FORMULA NUMBER — SOURCE STATEMENT — INTERN
0
SUBROUTINE OUTPUT(TSPEED,NH,NDIFF)
C
C PRODUCES HEIGHT SPECTRUM AND PERFORMS CORRELATION ANALYSIS.
C
DIMENSION TSPEED(750)
WRITE(3,1)
1 FORMAT(1X,10X7HDELTA H,5X10HE(DELTA H),
15X11HCORRELATION,3X13HSIGNIF    1-G /1X)
NEND=5 * NDIFF
LINE=0
DO125K=1,NEND
LINE=LINE+1
DELAH=FLOAT(K) * 0.2
SUM=0.0
ENERGY=0.0
ERGX=0.0
GJPKXJ=0.0
SQJ=0.0
SQJPK=0.0
DO123J=1,NH
IF(NH-J-K)124,122,122
122 JPK=J+K
ENERGY=ENERGY+(TSPEED(JPK)-TSPEED(J)) ** 2
SUM=SUM+1.0
GJPKXJ=GJPKXJ+TSPEED(JPK) * TSPEED(J)
SQJ=SQJ+TSPEED(J) ** 2
SQJPK=SQJPK+TSPEED(JPK) ** 2
123 CONTINUE
124 IF(SUM)117,117,118
117 G=0.0
SIGNIF=9.99
GOTO119
118 ENERGY=ENERGY/SUM
G=GJPKXJ/SQRT(SQJ * SQJPK)
SIGNIF=(1.0-G ** 2)/SQRT(SUM-1.0)
119 DIFF=1.0-G
IF(LINE-50)125,125,116
116 WRITE(3,2)
2 FORMAT(1H1/1X)
WRITE(3,1)
LINE=0
125 WRITE(3,115)DELAH,ENERGY,      G,SIGNIF,DIFF
115 FORMAT(1X,6XF8.1, 7XF8.1 ,8XF8.3,F11.3,F8.2)
RETURN
END

```

\$IBJOB GO
\$IBFTC NORMAL M94,XR7

NORMAL
EXTERNAL FORMULA NUMBER — SOURCE STATEMENT — INTE

SUBROUTINE NORMAL (ZONAL,ERID,ZI,NI,BZ,BM,NP,NQ)
C DETERMINES BEST FIT PROFILE TO THE NORMALIZED TOTAL HEIGHT RANG
C
DIMENSION ZONAL(750),ERID(750),ZI(750),BZ(1C),BM(1C),ZINORM(750)
DO1J=1,NI
ZINORM(J) = (2.0 * ZI(J)-ZI(NI)-ZI(1))/(ZI(NI)-ZI(1))
1 CONTINUE
CALL FIT (ZONAL, NP, BZ, NI, ZINORM)
CALL FIT (ERID, NQ, BM, NI, ZINORM)
RETURN
END

\$IBJOB GO
\$IBFTC TRADE M94,XR7

TRADE 08/
EXTERNAL FORMULA NUMBER — SOURCE STATEMENT — INTERNAL

SUBROUTINE TRADE(J,K)
C CALCULATES TURBULENT WINDSPEED PROFILE
C
DIMENSION ZI(750)
DIMENSION WINDI(750),AZRADI(750),ZONAL(750),ERID(750),TZONAL(750),
1TMRID(750),TSPEED(750)
COMMON ZI, WINDI,AZRADI,ZONAL,ERID,TZONAL,TMRID,TSPEED
TSPEED(J) = WINDI(K)-SQRT((ZONAL(K)-TZONAL(J)) * * 2+(ERID(K)-TMRID(J)
1) * * 2)
RETURN
END

\$IBFTC FIT M94,XR7

08/17

FIT
EXTERNAL FORMULA NUMBER -- SOURCE STATEMENT -- INTERNAL FO

SUBROUTINE FIT (BLOW,NSPEC,A,N,X)

C FITS A HEIGHT PROFILE SPECIFIED BY NSPEC TO THE MEASURED DATA
C BLOW, DETERMINING THE COEFFICIENTS A BY THE METHOD OF LEAST
C SQUARES. PROFILE FITTED OVER TOTAL HEIGHT RANGE OF INPUT DATA.
C
C DIMENSION BLOW(750), A(10), X(750), S(10,11)
C DO3J=1,10
3 A(J)=0.0
 IF(NSPEC)100,100,4
4 NADD=NSPEC+1
 DO10J=1,NSPEC
 DO10K=1,NADD
10 S(J,K)=0.0
 DO5J=1,NSPEC
 DO5K=1,NSPEC
 DO5I=1,N
5 S(J,K)=S(J,K)+X(I) ** (K+J-2)
 DU6J=1,NSPEC
 K=0
 DO6I=1,N
 K=K+1
6 S(J,NADD)=S(J,NADD)+X(I) ** (J-1) * BLOW(K)
 CALL MATS(S,A,NSPEC,MISS)
 IF(MISS)100,100,7
7 WRITE(3,8)
8 FORMAT(1X75HERROR IN INPUT DATA HAS RESULTED IN MATRIX S BEING UNS
1UITABLE FOR INVERSION ////1X20HEXECUTION TERMINATED ///////)
 PRINT 8
 CALL EXIT
100 RETURN
 END

MATS 08/17
 EXTERNAL FORMULA NUMBER — SOURCE STATEMENT — INTERNAL FO

SUBROUTINE MATS (S,A,NSPEC,MISS)

C REDUCES THE AUGMENTED MATRIX S TO PRODUCE THE COEFFICIENTS A

C DIMENSION S(10,11), A(10)

MISS = -1

MM = NSPEC + 1

N = NSPEC

DO15I = 2,N

70 II = I - 1

7 DO15J = 1,II

8 IF(S(I,J))9,15,9

9 IF(ABS(S(J,J))-ABS(S(I,J)))11,10,10

10 R = S(I,J)/S(J,J)

GOTO 130

11 R = S(J,J)/S(I,J)

DO12K = 1,MM

B = S(J,K)

S(J,K) = S(I,K)

12 S(I,K) = B

130 JJ = J + 1

13 DO14K = JJ,MM

14 S(I,K) = S(I,K) - R * S(J,K)

15 CONTINUE

IF(ABS(S(N,N))-1.0E-10)16,16,17

16 MISS = +1

GOTO29

17 A(N) = S(N,MM)/S(N,N)

DO28I = 2,N

JJ = N - I + 1

B = 0.0

II = N - I + 2

DO25K = II,N

25 B = B + S(JJ,K) * A(K)

IF(ABS(S(JJ,JJ))-1.0E-10)16,16,28

28 A(JJ) = (S(JJ,MM)-B)/S(JJ,JJ)

29 RETURN

END

PLANETARY ATMOSPHERES

1095

08/17

\$IBFTC MATS M94,XR7

08/17

\$IBFTC PAGE M94,XR7

PAGE 08/17
EXTERNAL FORMULA NUMBER — SOURCE STATEMENT — INTERNAL FO

SUBROUTINE PAGE (RESULT, START)

C
C TURNS PAGE, NUMBERS IT, AND WRITES HEADING AS APPEARING
C ON RESULT CARD.
C
DIMENSION RESULT (12)
IF(START)1,1,2
1 NOP=0
2 NOP=NOP+1
WRITE (3,3) RESULT, NOP
3 FORMAT (1H1/1X12A6,30X4HPAGE15//)
RETURN
END

APPENDIX III
Sample Data And Computer Output

PLANETARY ATMOSPHERES

1097

PRELIMINARY PAPER EGLIN DATA, MAY 21, 1963. 16/9/64.

PROFILE,5,5.

5 5

80 100

63 5 21 1910 69.0 34 255

63 5 21 1910 70.6 31 256

63 5 21 1910 71.0 27 270

63 5 21 1910 72.4 43 272

63 5 21 1910 72.6 20 290

63 5 21 1910 77.0 41 256

63 5 21 1910 80.4 25 358

63 5 21 1910 82.0 08 310

63 5 21 1910 82.4 28 202

63 5 21 1910 83.6 27 200

63 5 21 1910 84.0 54 190

63 5 21 1910 85.0 54 194

63 5 21 1910 85.4 30 108

63 5 21 1910 88.0 60 080

63 5 21 1910 91.6 76 095

63 5 21 1910 95.0 50 178

63 5 21 1910 96.0 40 120

63 5 21 1910 96.6 54 150

63 5 21 1910 97.6 40 115

63 5 21 1910 99.0 42 084

63 5 21 1910 99.6 64 078

63 5 21 1910 100.0 58 070

63 5 21 1910 100.8 65 069

63 5 21 1910 102.0 80 079

63 5 21 1910 103.0 93 094

63	5	21	1910	104.0	115	104
63	5	21	1910	104.2	111	120
63	5	21	1910	105.0	129	122
63	5	21	1910	105.6	140	130
63	5	21	1910	105.8	130	128
63	5	21	1910	107.0	125	132
63	5	21	1910	108.0	92	140
63	5	21	1910	109.0	50	160
63	5	21	1910	110.0	42	240
63	5	21	1910	111.0	56	250
63	5	21	1910	113.0	60	262
63	5	21	1910	114.0	84	274
63	5	21	1910	115.0	68	270
63	5	21	1910	117.2	72	282
63	5	21	1910	125.0	45	286
63	5	21	1910	130.0	30	296
63	5	21	1910	135.0	14	310
63	5	21	1910	140.0	15	316

← BLANK CARD

7
8

PLANETARY ATMOSPHERES

1099

TRIAL ANALYSIS. EGLIN DATA, MAY 21, 1963. 15/9/64.

PROFILE,5 5.

TOTAL NUMBER OF INPUT DATA POINTS 356

INCLUDING INTERPOLATION OF 313 POINTS

NUMBER OF DATA POINTS WITHIN THE HEIGHT RANGE 80. KM TO 100. KM 101

EAST WEST PROFILE SPECIFICATION 5

NORTH SOUTH PROFILE SPECIFICATION 5

TRIAL ANALYSIS. EGLIN DATA, MAY 21, 1963. CONTINUOUS PROFILE,^{5,5}.

CALCULATED ZONAL AND MERIDIONAL MEAN WIND PROFILES HEIGHT RANGE

HEIGHT	ZONAL		MERIDIONAL		WIND SPEED	
	DATA	MEAN	DATA	MEAN	DATA	MEAN
100	70.	34	20.	-21	72.	40
99	56.	37	21.	-21	60.	43
98	42.	39	4.	-22	42.	45
97	39.	41	-11.	-22	41.	47
96	34.	43	-35.	-22	48.	49
95	31.	45	-28.	-22	42.	50
94	6	46	-51.	-22	52.	51
93	31.	46	-51.	-21	59.	51
92	55.	47	-38.	-21	67.	51
91	73.	47	-13.	-21	74.	51
90	72.	46	-1.	-20	72.	50
89	67.	45	4.	-19	67.	49
88	62.	43	8.	-18	63.	47
87	55.	41	5.	-18	55.	45
86	44.	39	-4.	-16	44.	43
85	31.	36	-9.	-15	32.	39
84	-12.	33	-53.	-14	54.	36
83	-9.	29	-25.	-13	27.	32
82	-10.	24	-26.	-11	28.	27
81	-8.	19	10.	-10.	12.	22
80	-3.	14	23.	-8	23.	16

TRIAL ANALYSIS. EGLIN DATA, MAY 21, 1963. CONTINUOUS PROFILE, 5,5.

TURBULENT WIND PROFILE HEIGHT RANGE 80. KM TO 100. KM

HEIGHT	TZONAL	TMERIDIONAL	TSPEED
100	35.	41.	42.
99	19.	42.	26.
98	2.	26.	16.
97	-3.	11.	31.
96	-10.	-12.	32.
95	-14.	-6.	29.
94	-40.	-29.	8.
93	-16.	-29.	31.
92	8.	-16.	58.
91	26.	8.	62.
90	25.	19.	52.
89	22.	24.	45.
88	18.	27.	38.
87	13.	24.	33.
86	4.	13.	30.
85	-6.	7.	27.
84	-45.	-38.	18.
83	-39.	-12.	-5.
82	-35.	-14.	0.
81	-28.	20.	3.
80	-18.	31.	10.

TRIAL ANALYSIS. EGLIN DATA, MAY 21, 1963. 15/9/64.

PROFILE,5,5.

NORMALIZED HEIGHT RANGE

80. KM. TO 100. KM.

COEFFICIENTS GIVING BEST FIT TO ZONAL DATA

0.386E 02 -0.126E 03 -0.244E 03 0.174E 03 0.205E 03

COEFFICIENTS GIVING BEST FIT TO MERIDIONAL DATA

-0.304E 02 0.198E 02 0.148E 03 -0.168E 02 -0.125E 03

RMS TURBULENT VELOCITY

ZONAL 22.METRES/SEC.

MERIDIONAL 23.METRES/SEC.

WIND SPEED 17.METRES/SEC.

TRIAL ANALYSIS. EGLIN DATA, MAY 21, 1963. CONTINUOUS PROFILE,5,5.

ENERGY SPECTRUM OF ZONAL WIND HEIGHT VARIATION			HEIGHT RANGE 80.	
DELTA H	DELTA V * * 2	CORRELATION	SICNIF	I-G
0.2	24.3	0.979	0.004	0.02
0.4	64.9	0.943	0.011	0.06
0.6	113.7	0.900	0.019	0.10
0.8	169.4	0.851	0.028	0.15
1.0	230.7	0.797	p 037	0.20
1.2	297.1	0.739	0.047	0.26
1.4	369.4	0.676	0.056	0.32
1.6	450.4	0.604	0.066	0.40
1.8	534.8	0.525	0.076	0.47
2.0	619.9	0.449	0.084	0.55
2.2	703.2	0.374	0.091	0.63
2.4	789.0	0.297	0.097	0.70
2.6	877.1	0.217	0.102	0.78
2.8	964.9	0.136	0.106	0.86
3.0	1054.0	0.053	0.108	0.95
3.2	1133.4	-0.023	0.109	1.02
3.4	1209.9	-0.099	0.109	1.10
3.6	1285.2	-0.176	0.107	1.18
3.8	1360.8	-0.257	0.104	1.26
4.0	1436.0	-0.342	0.099	1.34
4.2	1507.0	-0.429	0.092	1.43
4.4	1567.1	-0.514	0.083	1.51
4.6	1614.3	-0.597	0.073	1.60
4.8	1681.4	-0.651	0.066	1.65
5.0	1745.7	-0.696	0.060	1.70
5.2	1804.0	-0.735	0.053	1.74
5.4	1852.3	-0.766	0.048	1.77
5.6	1885.5	-0.788	0.045	1.79
5.8	1897.3	-0.800	0.043	1.80
6.0	1880.3	-0.801	0.043	1.80
6.2	1863.6	-0.795	0.044	1.80
6.4	1847.4	-0.783	0.047	1.78
6.6	1827.7	-0.762	0.051	1.76
6.8	1803.8	-0.730	0.057	1.73
7.0	1775.0	-0.690	0.065	1.69
7.2	1740.9	-0.642	0.073	1.64
7.4	1701.2	-0.588	0.082	1.59
7.6	1656.5	-0.528	0.092	1.53
7.8	1608.4	-0.466	0.100	1.47
8.0	1555.6	-0.401	0.108	1.40
8.2	1497.1	-0.333	0.116	1.33
8.4	1432.6	-0.263	0.122	1.26
8.6	1361.9	-0.190	0.128	1.19
8.8	1285.1	-0.116	1.132	1.12
9.0	1202.6	-0.040	0.135	1.04
9.2	1114.7	0.038	0.136	0.96
9.4	1020.5	0.120	0.135	0.88
9.6	920.9	0.207	0.133	0.79
9.8	819.6	0.296	0.128	0.70
10.0	733.6	0.372	0.122	0.63

TRIAL ANALYSIS. EGLIN DATA, MAY 21, 1963. CONTINUOUS PROFILE,^{5,5.}

ENERGY SPECTRUM OF MERIDIONAL WIND HEIGHT VARIATION HEIGHT RANGE

DELTA H	DELTA V * * 2	CORRELATION	SIGNIF	I-G
0.2	31.3	0.973	0.005	0.03
0.4	94.1	0.917	0.916	0.08
0.6	164.4	0.853	0.028	0.15
0.8	241.7	0.781	0.040	0.22
1.0	326.3	0.701	0.052	0.30
1.2	418.3	0.612	0.064	0.39
1.4	515.2	0.518	0.076	0.48
1.6	616.0	0.420	0.086	0.58
1.8	723.6	0.316	0.094	0.68
2.0	825.3	0.219	0.100	0.78
2.2	935.1	0.116	0.105	0.88
2.4	1052.2	0.008	0.107	0.99
2.6	1175.9	-0.104	0.106	1.10
2.8	1305.7	-0.219	0.103	1.22
3.0	1429.3	-0.325	0.097	1.33
3.2	1534.6	-0.411	0.091	1.41
3.4	1614.7	-0.479	0.085	1.48
3.6	1667.7	-0.535	0.079	1.54
3.8	1711.0	-0.582	0.074	1.58
4.0	1741.1	-0.617	0.069	1.62
4.2	1756.8	-0.641	0.066	1.64
4.4	1758.3	-0.656	0.065	1.66
4.6	1745.6	-0.662	0.064	1.66
4.8	1776.6	-0.680	0.062	1.68
5.0	1836.6	-0.715	0.056	1.72
5.2	1878.5	-0.733	0.054	1.73
5.4	1900.7	-0.735	0.054	1.74
5.6	1902.8	-0.723	0.056	1.72
5.8	1885.6	-0.699	0.061	1.70
6.0	1853.4	-0.666	0.066	1.67
6.2	1809.8	-0.625	0.073	1.63
6.4	1751.9	-0.573	0.081	1.57
6.6	1679.1	-0.510	0.090	1.51
6.8	1592.6	-0.435	0.100	1.44
7.0	1494.3	-0.350	0.109	1.35
7.2	1385.9	-0.257	0.117	1.26
7.4	1269.8	-0.156	0.123	1.16
7.6	1149.0	-0.051	0.127	1.05
7.8	1028.4	0.057	0.128	0.94
8.0	912.5	0.164	0.126	0.84
8.2	802.4	0.266	0.121	0.73
8.4	697.1	0.366	0.114	0.63
8.6	598.6	0.459	0.105	0.54
8.8	508.4	0.544	0.094	0.46
9.0	427.7	0.620	0.083	0.38
9.2	357.9	0.684	0.072	0.32
9.4	302.8	0.735	0.063	0.27
9.6	260.1	0.774	0.056	0.23
9.8	231.1	0.801	0.050	0.20
10.0	219.4	0.812	0.048	0.19

TRIAL ANALYSIS. EGLIN DATA, MAY 21, 1963. CONTINUOUS PROFILE, 5,5.

DELTA H	DELTA V * * 2	CORRELATION	SIGNIF	HEIGHT RANGE 80.
0.2	15.1	0.993	0.001	0.01
0.4	47.1	0.979	0.004	0.02
0.6	83.2	0.964	0.007	0.04
0.8	122.0	0.947	0.011	0.05
1.0	161.5	0.930	0.014	0.07
1.2	200.6	0.914	0.017	0.09
1.4	240.7	0.898	0.020	0.10
1.6	286.9	0.879	0.024	0.12
1.8	337.0	0.859	0.028	0.14
2.0	382.2	0.841	0.031	0.16
2.2	421.0	0.827	0.034	0.17
2.4	455.3	0.815	0.036	0.19
2.6	483.4	0.805	0.038	0.20
2.8	502.9	0.799	0.039	0.20
3.0	512.5	0.797	0.040	0.20
3.2	517.8	0.796	0.040	0.20
3.4	528.9	0.793	0.041	0.21
3.6	542.8	0.789	0.042	0.21
3.8	561.7	0.783	0.043	0.22
4.0	584.0	0.775	0.045	0.22
4.2	606.6	0.768	0.046	0.23
4.4	628.3	0.761	0.048	0.24
4.6	650.9	0.755	0.049	0.25
4.8	679.5	0.746	0.051	0.25
5.0	712.5	0.734	0.053	0.27
5.2	748.8	0.722	0.056	0.28
5.4	785.1	0.710	0.058	0.29
5.6	818.7	0.700	0.060	0.30
5.8	847.5	0.692	0.062	0.31
6.0	870.6	0.686	0.063	0.31
6.2	894.8	0.680	0.065	0.32
6.4	919.4	0.674	0.066	0.33
6.6	943.4	0.668	0.068	0.33
6.8	968.1	0.661	0.069	0.34
7.0	996.2	0.653	0.071	0.35
7.2	1023.8	0.645	0.073	0.35
7.4	1048.3	0.638	0.075	0.36
7.6	1070.2	0.630	0.077	0.37
7.8	1088.9	0.623	0.078	0.38
8.0	1103.4	0.616	0.080	0.38
8.2	1114.0	0.608	0.082	0.39
8.4	1121.1	0.600	0.084	0.40
8.6	1120.2	0.593	0.086	0.41
8.8	1114.6	0.588	0.087	0.41
9.0	1103.8	0.585	0.089	0.42
9.2	1087.7	0.584	0.090	0.42
9.4	1066.1	0.586	0.090	0.41
9.6	1039.0	0.590	0.090	0.41
9.8	1007.8	0.596	0.090	0.40
10.0	973.4	0.603	0.090	0.40

N64-31451

TEMPERATURE, PRESSURE, DENSITY, AND WIND MEASUREMENTS WITH THE ROCKET GRENADE EXPERIMENT, 1960-1963*

W. SMITH, L. KATCHEN, P. SACHER, P. SWARTZ, AND J. THEON

Complete data from 28 rocket grenade experiments at Wallops Island, Virginia, and Fort Churchill, Canada, are presented. Pressures, temperatures, densities, and winds have been derived directly from the recorded times of explosions and sound arrivals; but no attempt has been made to analyze the meteorological significance of these measurements. Error analyses on 16 of the Wallops experiments are also included.

INTRODUCTION

During the period 1960-1963 a total of 28 rocket grenade experiments were carried out by Goddard Space Flight Center at Wallops Island, Virginia, and Fort Churchill, Canada. It is the purpose of this report to present the complete data from these experiments. The data have been reduced but not analyzed, i.e., the physical measurements (pressure, density, temperature and winds) have been derived directly from recordings of the times of grenade explosions and sound arrivals, and from the rocket trajectories; but no attempt has been made to analyze the measurements for their meteorological significance. Rather, this report should be considered as a record of the unsmoothed, raw measurements which may serve as the basis of further investigation and interpretation of the structure of the atmosphere. This is the first such report since the program started in 1960. As the program continues, future results will be documented in similar fashion.

The grenade experiment is one of the several techniques employed in NASA's Meteorological Rocket Sounding Program, the objective of which is to obtain as representative as possible a sample of the synoptic structure of the mesosphere and lower ionosphere. In order to extend the findings over the widest possible geographic area, and perhaps eventually to attain a global network

of soundings, the NASA launchings are coordinated whenever possible with soundings in other parts of the world. The instrumental details and methods of data reduction have been thoroughly described elsewhere.[†]

EXPERIMENTAL METHOD

One and two pound explosive charges (grenades) are carried aloft in the nosecone of a Nike-Cajun sounding rocket. The grenades are ejected and exploded at 4-6 km intervals. Either a precise radar such as the FPS-16 or a doppler tracking system, or both, are used to determine the rocket position and hence the exact position of the explosion. The time of the explosion is detected by small rocket borne infrared photocells and telemetered to the ground. A ground based array of hot wire microphones with frequency response peaked at 4 cycles per second is used to detect and record the sound waves from each exploding grenade. The measured experimental parameters are the times of the grenade explosions, the positions of the grenade explosions, and the times of arrival of the sound waves at the ground based microphones.

Elevation and azimuth angles are computed for each arriving sound wave front by applying a least-squares fit to the arrival times at the various microphones. Each wave is then analytically traced up through the atmosphere by means of Snell's law. Data from radiosonde ascents or

*Published as NASA Technical Report R-211, October 1964.

[†]Nordberg, W., and Smith W., "The Rocket Grenade Experiment," NASA Technical Note D-2107, March 1964.

from small meteorological rockets obtained at the time of the grenade soundings are used for this tracing up to the first explosion; above this, the results of the experiment itself are used for each successive explosion. This *apparent* position of the *wave* is then compared with the *known* position of the *wave source*, the grenade explosion. The amount by which the sound wave has been displaced horizontally from one explosion to the next is a measure of the average wind velocity vector in the layer between any two adjacent explosions. The average speed of the sound, and hence average temperature between two adjacent explosions, may also be determined. This analysis yields an altitude profile of temperatures and winds as a direct measurement. The temperature profile consists of discrete points, each representing an average value for an altitude layer between grenade explosions. It may be used to derive density and pressure profiles, if the pressure or density is

known at a given level at the bottom of the temperature profile; and the latter data are available from the accompanying radiosonde. Pressure is calculated by use of the hydrostatic equation, and the ideal gas law; an integration is performed over the temperature profile starting at the known pressure. The density at any level is then computed from the pressure, temperature, and universal gas constant.

During the period between July 8, 1960 and December 7, 1963, 23 successful rocket grenade soundings were conducted from Wallops Island, Virginia ($37^{\circ} 50'N$, $75^{\circ} 29'W$). In addition to offering excellent launch and tracking support, the geographical location of Wallops Island makes it a good middle-latitude observation site. Five soundings were conducted from a sub-arctic range, Fort Churchill, Canada, ($58^{\circ} 47'N$, $94^{\circ} 17'W$) in the period between December 1962 and March 1963. Originally, it was planned to distribute

Table 1

Dates, Times, and Locations of GSFC Grenade Experiments 1960-1963

Date	Local Time	Location
8 July 1960	2259	Wallops Island
14 February 1961	1850	Wallops Island
16 February 1961	2126	Wallops Island
5 April 1961	0757	Wallops Island
5 May 1961	1800	Wallops Island
5 May 1961	2354	Wallops Island
13 July 1961	1707	Wallops Island
14 July 1961	1102	Wallops Island
20 July 1961	0530	Wallops Island
16 September 1961	1855	Wallops Island
1 March 1962	1901	Wallops Island
2 March 1962	0615	Wallops Island
23 March 1962	1854	Wallops Island
27 March 1962	1904	Wallops Island
17 April 1962	0428	Wallops Island
6 June 1962	2005	Wallops Island
7 June 1962	2053	Wallops Island
1 December 1962	1625	Wallops Island
4 December 1962	0105	Fort Churchill
6 December 1962	0032	Wallops Island
5 December 1962	2343	Fort Churchill
20 February 1963	1734	Fort Churchill
20 February 1963	1847	Wallops Island
28 February 1963	1547	Fort Churchill
28 February 1963	1711	Wallops Island
8 March 1963	1901	Wallops Island
8 March 1963	1801	Fort Churchill
7 December 1963	0812	Wallops Island

the number of firings about equally between the two sites, but a fire early in 1961 destroyed part of the Fort Churchill launch facility, and it was not operational again until November 1962. Table 1 lists the soundings conducted. Four of the recent firings from each site were conducted nearly simultaneously.

The results of the 28 soundings are presented in Figures 1 through 43. In Figures 1 through 28, the *directly measured* parameters of temperatures and winds are tabulated (actual computer printouts) in the columns on the left side of the page

immediately above the graph. Tables of pressure and density *derived* from the temperature profiles are also shown. The temperatures were linearly interpolated between each of the measured points.

Winds and temperatures below 30 km obtained from radiosondes, and below 50 km from smaller meteorological sounding rockets (Arcas* and Hasp† whenever available) launched nearly

*"Data Report of the Meteorological Rocket Network, Spring 1961 Firings," U.S. Army Signal Missile Agency, White Sands Missile Range, New Mexico, September 1961.

†Private Communication from M. J. Parker, Naval Ordnance Laboratory, White Oak, Maryland.

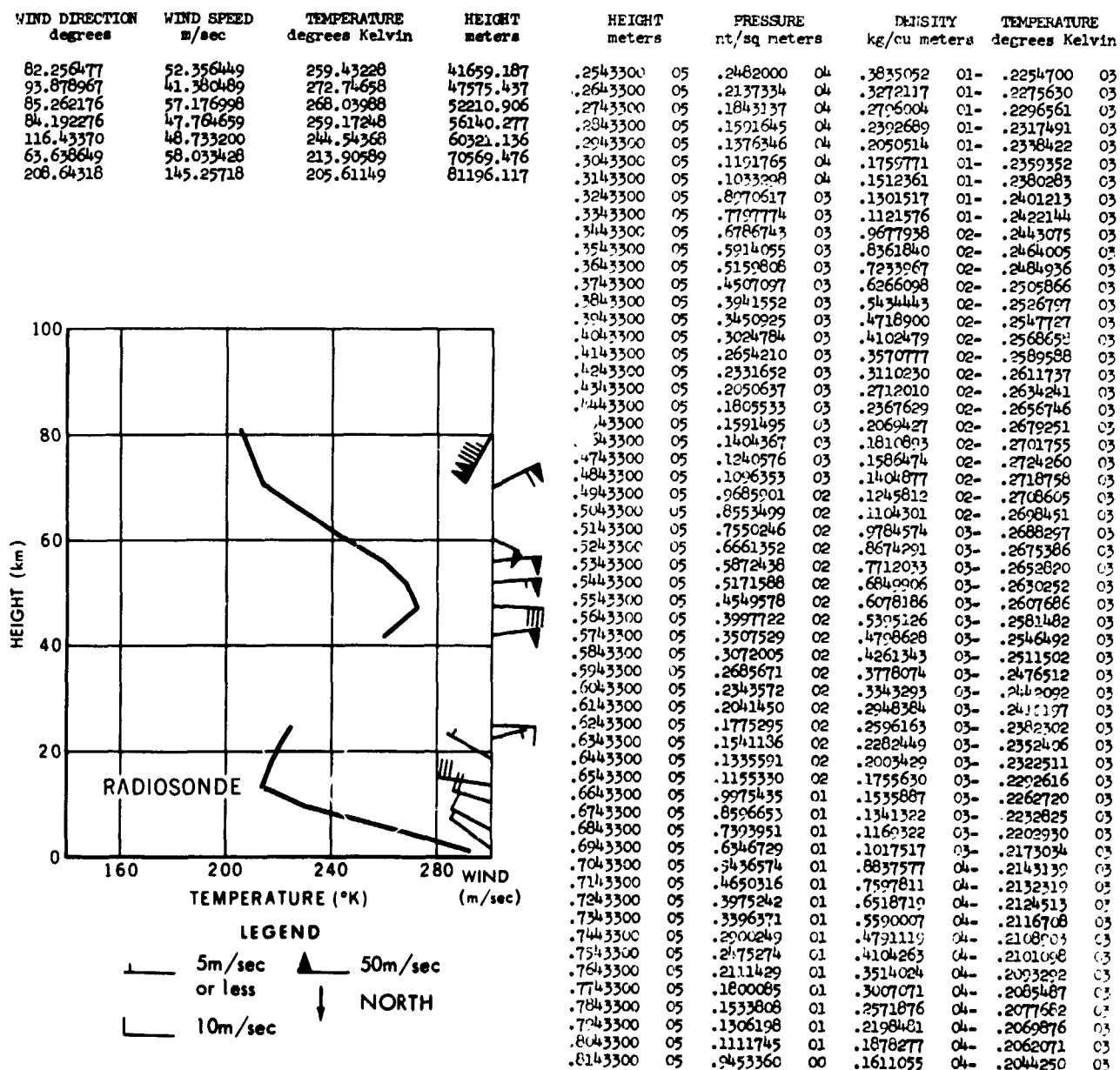


FIGURE 1

simultaneously with the grenade soundings are shown graphically. Winds and temperatures above 40 km from the grenade soundings are shown on the graph.

RESULTS

In the results from these soundings all data points, regardless of our degree of confidence, are presented in tabular form. Some individual data points may be subject to later revision, as there may be occasional errors in some of the records which have not yet been detected. In the preparation of these graphs some data points, where such errors seem obvious, were omitted and the graphs note the omissions. For the most part,

these occur at the upper altitude limit of the experiment where the signal-to-noise ratio of detected acoustic waves is poor. Random errors contained in either the measurements or in the data reductions can usually be recognized by comparing two adjacent data points. Since these errors will generally be contained in the parameters (time and space coordinates of the explosion) associated with one individual grenade explosion, the temperature data points both below and above this explosion will contain errors of approximately equal magnitude but opposite sign. Therefore, if large excursions of this nature occur between two adjacent data points, it is very likely that the recordings from the explosion between these two data points were in error.

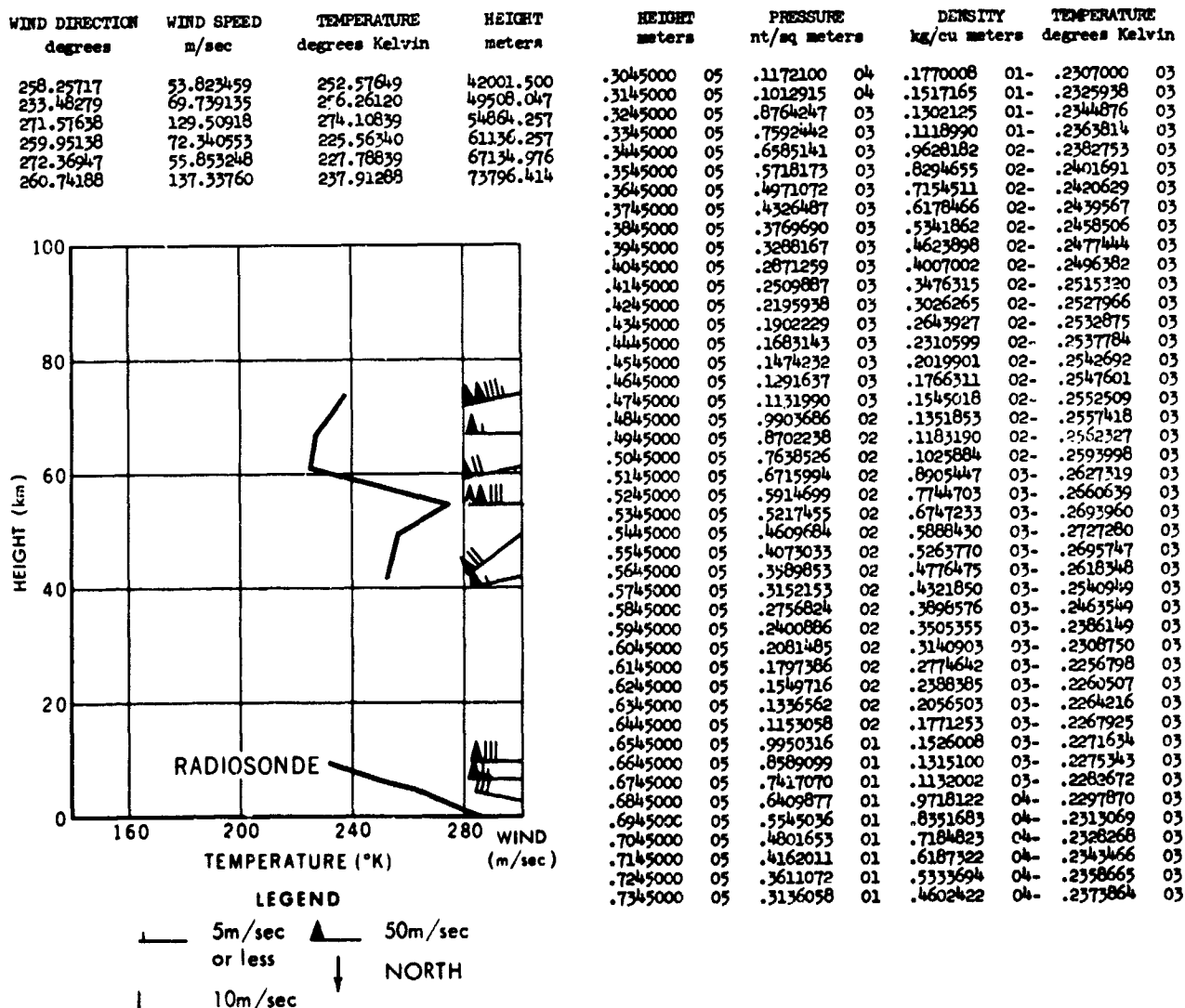


FIGURE 2

ERROR ANALYSIS

An error analysis was run with the aid of a digital computer on 16 of the 28 experiments reported. The firings considered were the first 16 conducted from Wallops Island. The following nomenclature is used in the error analysis:

Δw = Difference in west coordinate between successive grenade explosions.

Δn = Difference in north coordinate between successive grenade explosions.

h = Difference in altitude between successive grenade explosions.

w = Wind direction in the layer.

W = Wind speed in the layer.

c = Speed of sound in the layer = $k(T)^{1/2}$, where k is a proportionality constant depending on molecular mass, the ratio of specific heats, and the universal gas constant.

ϕ_u = Azimuth angle of sound wave for upper explosion.

r = Travel time of sound wave in layer.

$K = c_0 \sec \theta_u + W_0 \cos(\phi_u - \omega_0) - W \cos(\phi_u - \omega)$, where c_0 is the mean speed of sound over

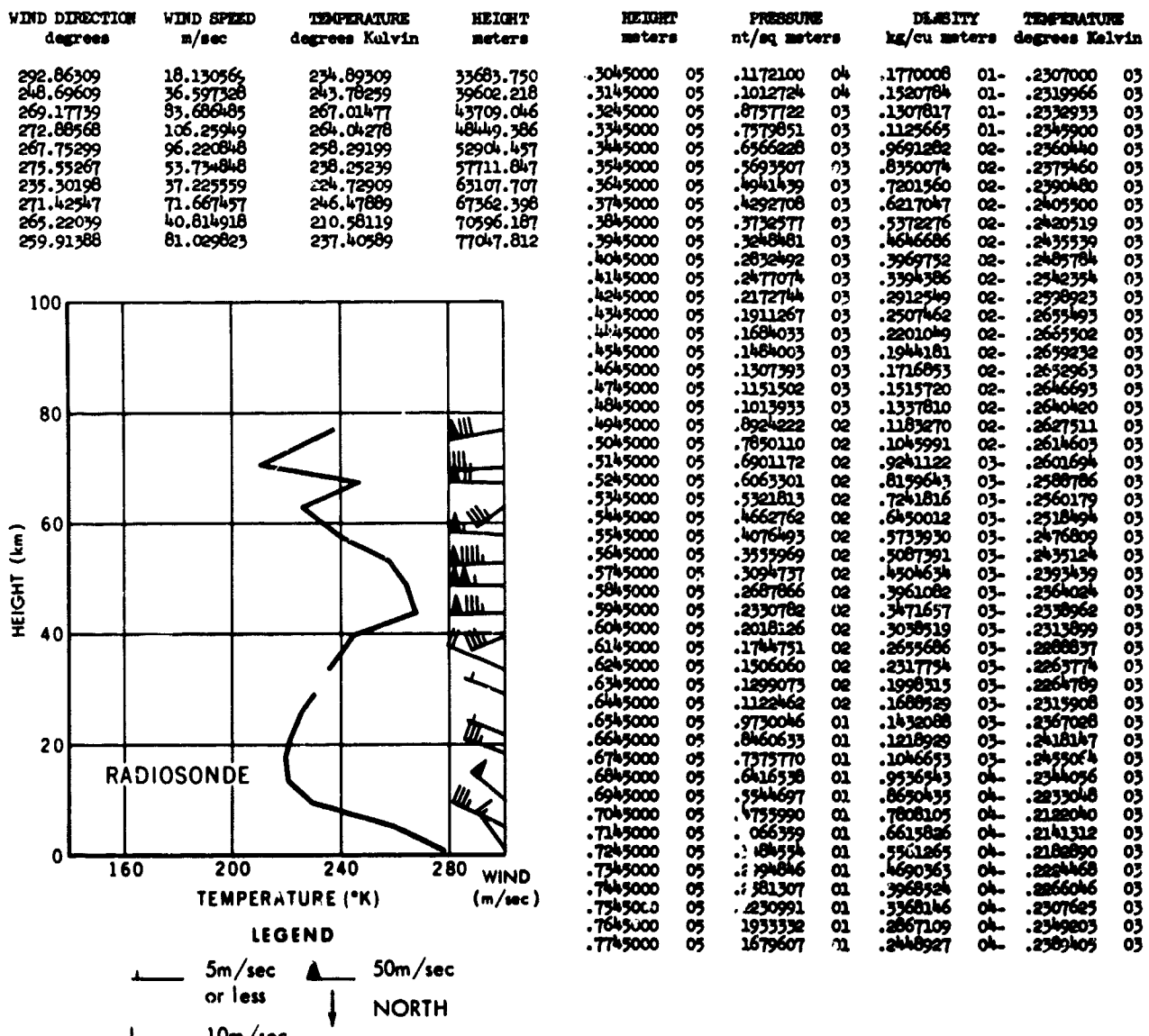


FIGURE 3

the microphone array; θ_0 is the elevation angle of sound wave for upper explosion; W_0 is the wind speed over the microphone array; and ω_0 is the wind direction over the microphone array.

t = Travel time of sound wave from grenade explosion to ground.

T = Mean temperature in layer.

Δt = Time difference between microphones introduced by changing the time of arrival at one microphone.

ϕ'_u = Elevation angle from ground to apparent position of upper grenade explosion as obtained by ray tracing.

In order to determine the error function, deliberate errors were introduced in the following experimental parameters:

A. Position of grenade explosions

1. North: 200 meters
2. West: 200 meters
3. Up: 50 meters

B. Travel time of sound from explosions to ground: 0.3 second.

C. Time of arrival at one of the 6 microphones relative to the other five microphones: 0.02 second.

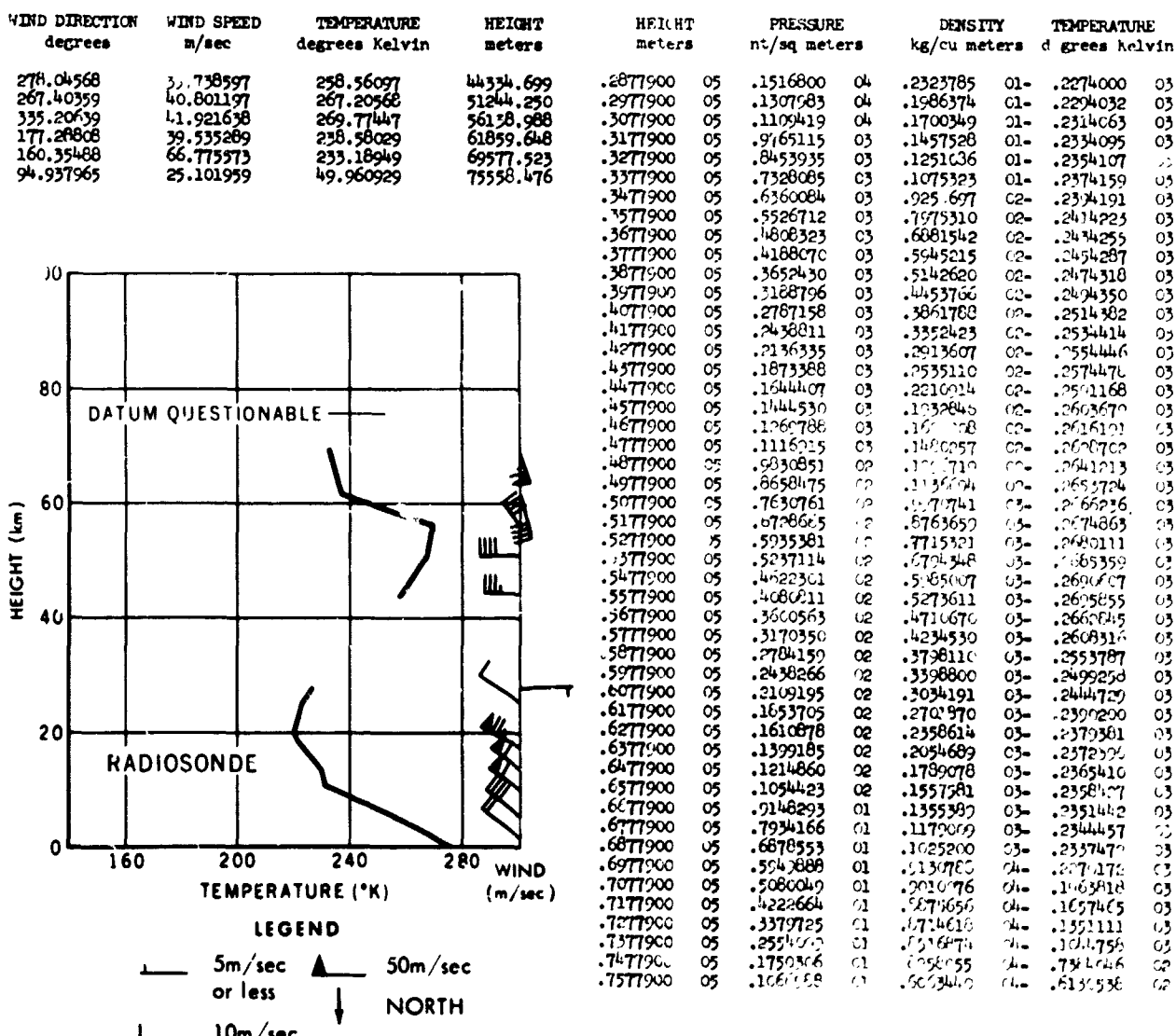


FIGURE 4

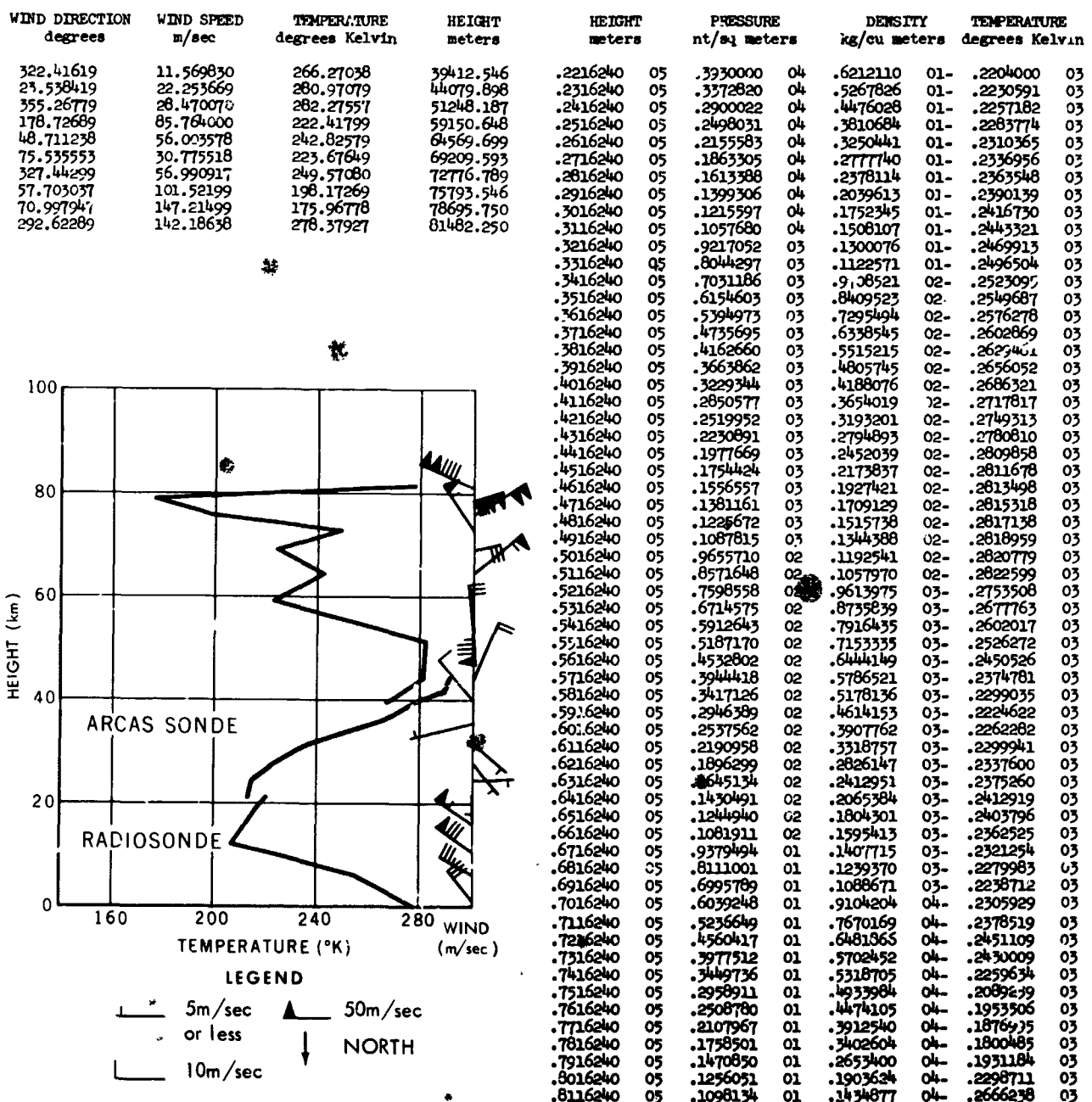


FIGURE 5

It was determined that an error in one of the foregoing parameters for any given grenade will cause wind and temperature errors in the two layers adjacent to the grenade. The temperature errors, in general, will be of opposite sign and approximately equal in magnitude. There are slight errors introduced in the remaining layers above the grenade; however, these are negligibly small. The errors in the temperatures and winds due to errors in the coordinates of the explosions are given by:

$$\frac{\partial W}{\partial \Delta w} = \frac{\sin \omega}{\tau}; \quad (1)$$

$$\frac{\partial W}{\partial \Delta n} = \frac{\cos \omega}{\tau}; \quad (2)$$

$$\frac{\partial W}{\partial h} = \frac{\cot \theta'_u}{\tau} \cos(\omega - \phi_u); \quad (3)$$

$$\frac{\partial c}{\partial \Delta w} = \frac{\sin \phi_u}{c \tau} \left[\frac{h^2 K}{\tau^2 (K^2 - 2c^2)} - \frac{c^2}{K} \right]; \quad (4)$$

$$\frac{\partial c}{\partial \Delta n} = \frac{\cos \phi_u}{c \tau} \left[\frac{h^2 K}{\tau^2 (K^2 - 2c^2)} - \frac{c^2}{K} \right]; \quad (5)$$

$$\frac{\partial c}{\partial h} = \frac{1}{c \tau} \left[\frac{h^2 K \cot \theta'_u - h K^2 \tau}{\tau^2 (K^2 - 2c^2)} + \frac{c^2 \cot \theta'_u}{K} \right]. \quad (6)$$

In the error analysis, the north and west coordinates of alternate grenades were changed by -200m, and the up coordinates were changed by -50m. This means that Δw and Δn for adjacent layers were alternatingly +200 and -200, and dh for adjacent layers were alternatingly +50 and -50. The azimuth angle changes slowly with altitude. Generally, $\sin \phi_u$ and $\cos \phi_u$ do not change sign during an experiment; thus the signs of $(\partial c / \partial \Delta w) \Delta w$ and $(\partial c / \partial \Delta n) \Delta n$ alternate regularly from layer to layer as the coordinates of alternate grenade explosions are changed. This accounts for the regular alternation of the temperature error, since all other signs in the equation for $\partial c / \partial \Delta w$, $\partial c / \partial \Delta n$ remain constant during an experiment. Similarly, it can be seen from the expression for $\partial c / \partial h$ that all the quantities retain

the same sign throughout an experiment. Thus, the same regular alternation for the signs of the $(\partial c / \partial h) dh$ will occur for successive grenades.

The situation is different, however, for $\partial W / \partial \Delta w$, $\partial W / \partial \Delta n$, $\partial W / \partial h$. The sign of $\partial W / \partial \Delta w$ depends on the sign of $\sin \omega$ which in turn depends on the value of ω . Since ω may vary from 0 to 360°, $\sin \omega$ may be either positive or negative. The same is true for the sign of $\partial W / \partial \Delta n$, which depends on $\cos \omega$. Hence, we expect no regular alternation from layer to layer in the sign of the wind error. The sign of $\partial W / \partial h$ depends on the sign of $\cos(\omega - \phi_u)$ which in turn depends on the value of $\omega - \phi_u$. Although ϕ_u changes slowly and in general remains in the same quadrant, ω can vary from 0 to 360°, and hence $\omega - \phi_u$ can be positive or negative. Thus, $(\partial W / \partial h) dh$ exhibits no regular alternation in sign. In summary, we can see that the signs of $\partial c / \partial \Delta w$, $\partial c / \partial \Delta n$, $\partial c / \partial h$ are constant and hence an error in the coordinates of one individual grenade explosion will cause a positive error in the measured temperatures in the layer below the explosion if a negative error is caused in the layer above the explosion, and vice versa. In general, the magnitudes of the temperature errors caused by an error of the explosion coordinates between two adjacent layers are approximately equal.

However, this does not hold for wind errors. The error functions for the wind speed are proportional to $\sin \omega$, $\cos \omega$ and $\cos(\omega - \phi_u)$, which may vary considerably from layer to layer. The error functions of c , however, are proportional to ϕ_u and θ'_u which do not vary greatly from layer to layer.

The two other parameters of importance to the errors in addition to the grenade explosion coordinates were investigated in a similar manner. These parameters were: the time differences, Δt , between arrival of the sound wave at any two microphones within the array of six; and the travel time, t , of the sound from the explosion to the ground. The parameter Δt is important because the direction of the arriving sound wave front is derived from those differences, while t enters primarily in the calculation of the speed of sound in the layer. An error of .02 second was introduced into the arrival time at one microphone without altering the arrival times at the remaining five microphones, while an error of

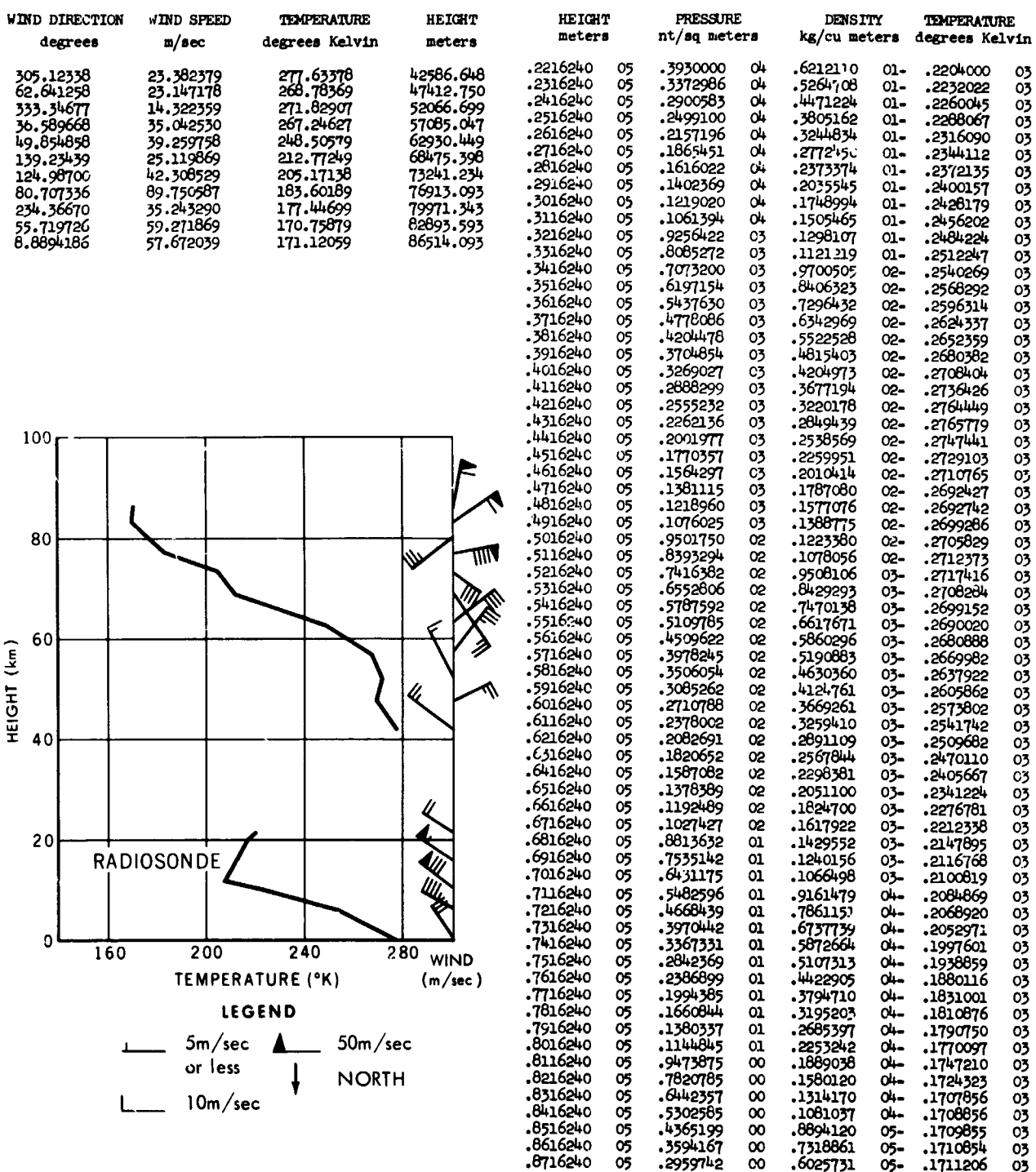


FIGURE 6

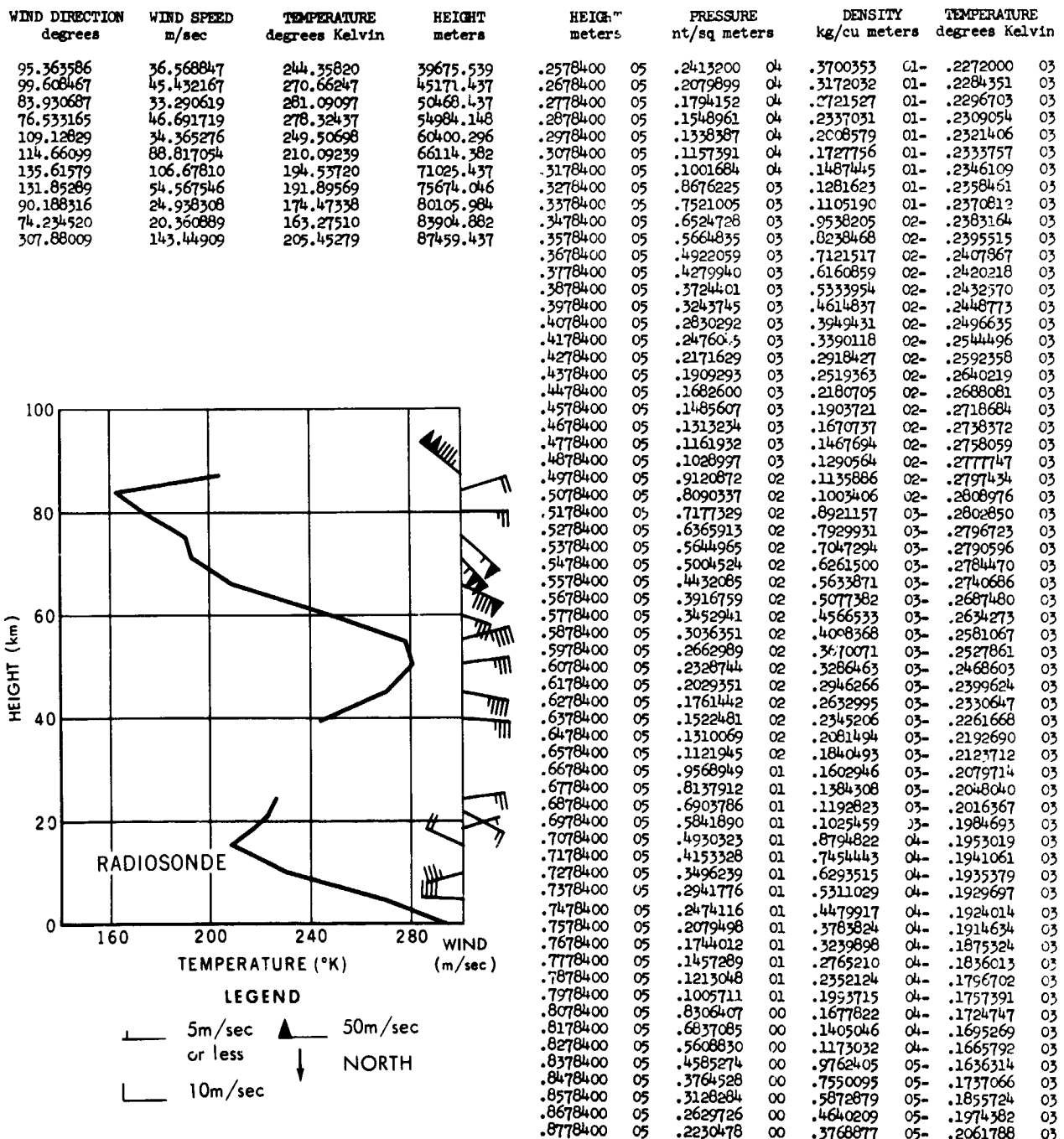


FIGURE 7

.3 second was introduced into t . As in the case of the coordinates of the grenade explosions, these errors were introduced only for alternate grenades.

A typical result of the error analysis is presented in Figures 29 through 38. From a study of these figures, the following conclusions can be reached:

1. Relative errors in the North and West coordinates of 200 meters will significantly affect only winds by about 10 m/sec but not the temperatures.
2. Relative errors in the up coordinates of 50 meters will cause significant errors of about 5°K in temperature, but not in winds.

3. An error of .3 second in t will give rise to large temperature errors—about 10°K—but in general only very small wind errors.

4. An error of .02 in the relative arrival times between microphones will cause the largest errors in both winds and temperatures: 10–40 m/sec and 10–25°K. The error analysis clearly shows that an error introduced into the input parameters of a grenade significantly affects only the layers adjacent to the particular grenade. No significant error is introduced into the calculated winds and temperature for suc-

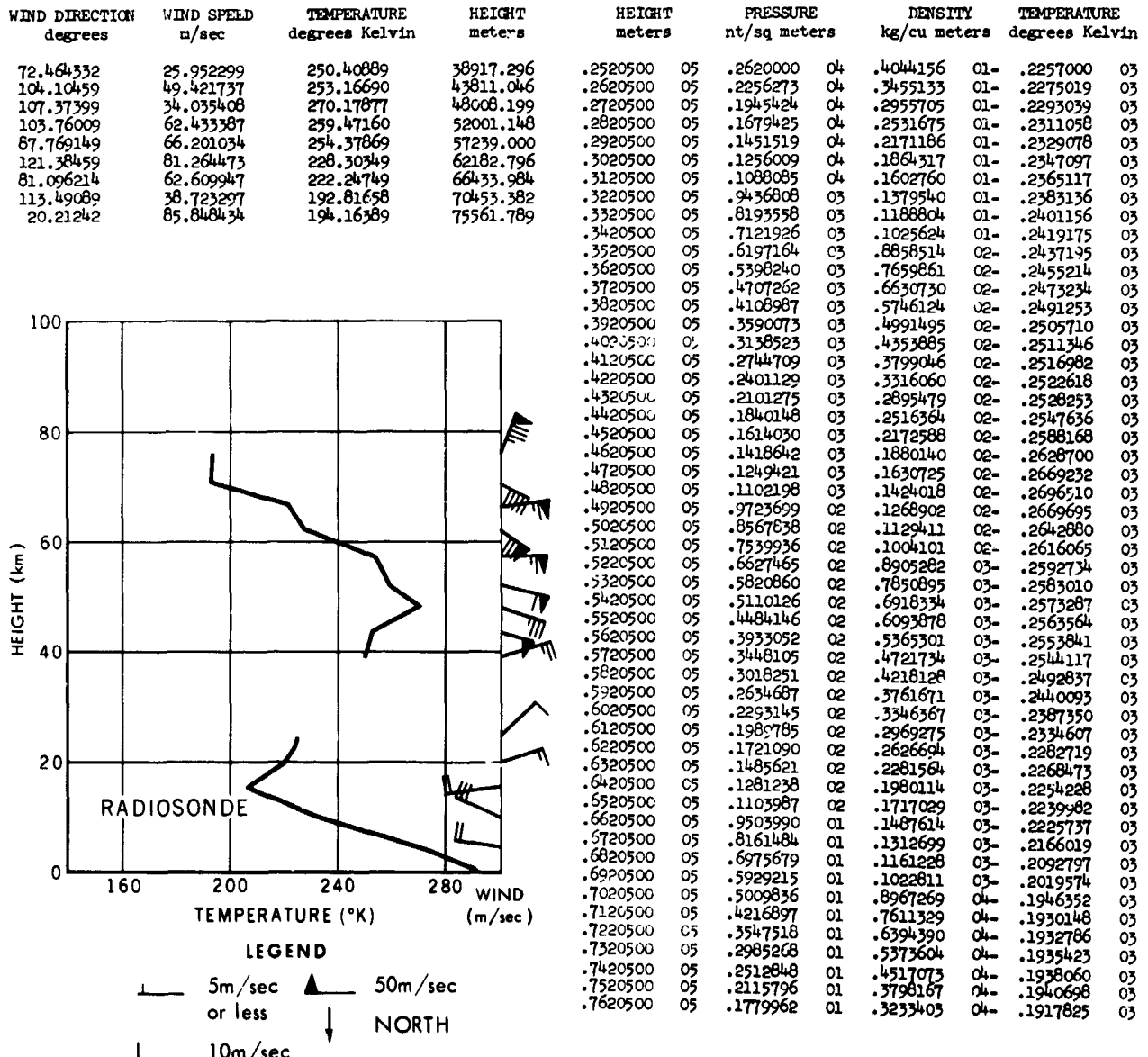


FIGURE 8

ceeding grenades, and hence only the layers adjacent to the grenade in question need be considered.

Table 2 gives the average error functions for the 16 firings tabulated by layers. Figures 39 and 40 are graphs of the two functions which are most strongly altitude dependent, $\partial T/\partial \Delta t$ and $\partial W/\partial \Delta t$, showing quite clearly the increase of the error function with altitude.

$\partial W/\partial \Delta h$, etc., by the value of the actual errors in Δw , Δn , h , Δt , and t . The maximum error is calculated by summing all the partial errors:

$$\left(\frac{\partial W}{\partial \Delta w} d\Delta w + \frac{\partial W}{\partial \Delta n} d\Delta n + \frac{\partial W}{\partial \Delta h} d\Delta h + \dots \text{etc.} \right)$$

The actual errors in coordinates and times are estimated in the following manner:

The position of the grenade explosion is determined by two totally independent tracking meth-

Table 2
Absolute Average Error Functions

Layer	t + .3 sec		North-200m		West-200m		Up-50m		$\Delta t + .02$ sec	
	Temp. (°K)	Wind (m/sec)	Temp. (°K)	Wind (m/sec)	Temp. (°K)	Wind (m/sec)	Temp. (°K)	Wind (m/sec)	Temp. (°K)	Wind (m/sec)
1	10.1	.5	.9	3.9	.7	9.2	5.4	.8	11.7	12.2
2	10.2	.7	.9	5.3	.7	10.6	5.6	.6	15.2	18.5
3	13.0	1.0	.9	5.2	.8	11.9	6.7	.8	16.3	22.0
4	10.5	1.1	.6	4.6	.6	10.7	5.8	.6	17.8	22.3
5	8.4	.9	.4	2.5	.4	9.5	4.6	.5	12.0	16.9
6	7.7	1.0	.4	3.7	.5	8.7	4.5	.7	15.1	26.4
7	10.0	1.3	.4	6.0	.5	10.6	5.6	.8	16.3	25.3
8	9.2	1.2	.4	6.3	.7	10.3	5.6	.7	20.9	31.9
9	11.7	2.3	.5	5.8	.8	12.1	6.4	.8	21.4	30.5
10	8.3	2.4	.5	8.2	.8	9.3	5.4	.7	22.5	41.1
11	11.5	5.2	.4 ^a	9.8	.7	11.4	6.4	.5	22.4	35.2

Figure 41 shows the dependence of $\partial T/\partial \Delta t$ upon zenith angle. As the zenith angle increases, the error function increases nearly linearly. Thus, to make the experiments as accurate as possible, it is desirable that the sound propagation be as nearly vertical as possible. A zenith angle of 0° would, of course, be ideal; however, range safety considerations make this impossible, and at Wallops Island the zenith angles usually lie in the range from 15° — 30° . The zenith angles at Fort Churchill are generally less than 10° , and the probable error in the Fort Churchill data is therefore correspondingly less.

The magnitudes of the errors assumed in this analysis were chosen arbitrarily large for convenience in calculation. The actual resulting errors will be much smaller, as will be shown below. The magnitude of the actual errors in the rocket grenade experiment is determined by multiplying the error functions $\partial W/\partial \Delta w$, $\partial W/\partial \Delta n$,

ods, DOVAP and radar. The agreement of these two systems with regard to the coordinates Δn , Δw and h in general is better than 20 meters. The result is a maximum temperature error of $1^\circ K$ and maximum wind error of 1–2 meters/sec, according to the error functions. The time of the grenade explosion, determined primarily by rocket borne infrared photocells, is telemetered to the ground equipment. The time of grenade explosions may also be determined by ground based flash detectors or radar signal strength records. It has been shown that this time can generally be determined within $\pm .001$ second. The errors in determining the arrival time of the sound at the ground range from $\pm .001$ to $\pm .010$ second. Thus, the maximum error expected in determining the travel time (t) of the sound between explosion and ground is approximately .01 second, which results in a temperature error of $0.3^\circ K$ and virtually no errors in winds. By far the largest contribution

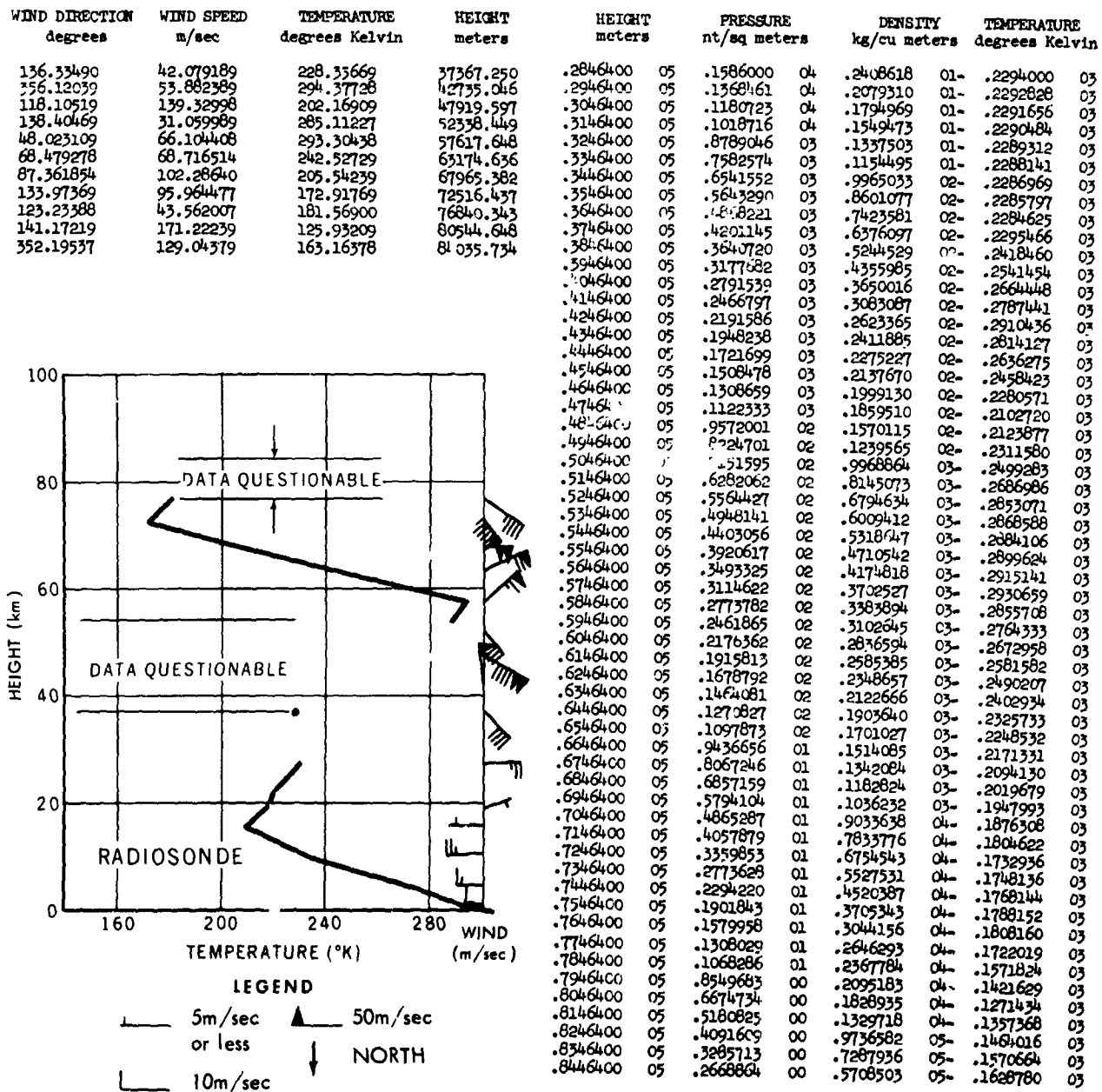


FIGURE 9

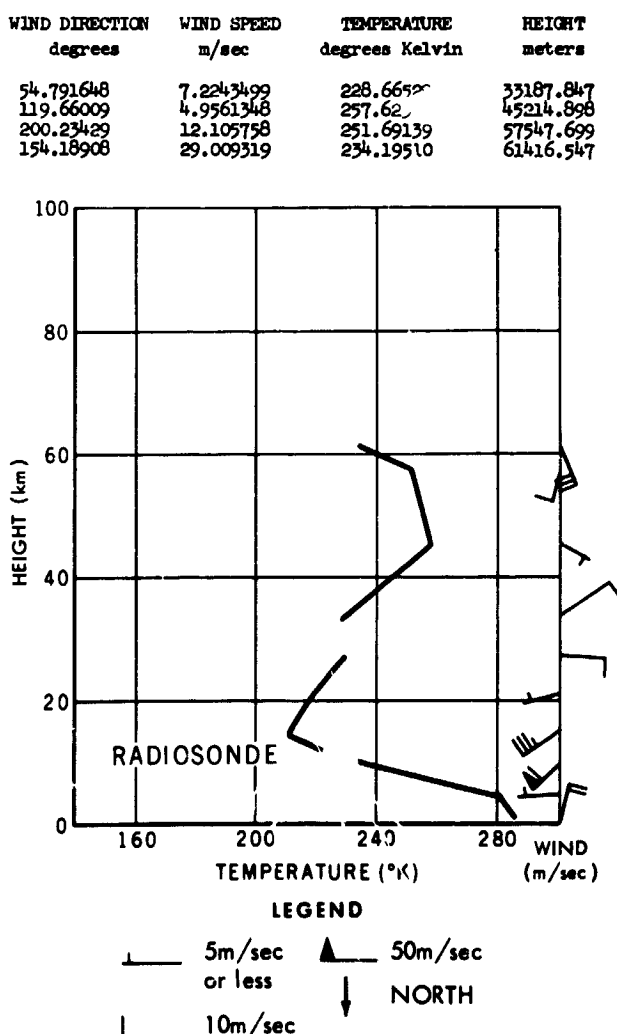
to the total error comes from errors in Δt , which also range from .001 to .010 second, depending upon the background noise level and the altitude of the explosion. The error in Δt is obtained by determining typical discrepancies among a number of independent Δt readings for each explosion. These errors result in temperature errors ranging from 1°K at 40 km to 15°K at 90 km, and wind errors from 1 to 16 m/sec over the same altitude range.

The maximum errors in the 16 soundings considered in this error analysis are presented in Figures 42 and 43, which clearly show the increase of the maximum errors with altitude. This increase is to be expected, since the amplitude of the sound waves will decrease rapidly with increasing

altitudes, making it difficult to distinguish the grenade explosion from the background noise level. Since the determination of the relative arrival times between microphones is by far the most critical measured parameter, the largest part of the maximum error is due to the attenuation of the sound wave with altitude.

ACKNOWLEDGMENTS

The authors greatly appreciate the contributions of: Superior Engineering Company in designing and constructing the payload instrumentation for the grenade experiment; Texas Western College in conducting the sound ranging portion of this experiment; and New Mexico State University in operating the DOVAP tracking system.



HEIGHT meters	PRESSURE nt/sq meters	DENSITY kg/cu meters	TEMPERATURE degrees Kelvin
.2842900	05 .1585800	04 .2421628	01-.2281200 03
.2942900	05 .1367266	04 .2087035	01-.2282346 03
.3042900	05 .1178998	04 .1798754	01-.2283492 03
.3142900	05 .1016779	04 .1550405	01-.2284637 03
.3242900	05 .8716945	03 .1336642	01-.2285783 03
.3342900	05 .7566287	03 .1149845	01-.2292459 03
.3442900	05 .6534624	03 .9827423	02-.2316536 03
.3542900	05 .5652446	03 .8413269	02-.2340614 03
.3642900	05 .4896843	03 .7214396	02-.2364691 03
.3742900	05 .4248608	03 .6196276	02-.2388769 03
.3842900	05 .3691600	03 .5330196	02-.2412846 03
.3942900	05 .3212236	03 .4592231	02-.2436923 03
.4042900	05 .2799064	03 .3962408	02-.2461001 03
.4142900	05 .2442411	03 .3424025	02-.2485078 03
.4242900	05 .2134095	03 .2963086	02-.2509156 03
.4342900	05 .1867181	03 .2567850	02-.2533233 03
.4442900	05 .1635784	03 .2228439	02-.2557310 03
.4542900	05 .1434675	03 .1940888	02-.2575203 03
.4642900	05 .1258761	03 .1706489	02-.2570393 03
.4742900	05 .1104189	03 .1499393	02-.2565583 03
.4842900	05 .9684000	02 .1317473	02-.2560773 03
.4942900	05 .8491356	02 .1157392	02-.2555963 03
.5042900	05 .7444053	02 .1016555	02-.2551154 03
.5142900	05 .6524572	02 .8926745	03-.2546344 03
.5242900	05 .5717470	02 .7837294	03-.2541534 03
.5342900	05 .5009164	02 .6879393	03-.2536724 03
.5442900	05 .4387682	02 .6037321	03-.2531914 03
.5542900	05 .3842498	02 .5297227	03-.2527101 03
.5642900	05 .3361340	02 .4646889	03-.2522294 03
.5742900	05 .2945059	02 .4075542	03-.2517485 03
.5842900	05 .2575032	02 .3621634	03-.2477058 03
.5942900	05 .2246321	02 .3218074	03-.2431835 03
.6042900	05 .1956639	02 .2853272	03-.2386611 03
.6142900	05 .1696355	02 .2524733	03-.2340774 03

FIGURE 10

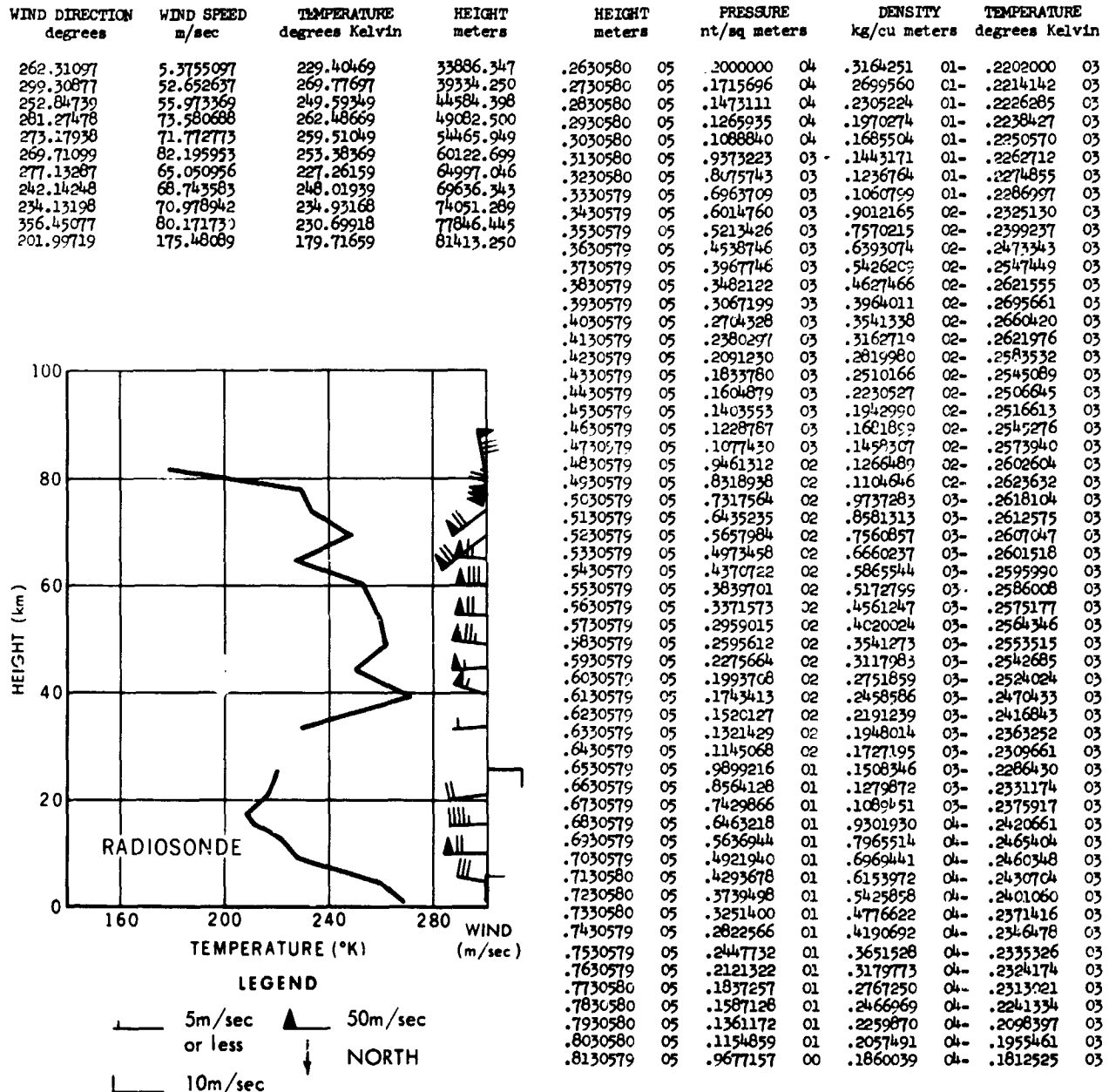


FIGURE 11

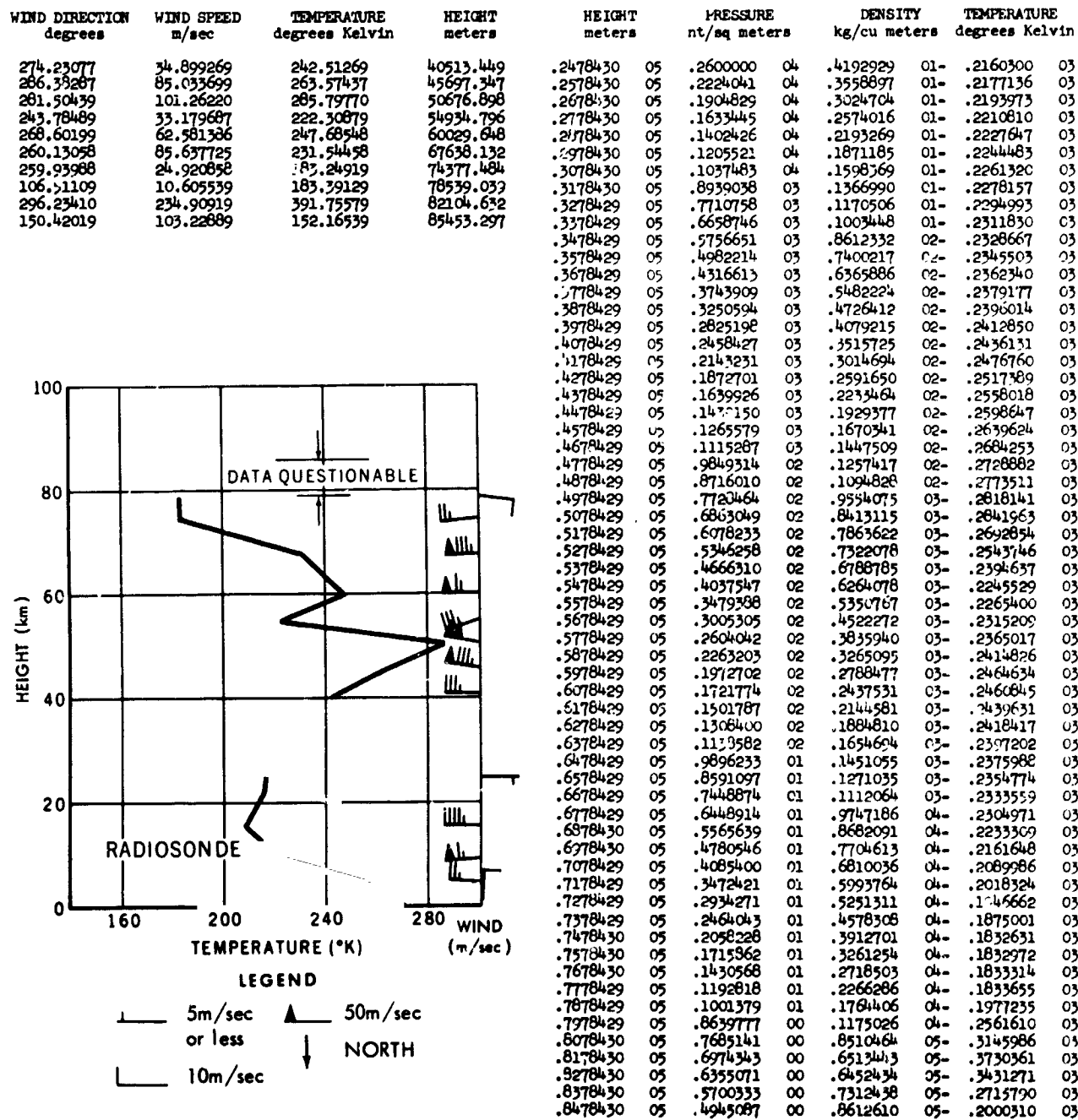


FIGURE 12

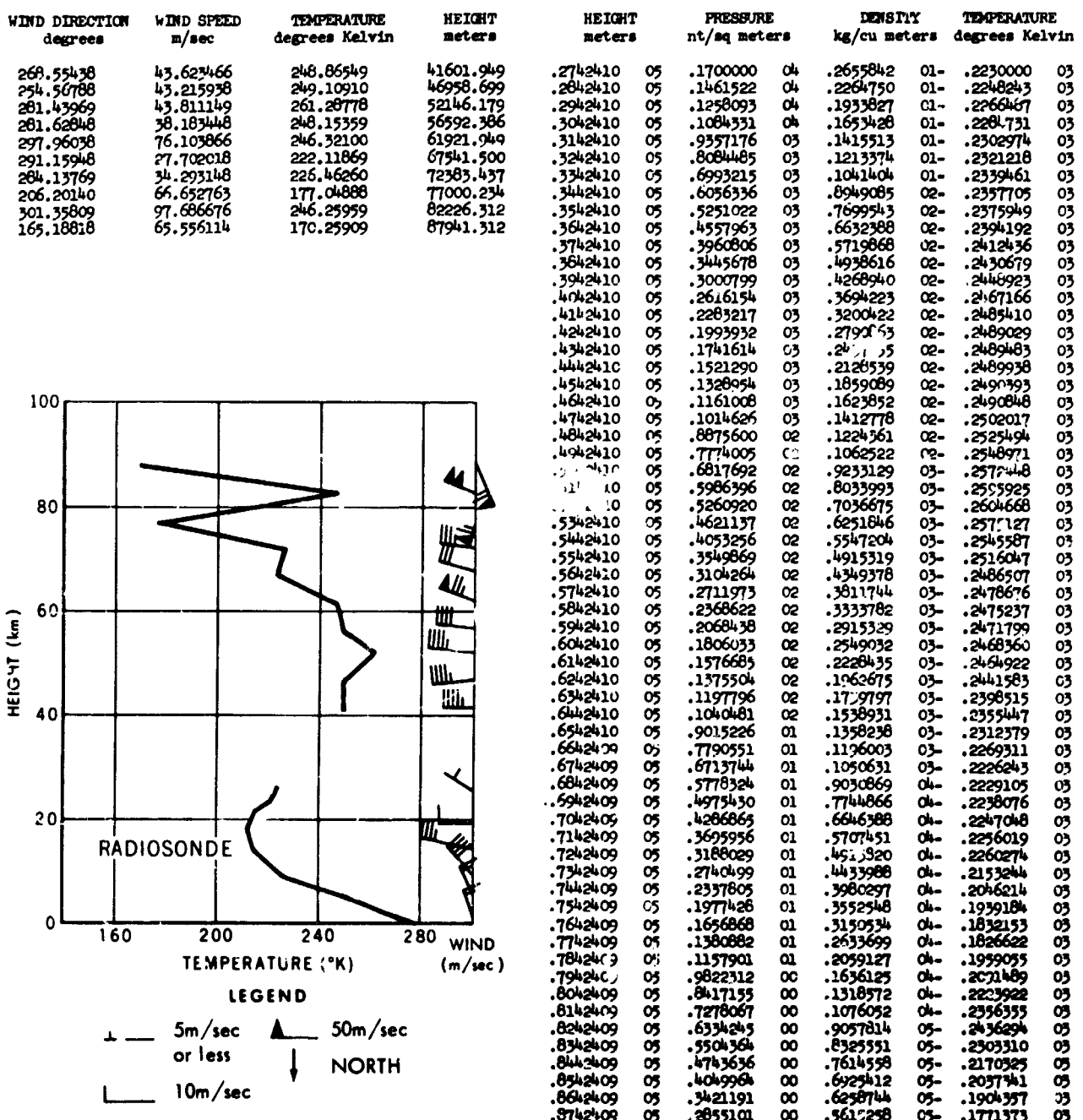
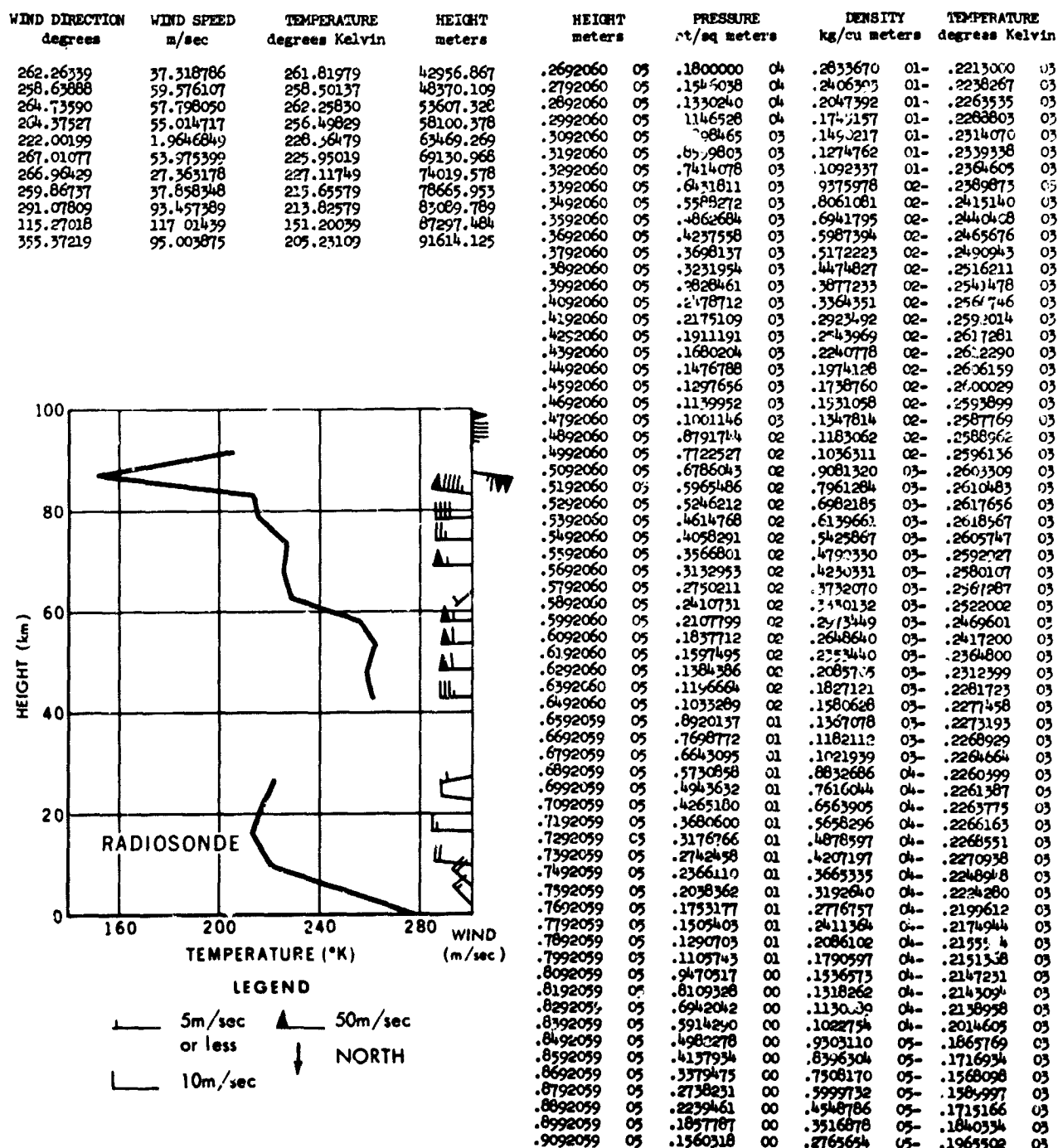


FIGURE 13



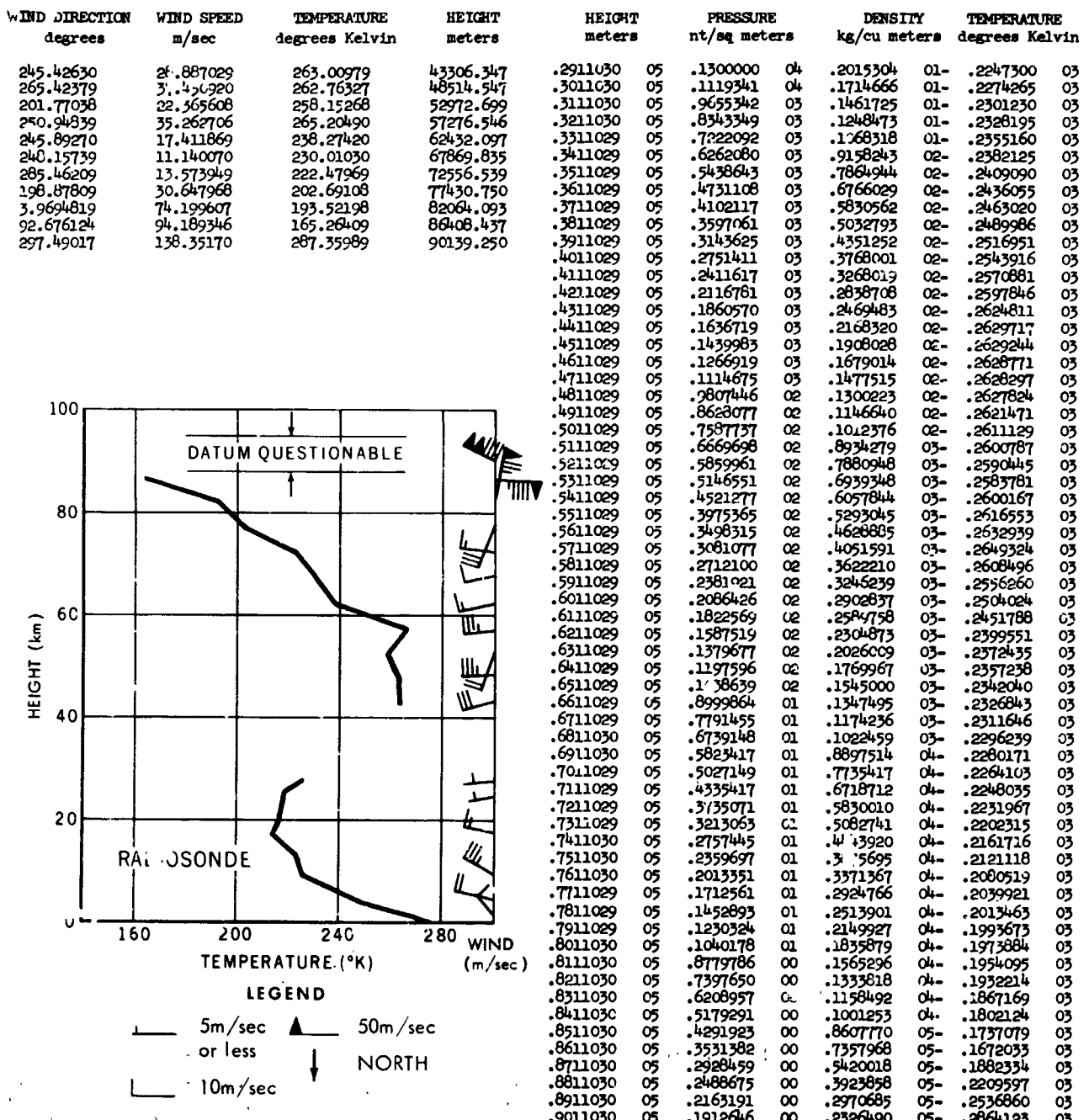


FIGURE 15

WIND DIRECTION degrees	WIND SPEED m/sec	TEMPERATURE degrees Kelvin	HEIGHT meters	HEIGHT meters	PRESSURE nt/sq meters	DENSITY kg/cu meters	TEMPERATURE degrees Kelvin
100.23349	35.039177	271.12729	45967.500	.2782370	05 .1700000	04 .2561204	01- .2312400
112.12339	31.585488	265.44738	51428.398	.2882370	05 .1469582	04 .2193208	01- .2334304
85.151590	20.540390	268.92038	56624.398	.2982370	05 .1272189	04 .1880904	01- .2356366
76.249366	37.992378	241.96479	62684.597	.3082370	05 .1102634	04 .1615445	01- .2376352
86.465759	47.108570	208.31379	69435.039	.3182370	05 .0973240	03 .1389457	01- .2400356
102.19909	72.066656	197.25399	75832.382	.3282370	05 .0832120	03 .1196778	01- .2422320
100.33849	77.084068	168.90759	81279.049	.3382370	05 .0742419	03 .1032254	01- .2444504
219.76649	81.912193	174.49778	85927.898	.3482370	05 .0611593	03 .8915658	02- .2466288
5.6612997	193.16529	167.00509	89940.898	.3582370	05 .0507353	03 .7710869	02- .2488272
97.556236	223.62478	145.78129	93665.695	.3682370	05 .0401159	03 .6677687	02- .2510256
				.3782370	05 .0420880	03 .5790443	02- .2532240
				.3882370	05 .0368567	03 .5027484	02- .2554224
				.3982370	05 .03231886	03 .4370523	02- .2576207
				.4082370	05 .02637027	03 .3804088	02- .2598191
				.4182370	05 .02493247	03 .3315073	02- .2620175
				.4282370	05 .02193578	03 .2892359	02- .2642159
				.4382370	05 .01932052	03 .2526500	02- .2664143
				.4482370	05 .01703549	03 .2209460	02- .2686127
				.4582370	05 .01503671	03 .1934393	02- .2708111
				.4682370	05 .01327794	03 .1711766	02- .2702367
				.4782370	05 .01172096	03 .1516882	02- .2691966
				.4882370	05 .01034197	03 .1343609	02- .2681565
				.4982370	05 .0912133	02 .1189615	02- .2671164
				.5082370	05 .08040792	02 .1052812	02- .2660763
				.5182370	05 .07086315	02 .9291121	03- .2657116
				.5282370	05 .06245859	02 .8168621	03- .2663800
				.5382370	05 .05507040	02 .7184333	03- .2670483
				.5482370	05 .04857337	02 .6320927	03- .2677168
				.5582370	05 .04285786	02 .5563270	03- .2683892
				.5682370	05 .03781911	02 .4915637	03- .2680339
				.5782370	05 .03333633	02 .4406094	03- .2635059
				.5882370	05 .02932304	02 .3942177	03- .2591379
				.5982370	05 .02573672	02 .3520461	03- .2546900
				.6082370	05 .02253809	02 .3137727	03- .2502420
				.6182370	05 .01969090	02 .27190933	03- .2457940
				.6282370	05 .01716138	02 .2478020	03- .2412713
				.6382370	05 .01491656	02 .2199319	03- .2362863
				.6482370	05 .01292725	02 .1947090	03- .2313013
				.6582369	05 .01116886	02 .1719297	03- .2263163
				.6682369	05 .09618718	01 .1514023	03- .2213313
				.6782369	05 .0855966	01 .1329464	03- .2163463
				.6882369	05 .07061436	01 .1163927	03- .2113613
				.6982369	05 .06020476	01 .1010123	03- .2076419
				.7082369	05 .0512246	01 .08666698	04- .2059131
				.7182369	05 .04352695	01 .7426672	04- .2041842
				.7282369	05 .03693669	01 .6356042	04- .2024554
				.7382369	05 .03130174	01 .5432774	04- .2007266
				.7482369	05 .02648987	01 .4637561	04- .1989978
				.7582369	05 .02238624	01 .3953489	04- .1972690
				.7682369	05 .01886279	01 .3420963	04- .1920948
				.7782369	05 .01582039	01 .2949091	04- .1868905
				.7882369	05 .01320369	01 .2531813	04- .1816861
				.7982369	05 .01096266	01 .2164086	04- .1764818
				.8082369	05 .09052001	00 .1841207	04- .1712774
				.8182369	05 .07445886	00 .1529835	04- .1695625
				.8282369	05 .06123329	00 .1249943	04- .1707650
				.8382369	05 .05042907	00 .1021628	04- .1719675
				.8482369	05 .04158986	00 .08367063	05- .1731700
				.8582369	05 .03434779	00 .06862448	05- .1743725
				.8682369	05 .02836304	00 .05717470	05- .1728252
				.8782369	05 .0233198	00 .04764040	05- .1709581
				.8882369	05 .01922939	00 .03961897	05- .1690910
				.8982369	05 .0178369	00 .03288277	05- .1672239
				.9082369	05 .01490065	00 .02774782	05- .1619749
				.9182369	05 .01047229	00 .02334559	05- .1562769
				.9282369	05 .08435857	01- .01951745	05- .1505790
				.9382369	05 .06706524	01- .01684508	05- .1387020

FIGURE 16

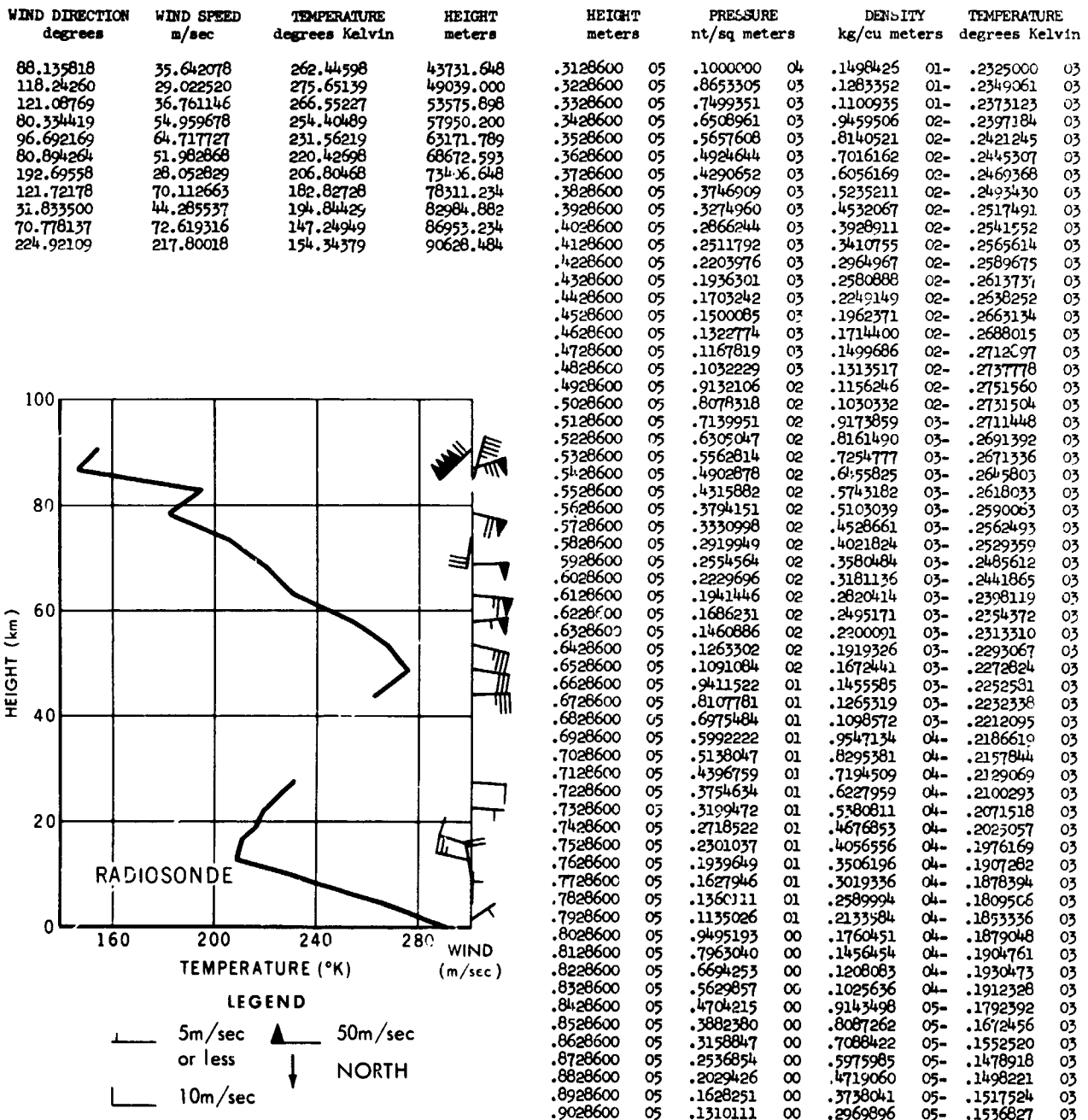


FIGURE 17

PLANETARY ATMOSPHERES

1127

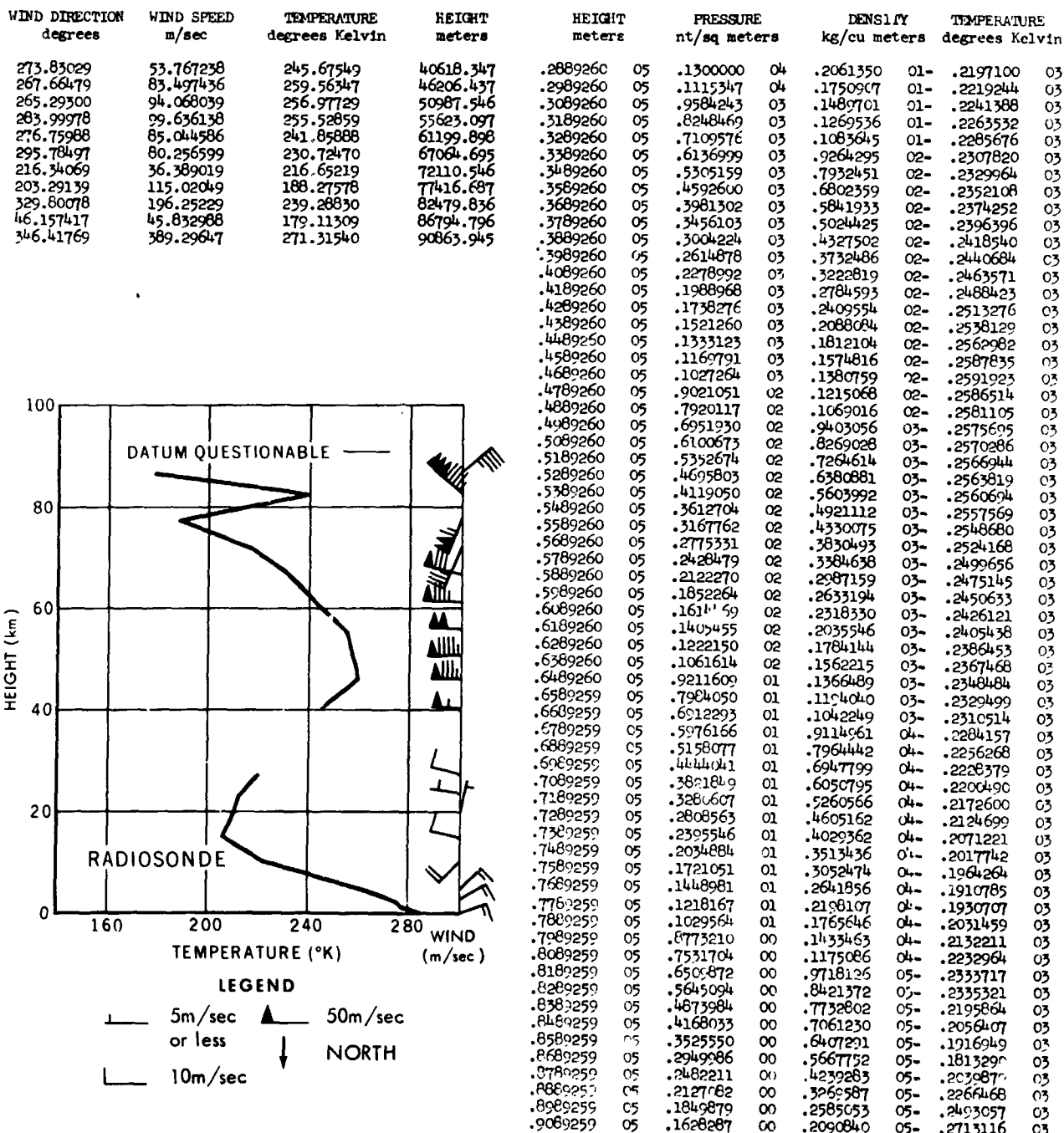


FIGURE 18

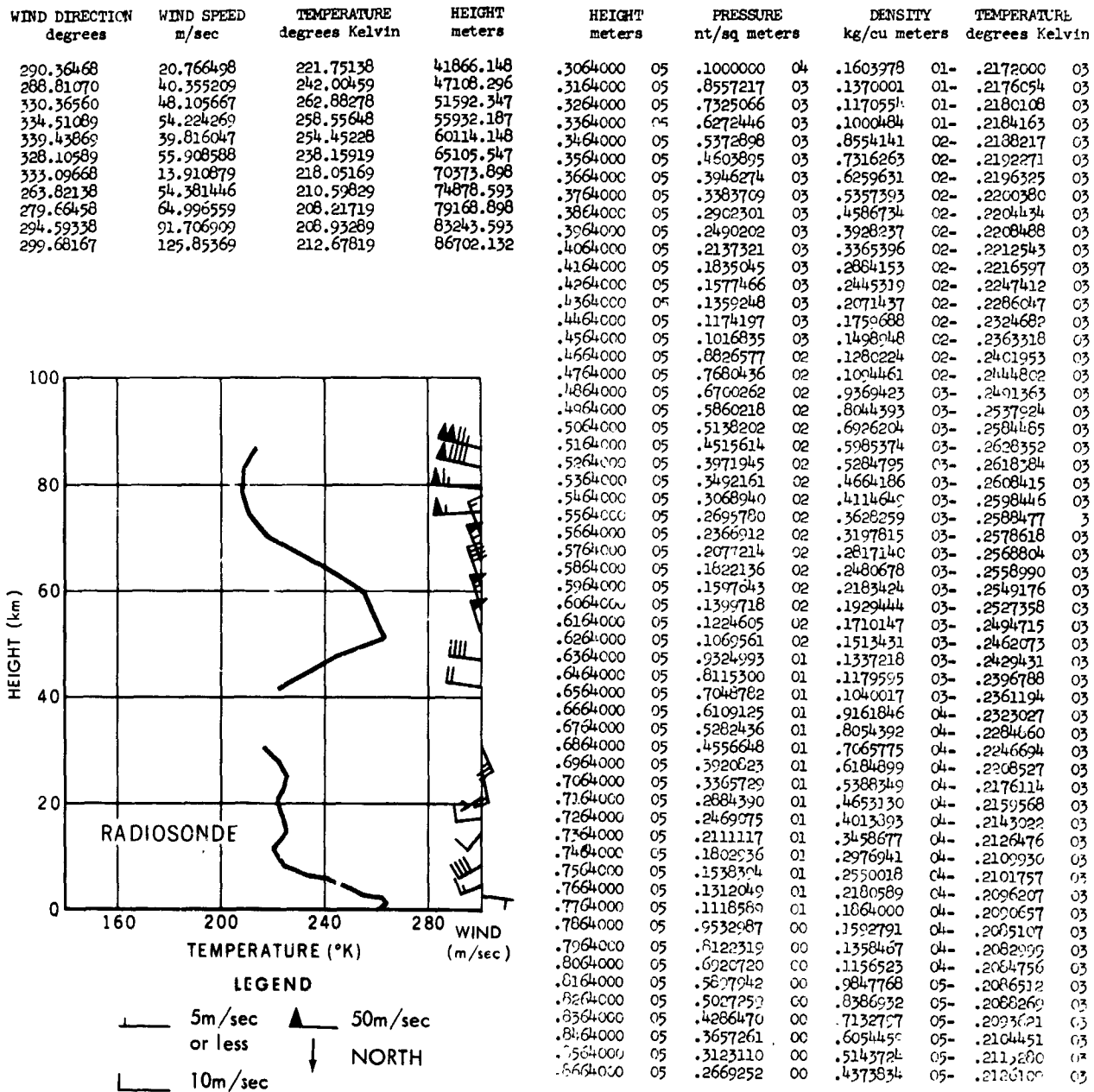


FIGURE 19

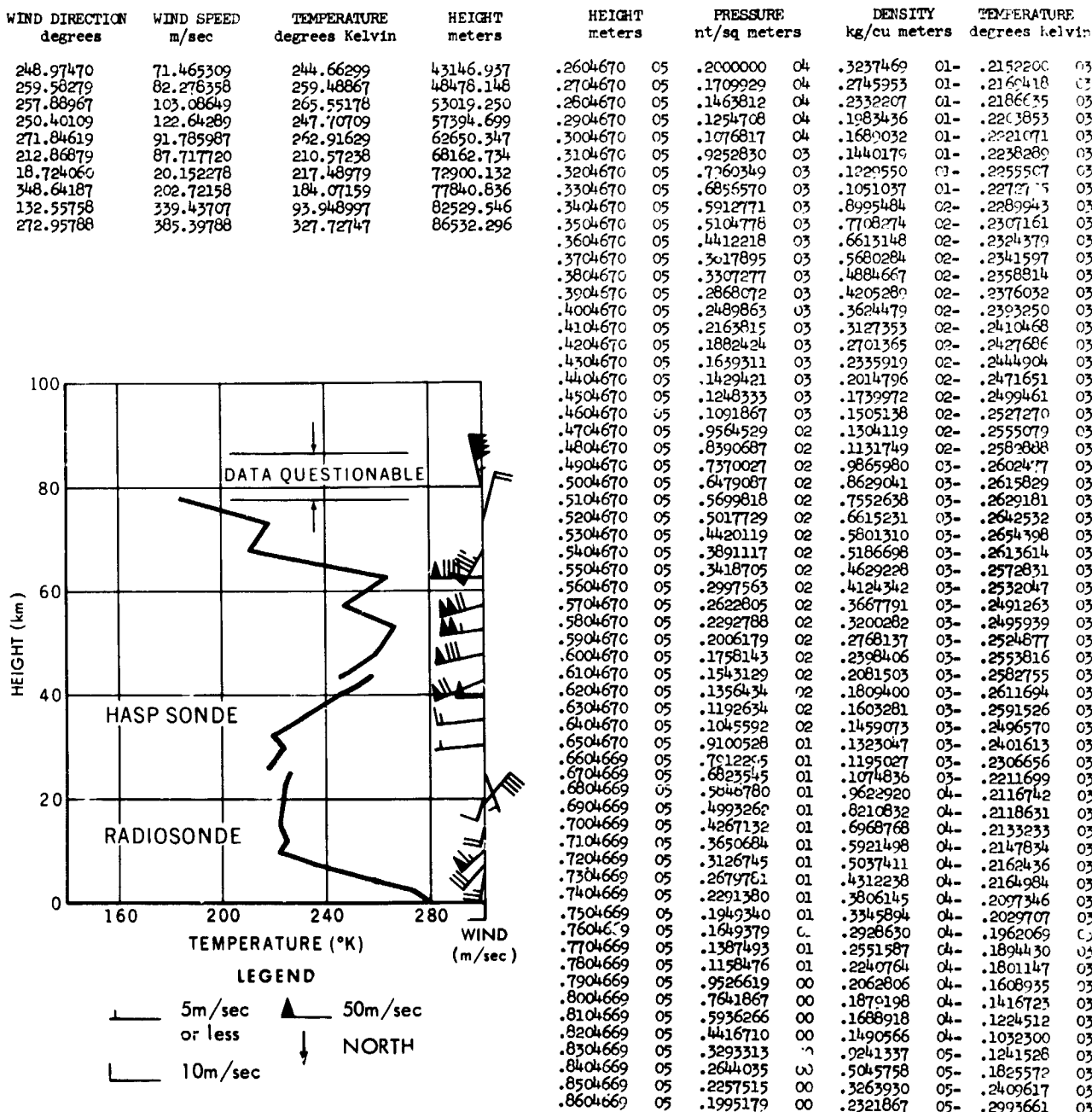


FIGURE 20

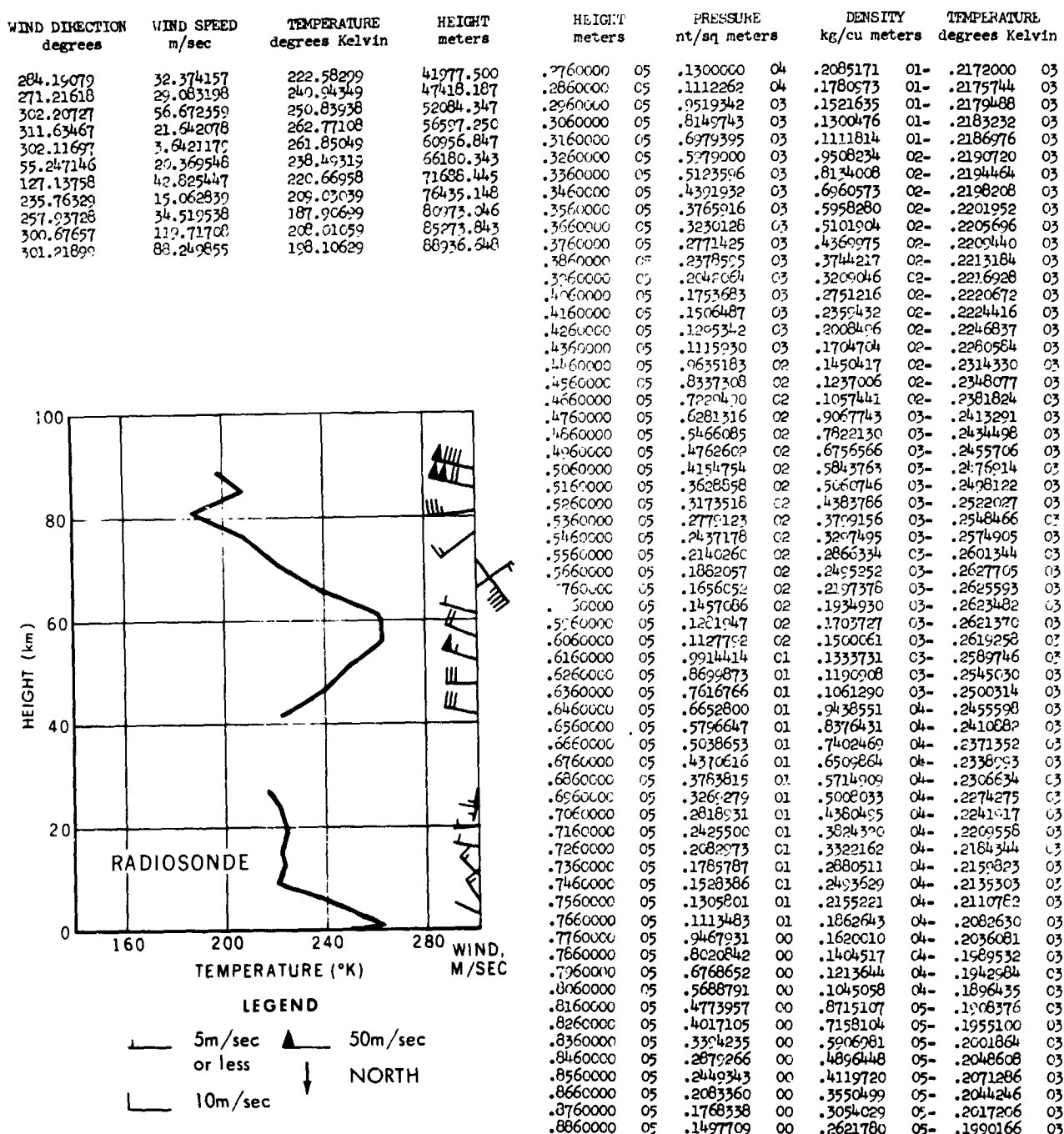


FIGURE 21

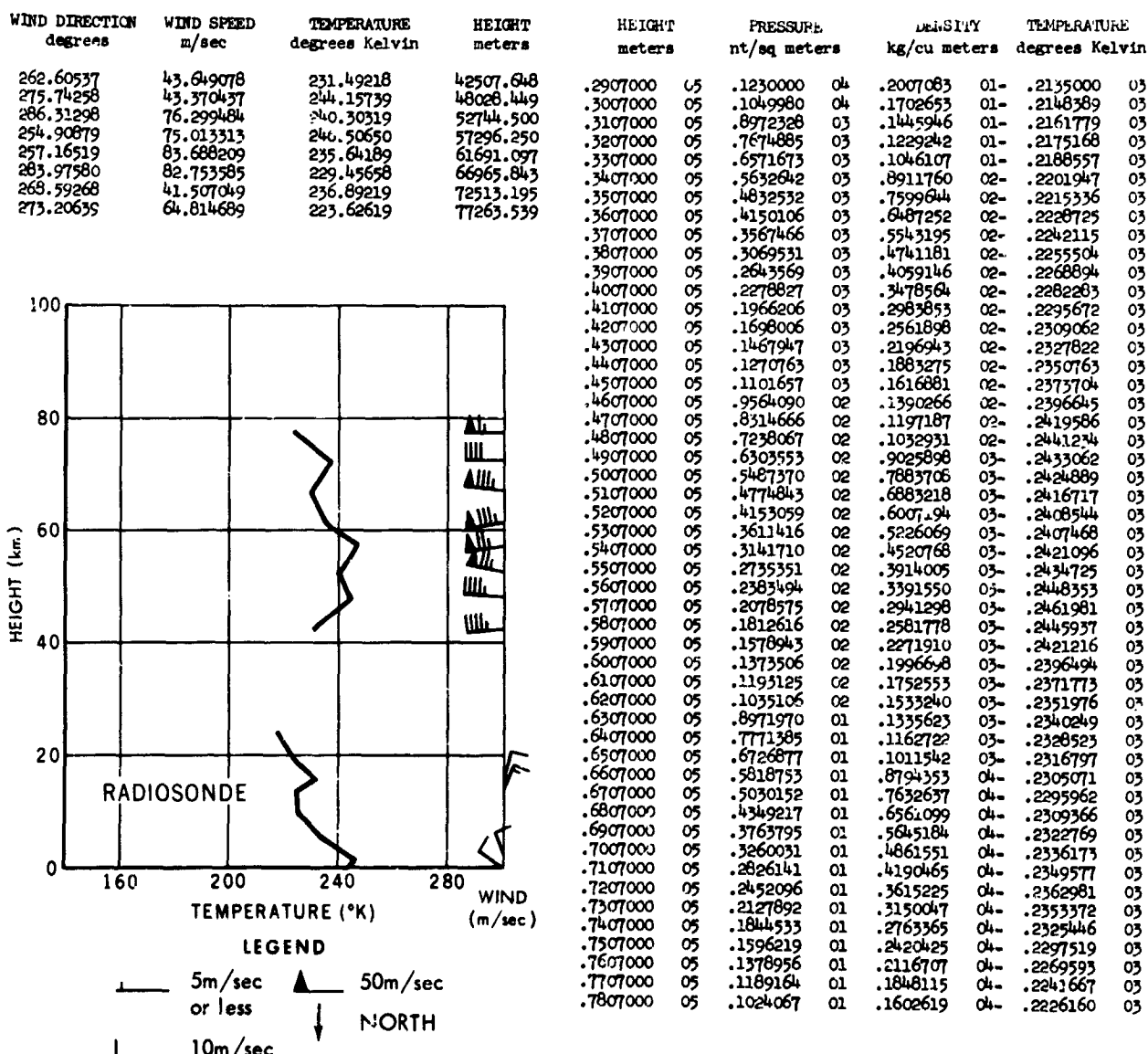


FIGURE 22

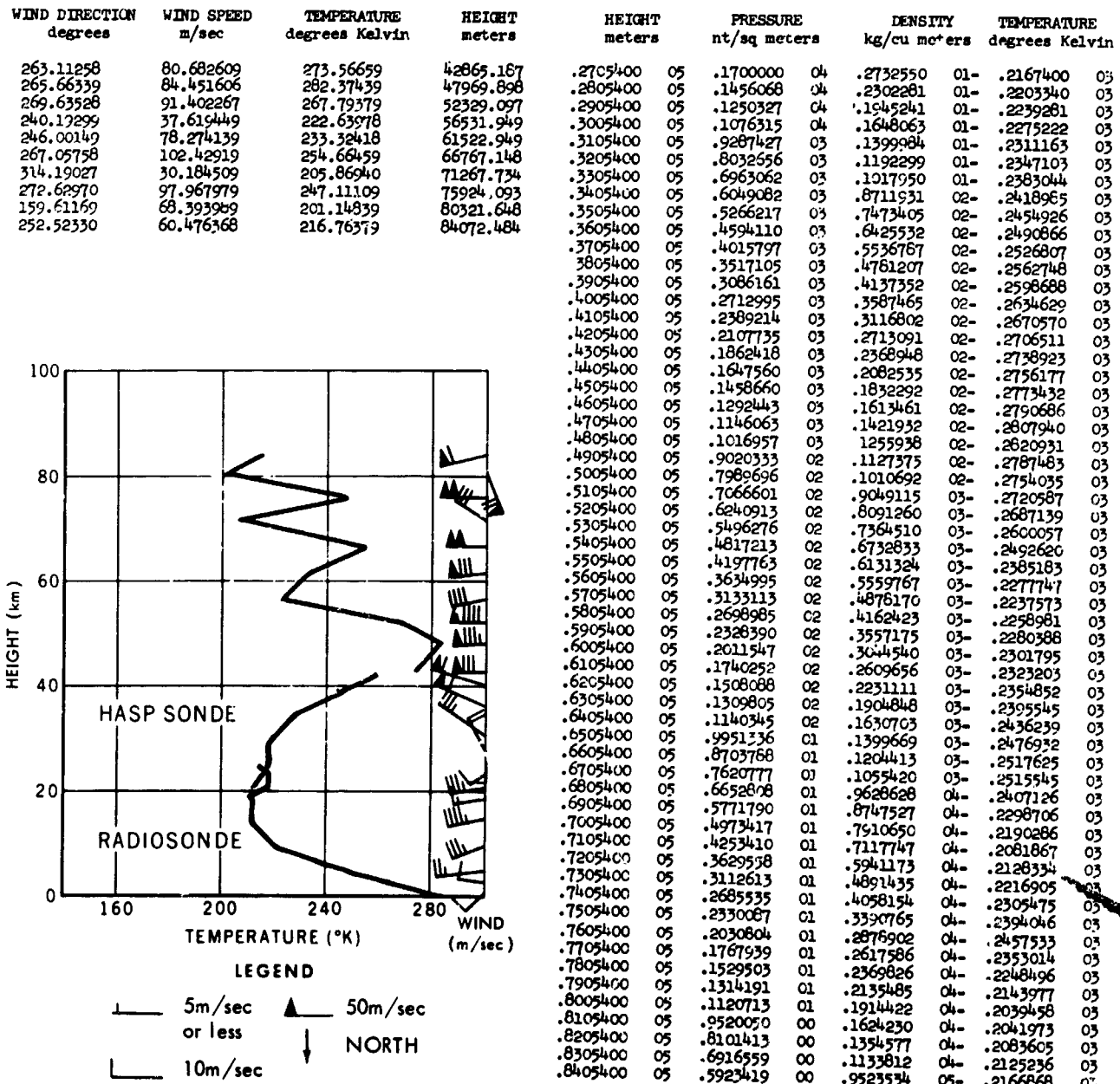


FIGURE 23

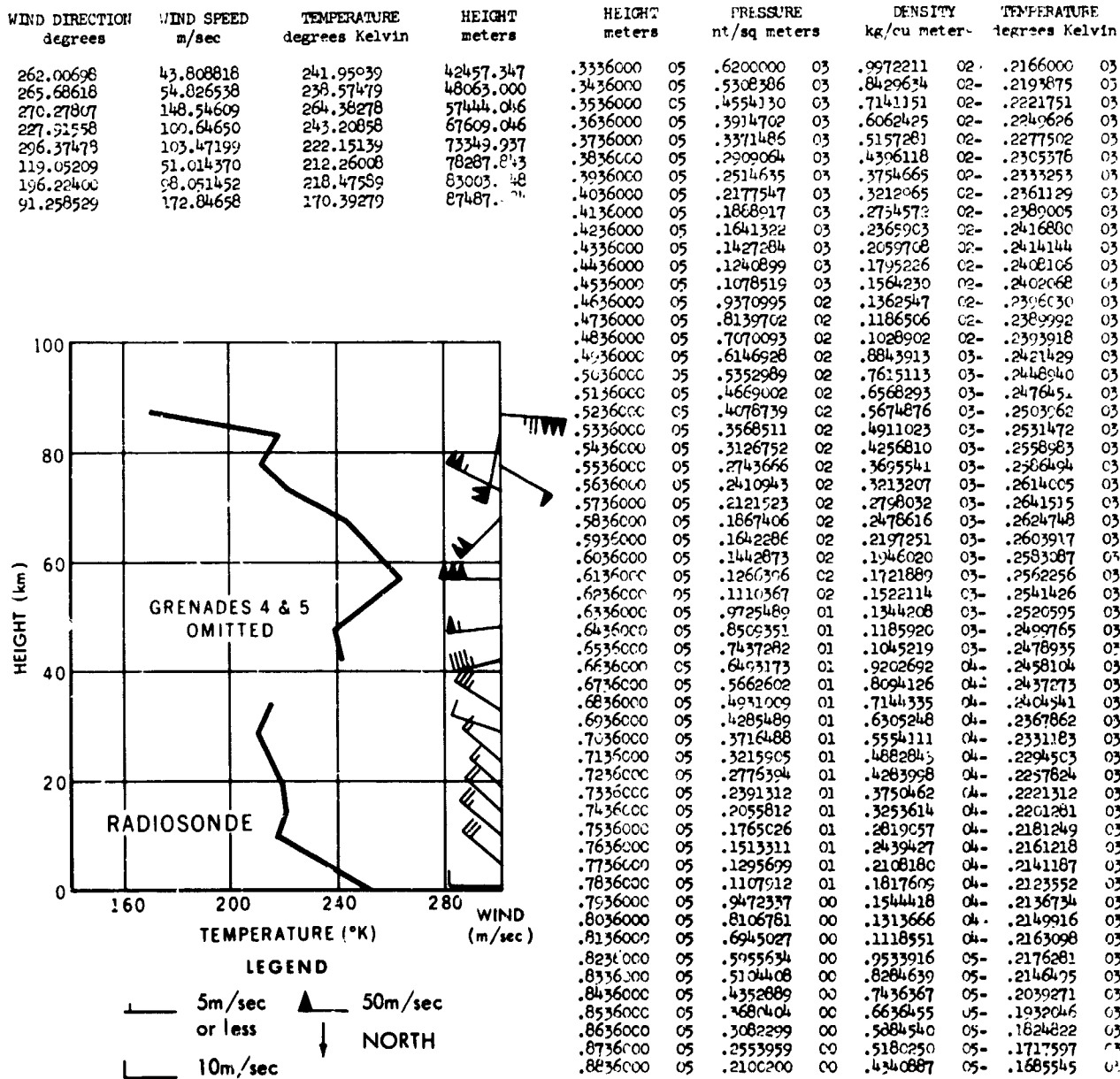


FIGURE 24

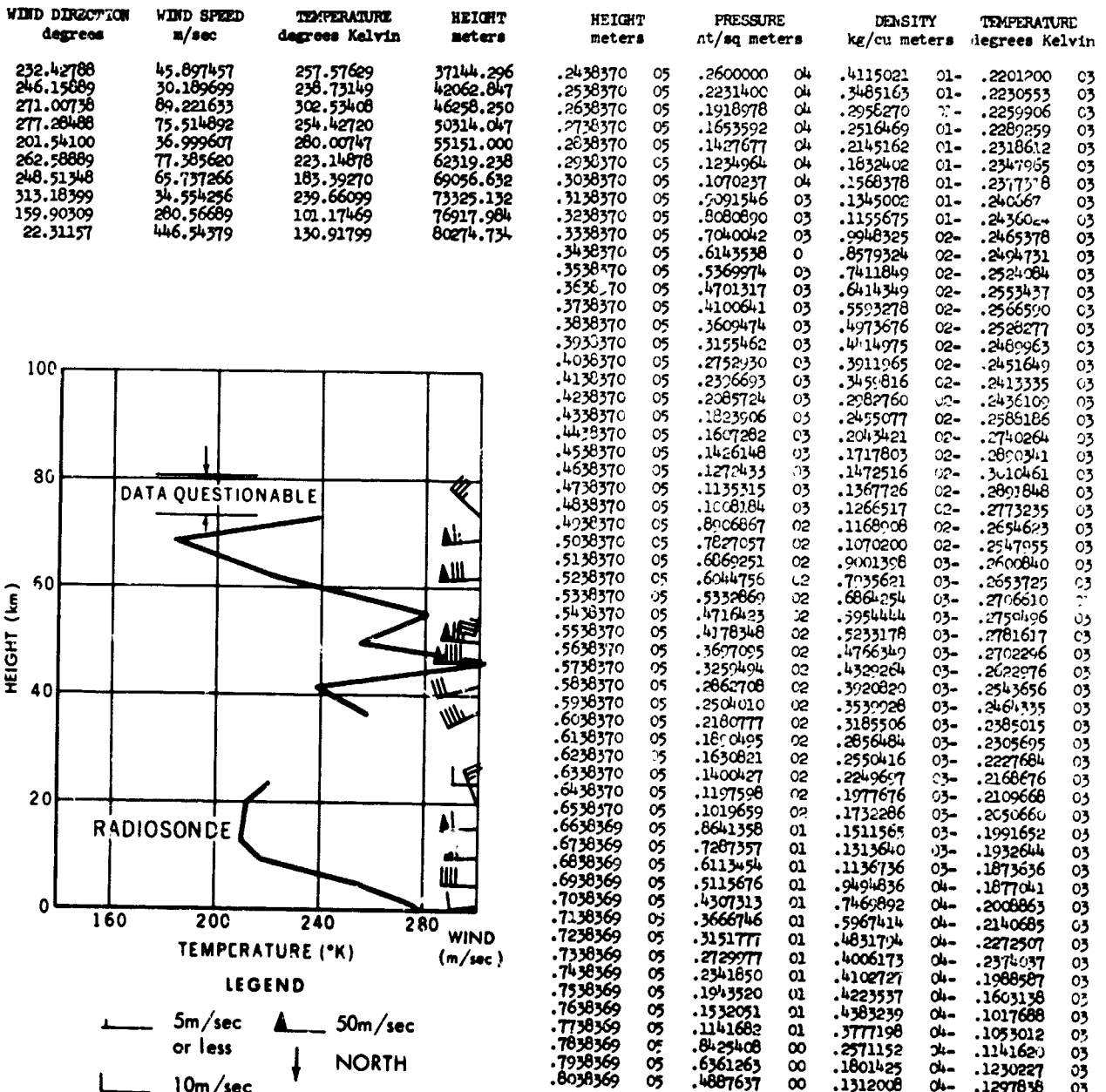


FIGURE 25

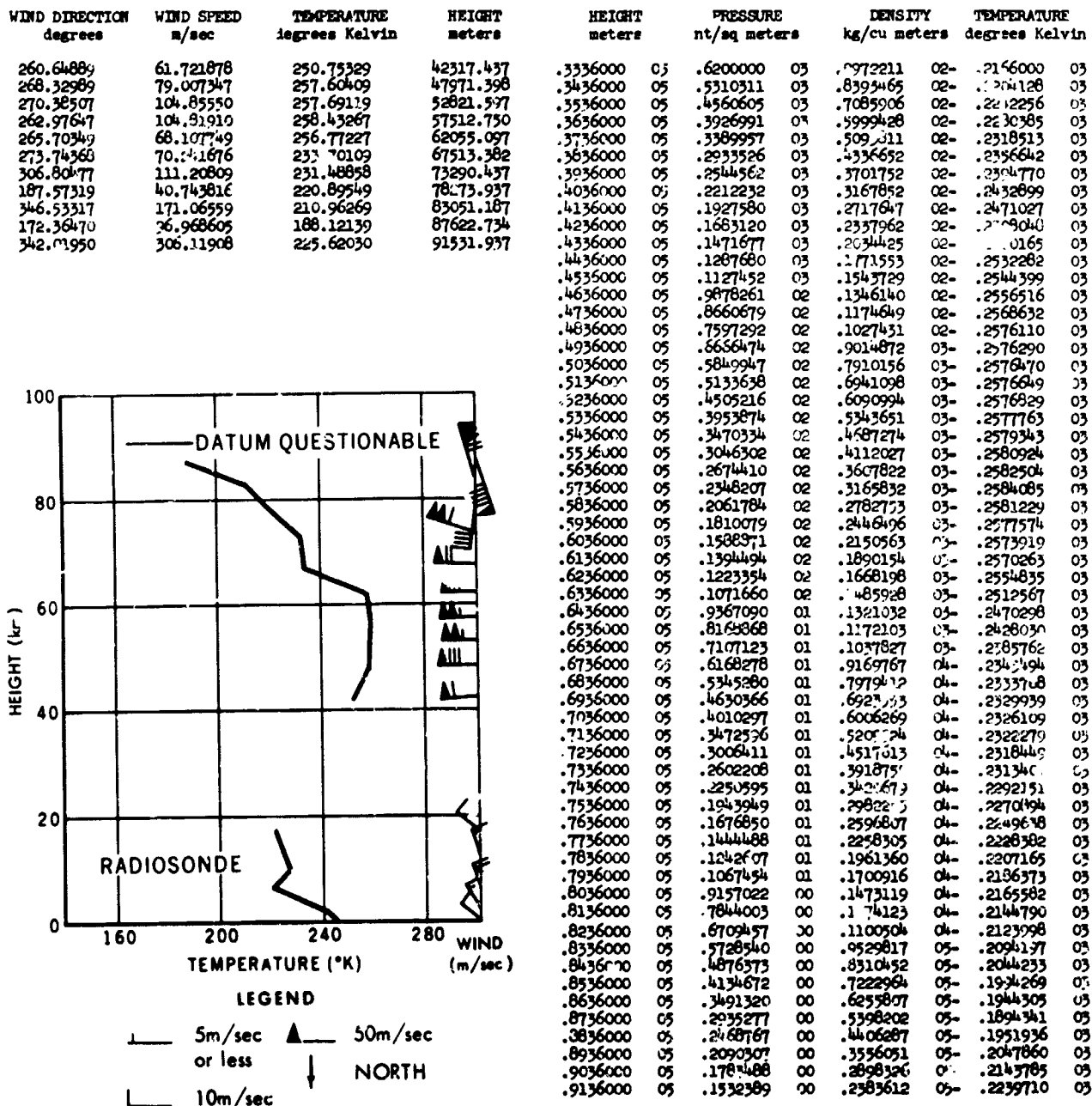


FIGURE 26

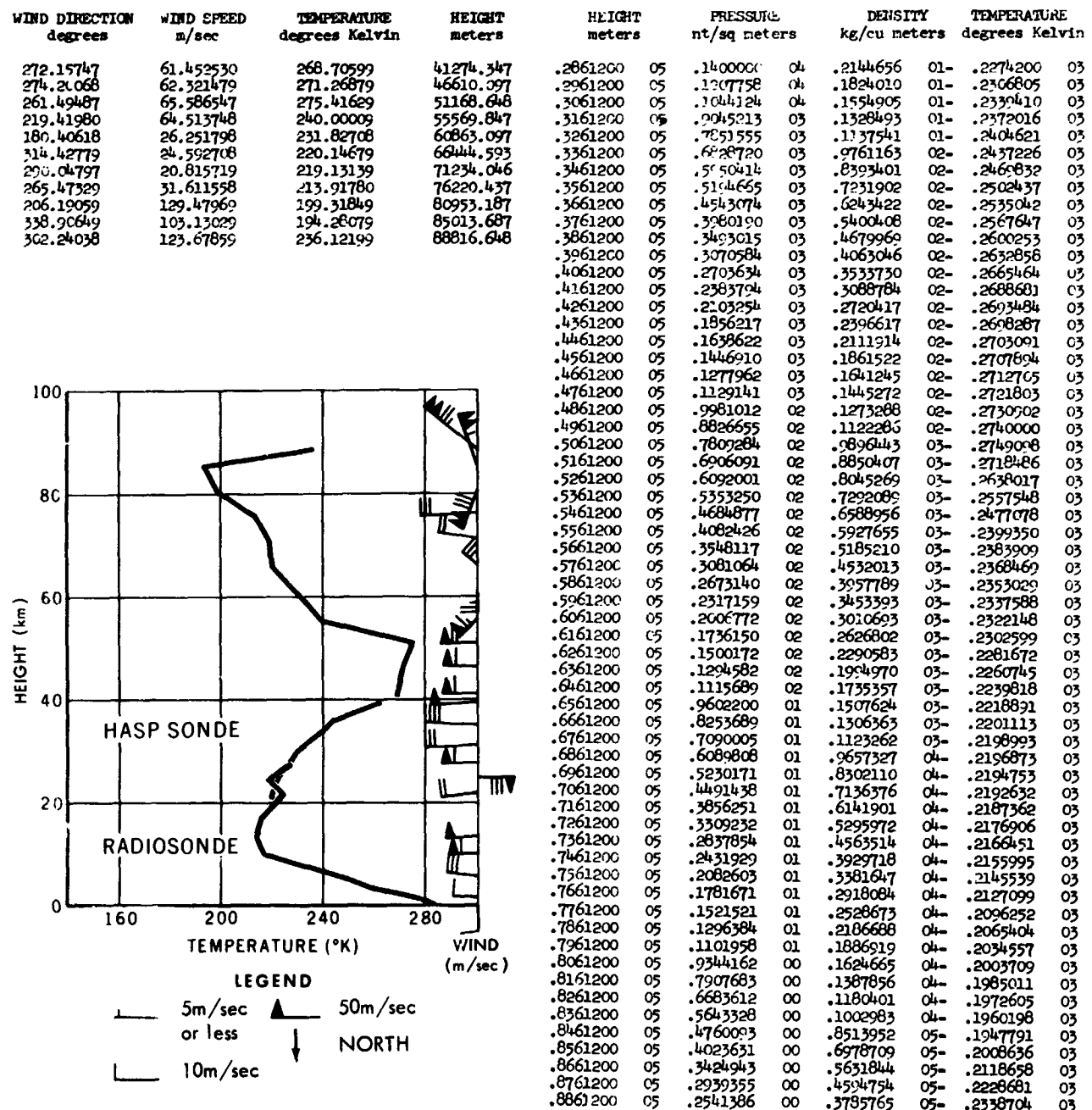


FIGURE 27

WIND DIRECTION degrees	WIND SPEED m/sec	TEMPERATURE degrees Kelvin	HEIGHT meters	HEIGHT meters	PRESSURE nt/sq meters	DENSITY kg/cu meters	TEMPERATURE degrees Kelvin
251.04699	49.156208	225.17968	34084.500	.3371160	.6000000	.8953968	02-.2334500 03
266.78720	120.79139	250.57888	38644.847	.3471160	.5183956	.7897794	02-.2286723 03
274.32379	130.62210	243.76129	43035.796	.3571160	.4480216	.6663348	02-.2342419 03
260.92868	95.027588	258.45147	47755.898	.3671160	.3085483	.5644600	02-.2398115 03
271.01498	79.796524	239.92878	52804.097	.3771160	.3380882	.4800066	02-.2453811 03
265.85369	104.42839	248.69580	58059.597	.3871160	.2950756	.4104183	02-.2504752 03
247.35418	84.380134	239.13979	63433.289	.3971160	.2577956	.3608024	02-.2489226 03
262.06008	85.245559	215.70478	68496.437	.4071160	.2250448	.3169423	02-.2473699 03
271.16949	147.49569	236.68159	73204.734	.4171160	.1962951	.2781987	02-.2458173 03
231.80848	67.915214	223.47479	77866.046	.4271160	.1710773	.2440001	02-.2442646 03
				.4371160	.1491077	.2112620	02-.2458045 03
				.4471160	.1301350	.1820931	02-.2489768 03
				.4571160	.1137774	.1572334	02-.2520891 03
				.4671160	.9963715	.1360180	02-.2552013 03
				.4771160	.8740130	.1178769	02-.2583136 03
				.4871160	.7666611	.1047648	02-.2549448 03
				.4971160	.6712982	.9307289	03-.2512757 03
				.5071160	.58666743	.8254546	03-.2476065 03
				.5171160	.5117097	.7308085	03-.2439373 03
				.5271160	.4454194	.6458490	03-.2402682 03
				.5371160	.3874565	.5590685	03-.2414438 03
				.5471160	.3373267	.4833930	03-.2431132 03
				.5571160	.2939739	.4183948	03-.2447826 03
				.5671160	.2586433	.3625076	03-.2464521 03
				.5771160	.2239200	.3144030	03-.2481215 03
				.5871160	.1955870	.2752715	03-.2475300 03
				.5971160	.1707354	.2420376	03-.2457529 03
				.6071160	.1489009	.2126223	03-.2439758 03
				.6171160	.1297344	.1866129	03-.2421987 03
				.6271160	.1129253	.1636349	03-.2404216 03
				.6371160	.9817432	.1437974	03-.2378510 03
				.6471160	.8517133	.1272275	03-.2332226 03
				.6571159	.7368373	.1122961	03-.2285942 03
				.6671159	.6355982	.9886879	04-.2239657 03
				.6771159	.5466049	.8681987	04-.2193373 03
				.6871159	.4689100	.7539841	04-.2166633 03
				.6971159	.4025276	.6342033	04-.2211186 03
				.7071159	.3466127	.5353203	04-.2255739 03
				.7171159	.2993529	.4533761	04-.2300292 03
				.7271159	.2592765	.3852185	04-.2344845 03
				.7371159	.2249351	.3331150	04-.2352455 03
				.7471159	.1950275	.2923446	04-.2324122 03
				.7571159	.1688084	.2561652	04-.2289739 03
				.7671159	.1456590	.2241054	04-.2267457 03
				.7771159	.1258039	.1957375	04-.2239124 03

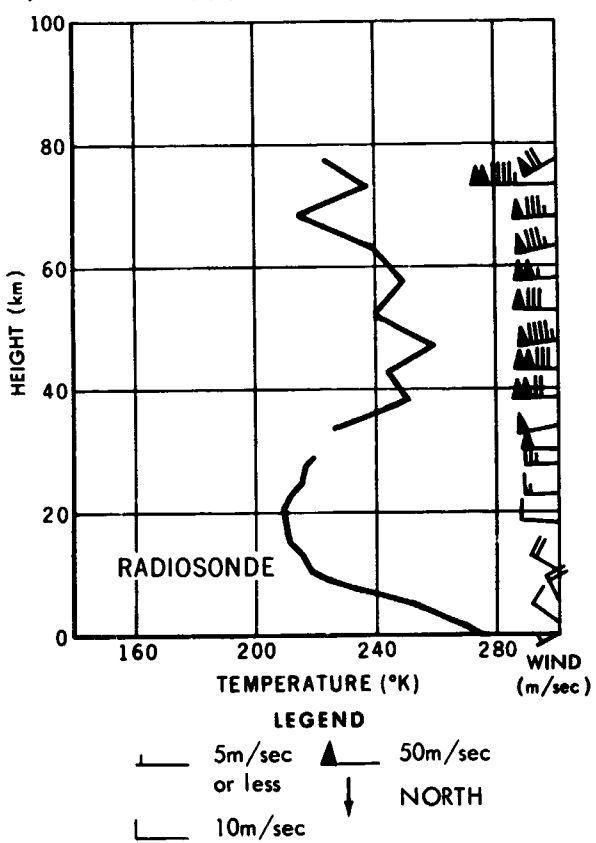


FIGURE 28

PUBLICATIONS OF GSFC, 1964: I. SPACE SCIENCES
 ERROR ANALYSIS 7/JUNE/62 NORTH COÖRD. - 200m

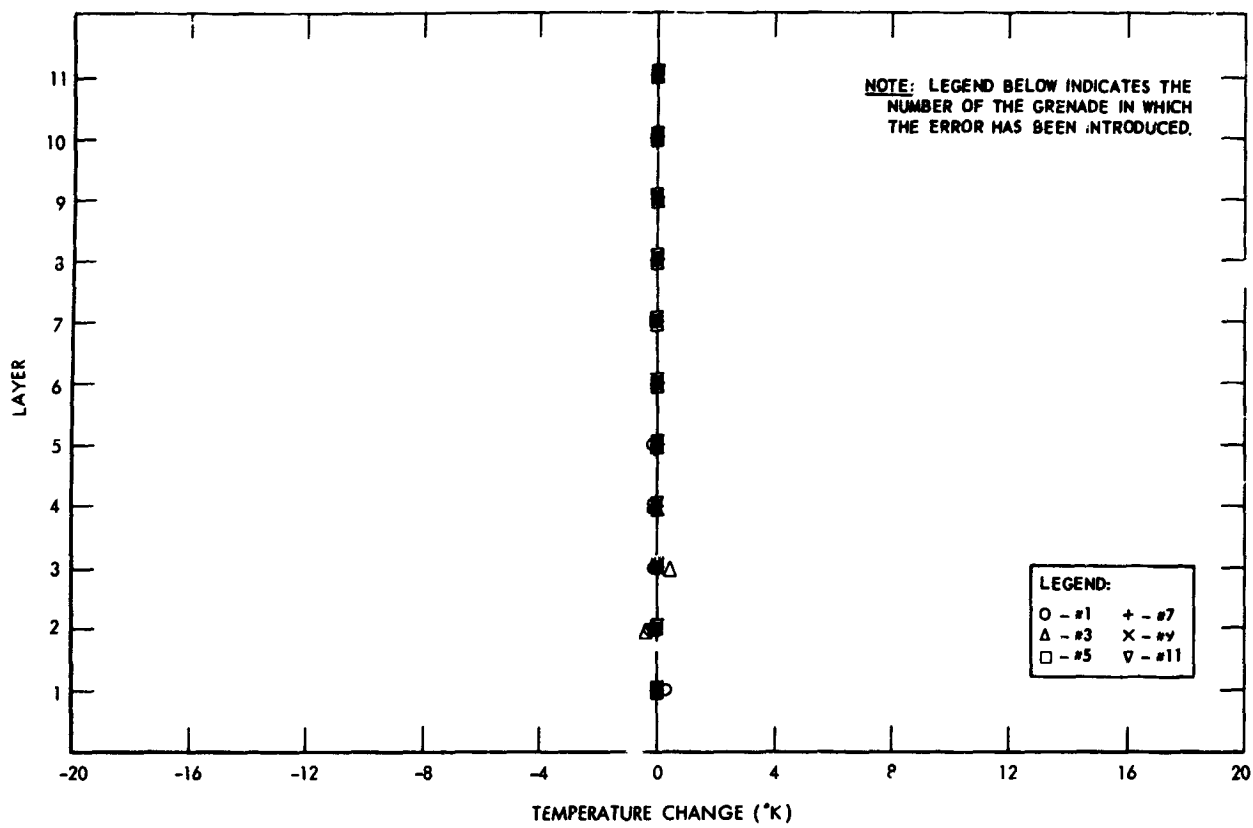


FIGURE 29

ERROR ANALYSIS 7/JUNE/62 NORTH COÖRD. - 200m

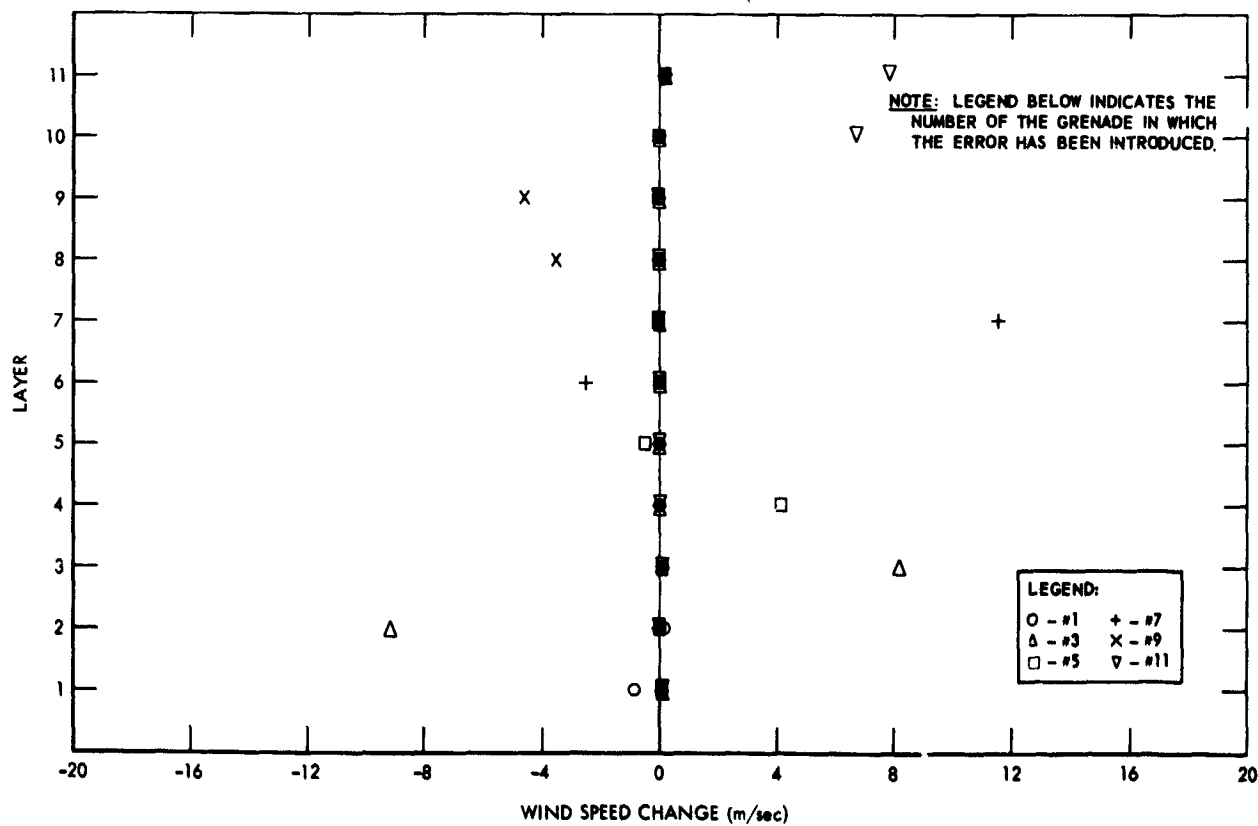


FIGURE 30

PLANETARY ATMOSPHERES

1139

ERROR ANALYSIS 7/JUNE/62 WEST COÖRD. - 200m

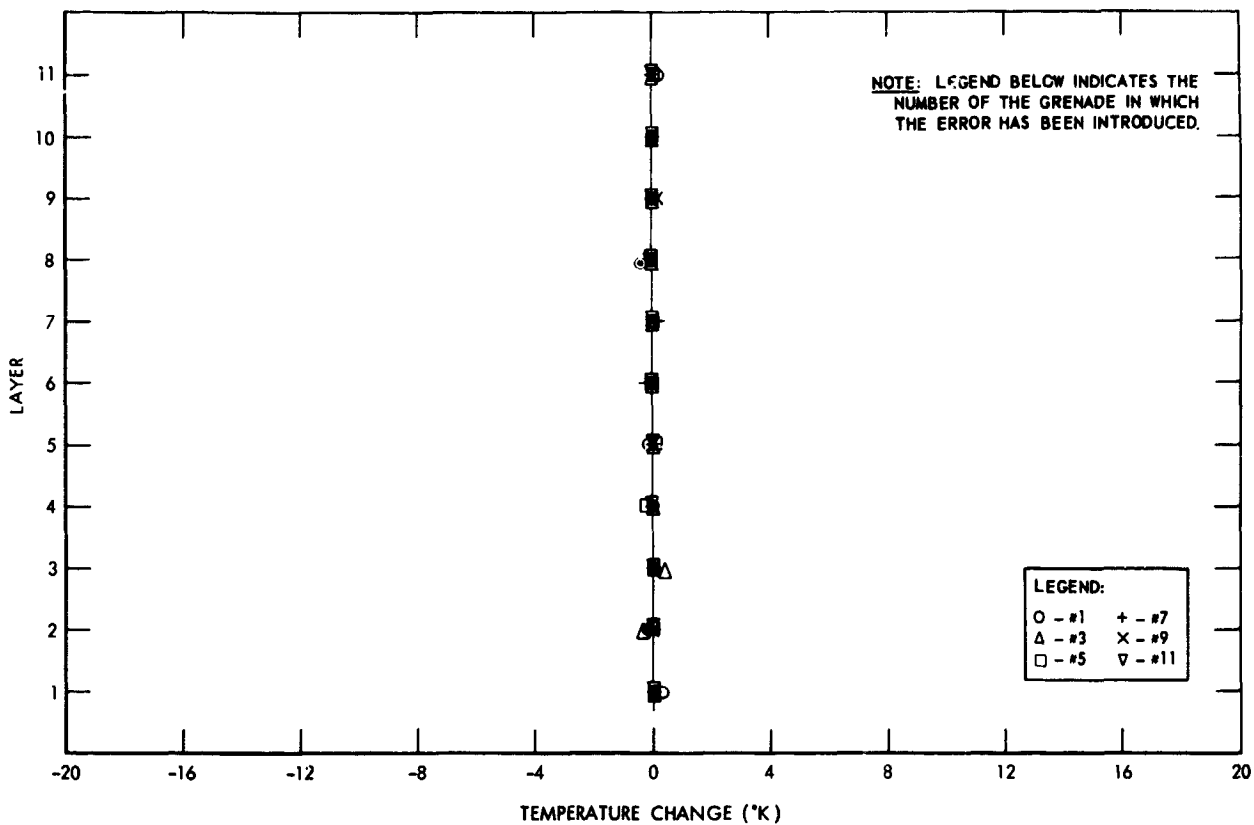


FIGURE 31
ERROR ANALYSIS 7/JUNE/62 WEST COORD. - 200m

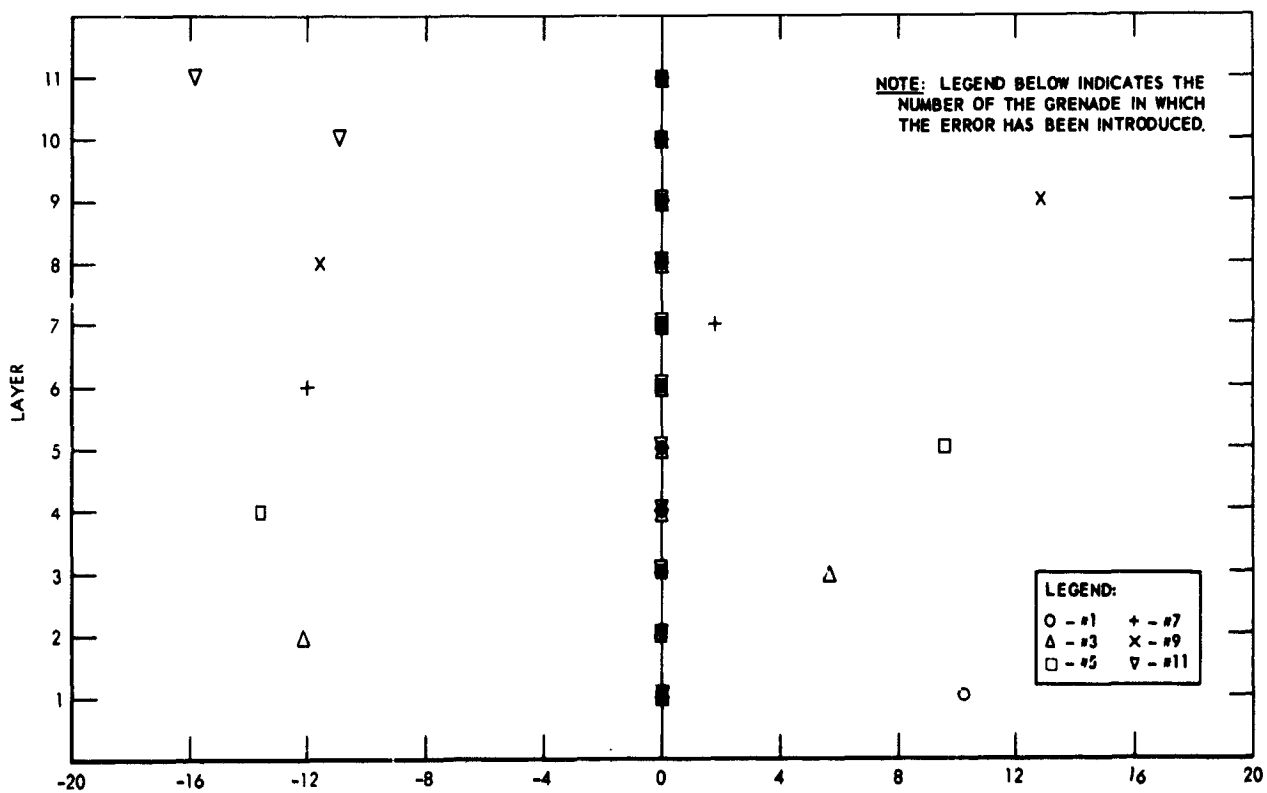


FIGURE 32

ERROR ANALYSIS 7/JUNE/62 UP COÖRD. - 50m

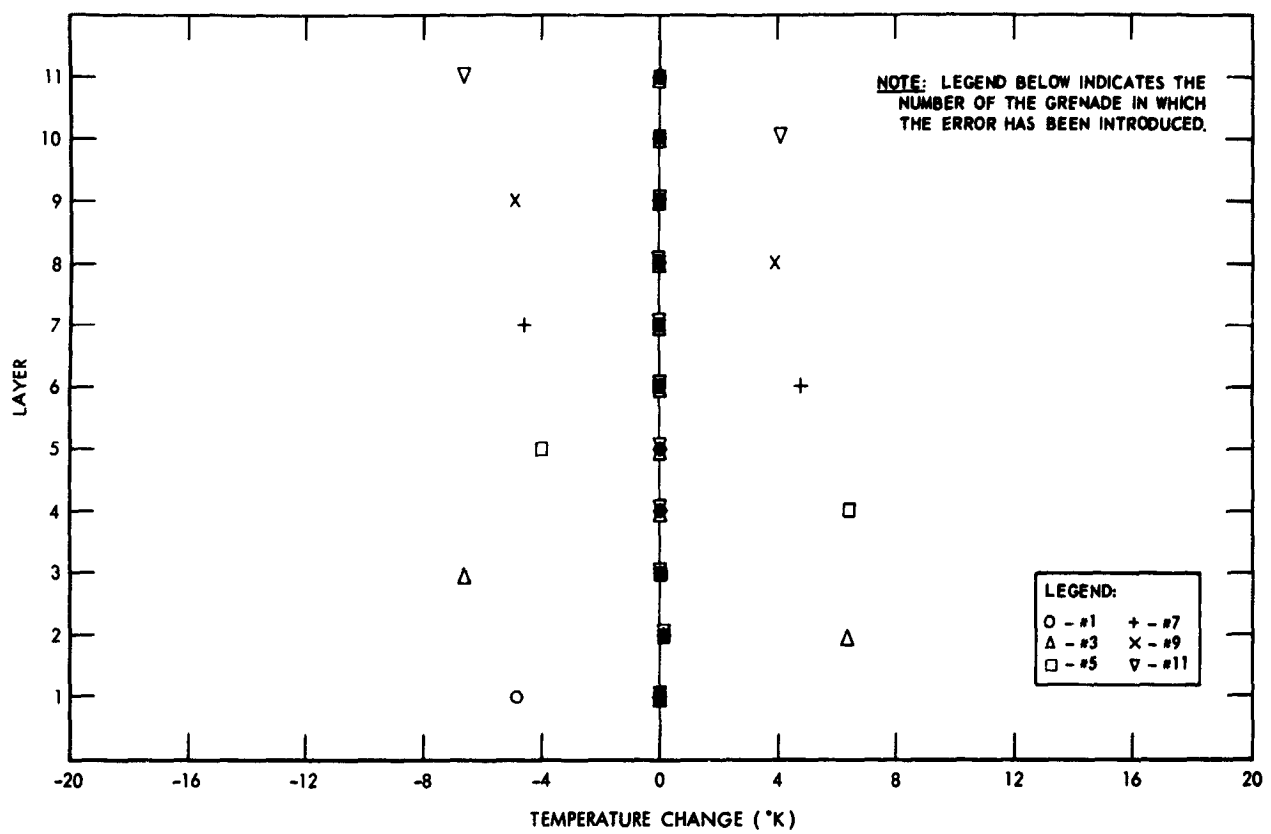


FIGURE 33

ERROR ANALYSIS 7/JUNE/62 UP COÖRD. - 50m

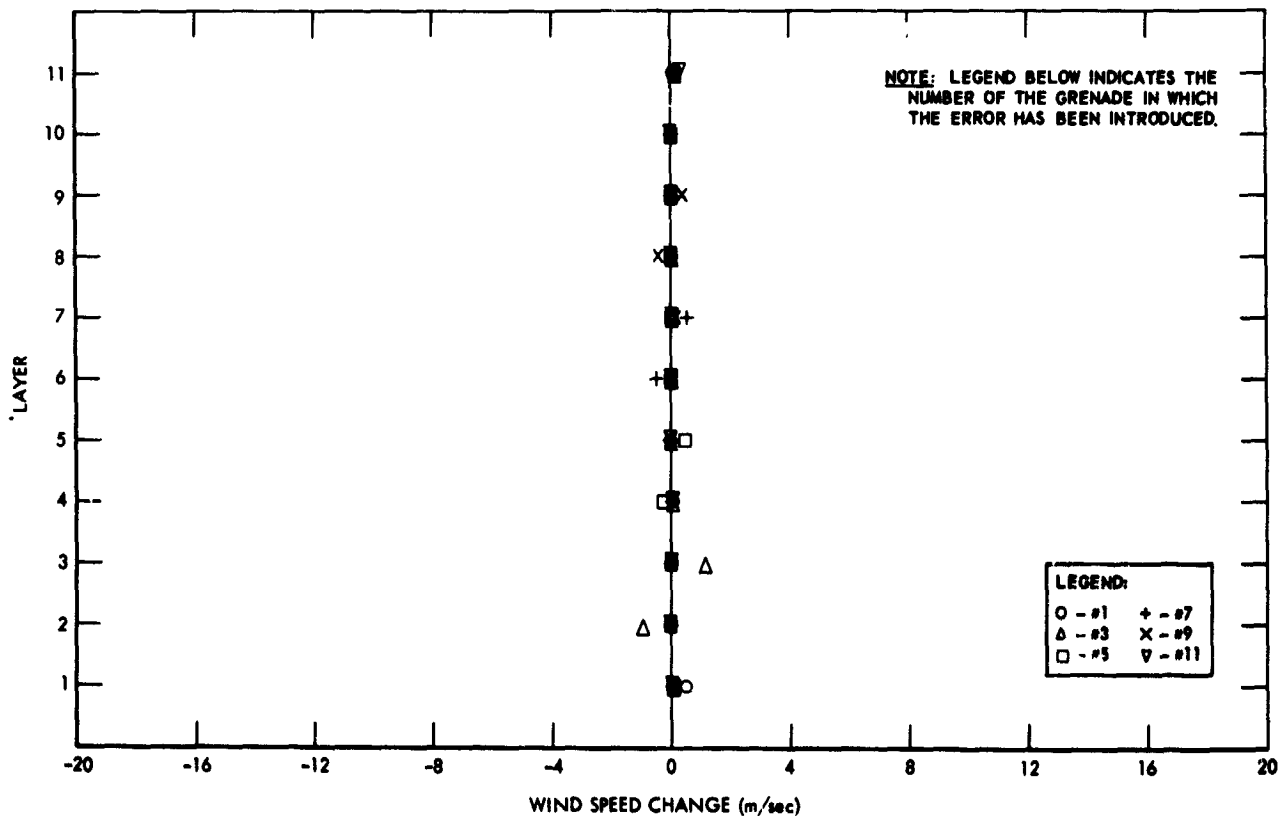


FIGURE 34

PLANETARY ATMOSPHERES

1141

ERROR ANALYSIS 7 JUNE '62 $t + .3 \text{ sec}$

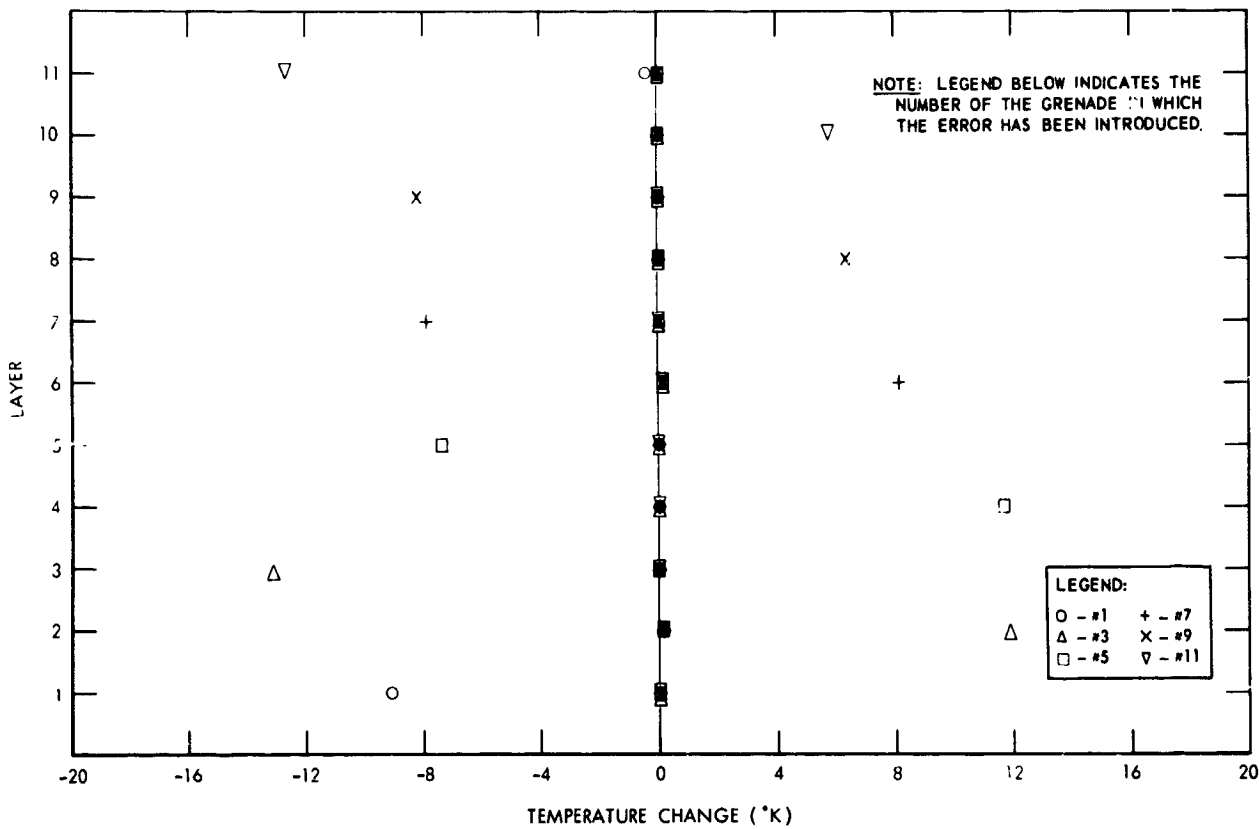


FIGURE 35

ERROR ANALYSIS 7/JUNE/62 $t + .3 \text{ sec}$

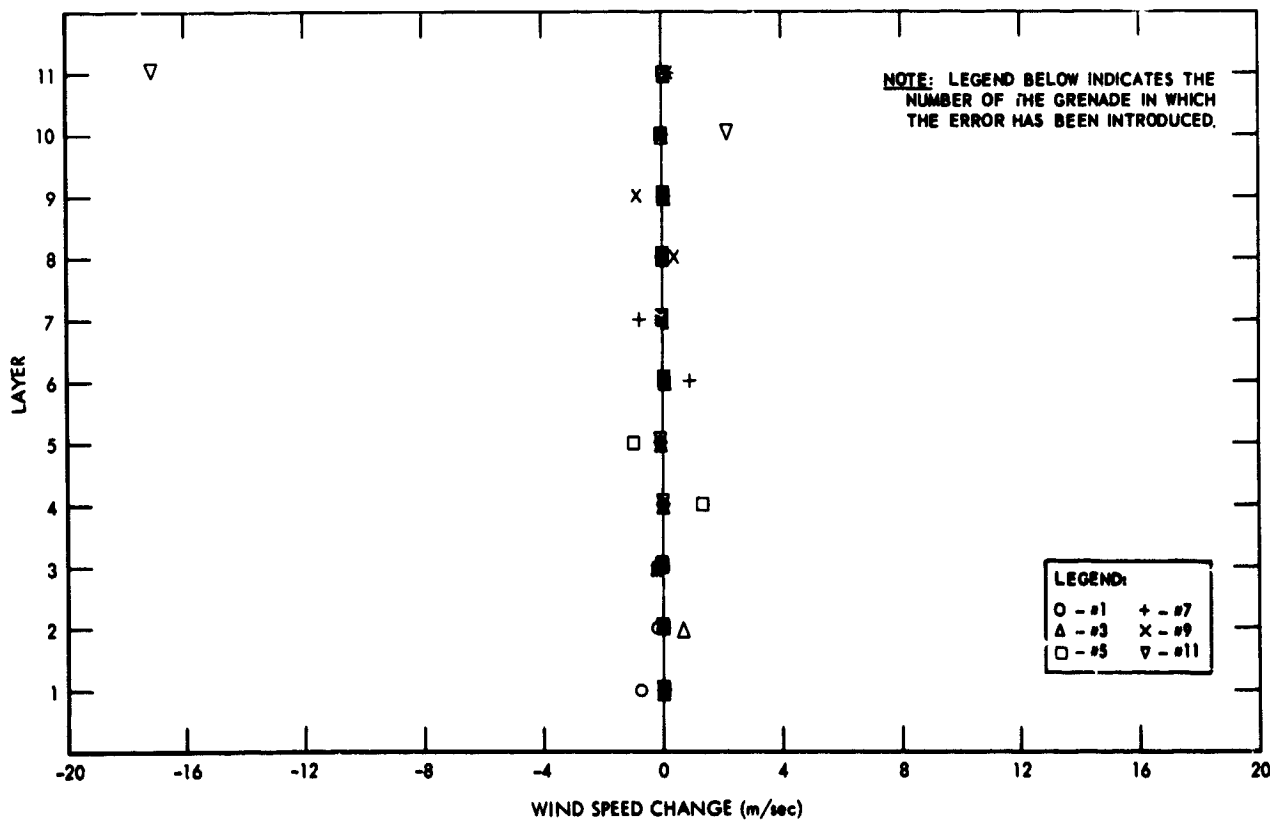


FIGURE 36

PUBLICATIONS OF GSFC, 1964: I. SPACE SCIENCES

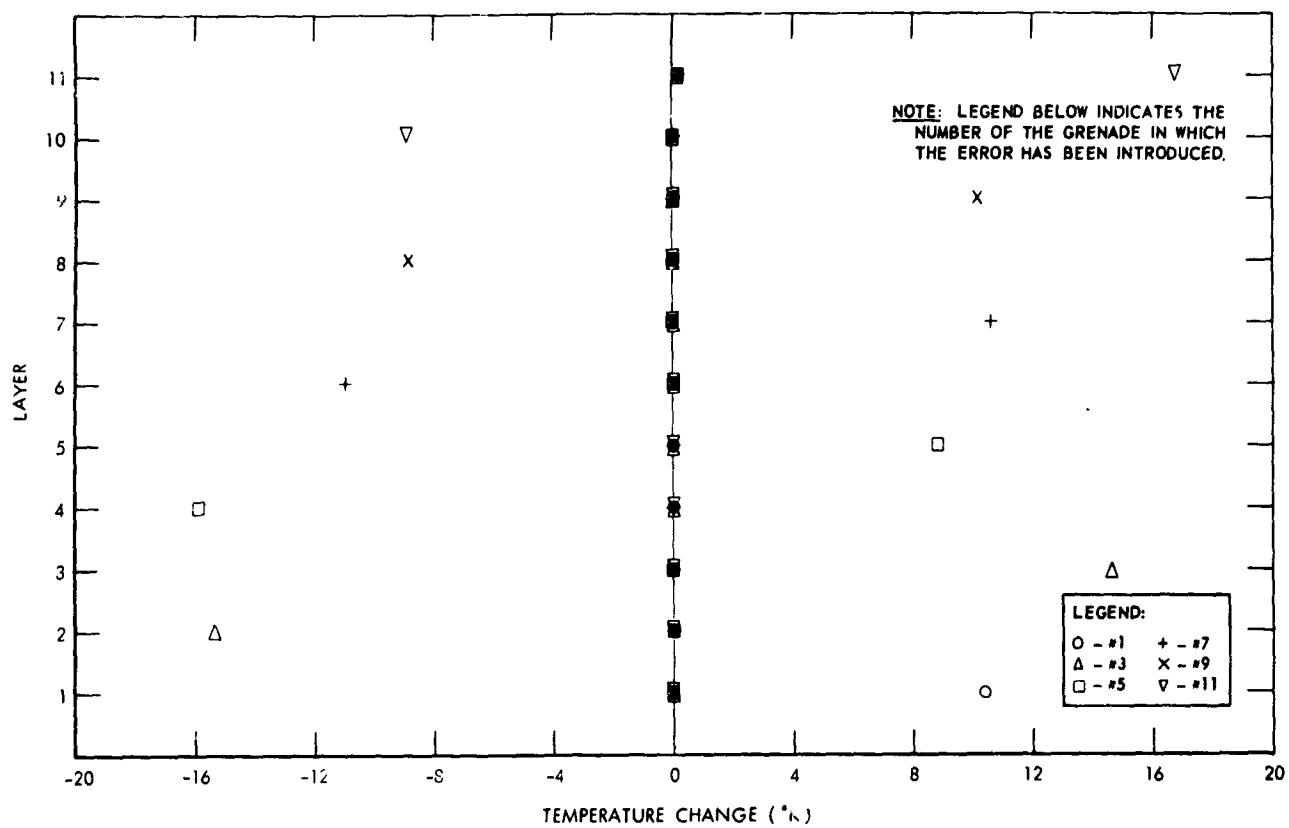
ERROR ANALYSIS 7 JUNE 62 $\Delta t = .02$ sec

FIGURE 37

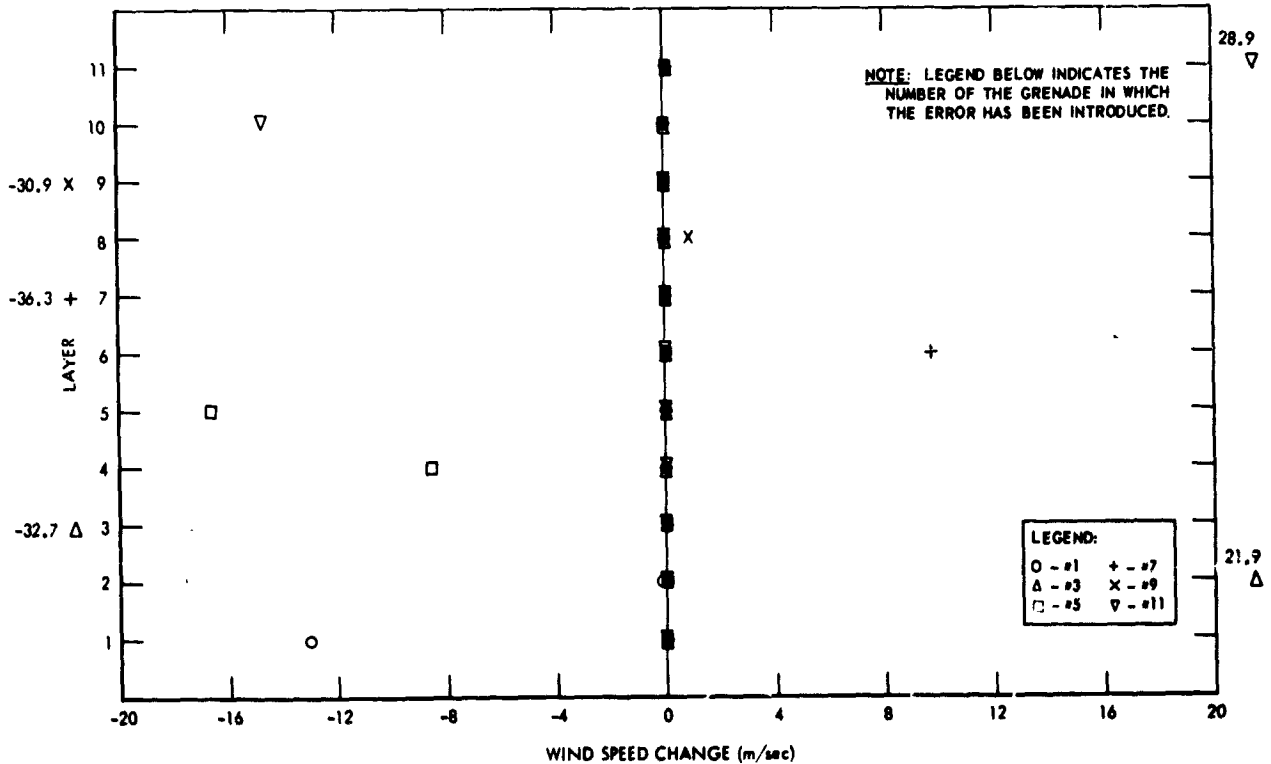
ERROR ANALYSIS 7/JUNE/62 $\Delta t = .02$ sec

FIGURE 38

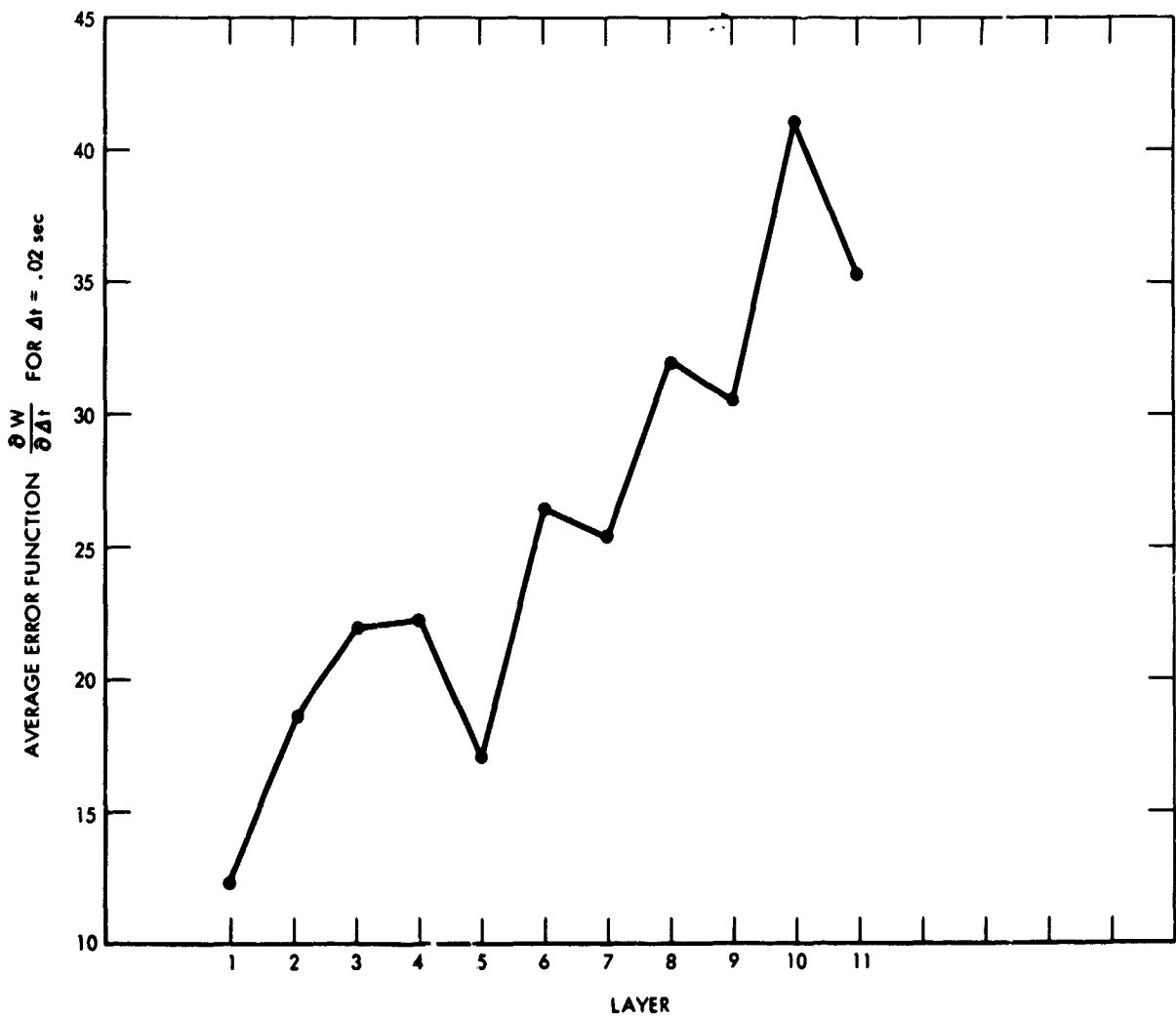


FIGURE 39.—Graph of $\frac{\partial T}{\partial \Delta t}$ vs. layer where $\Delta t = .02$ sec. (average of 16 firings).

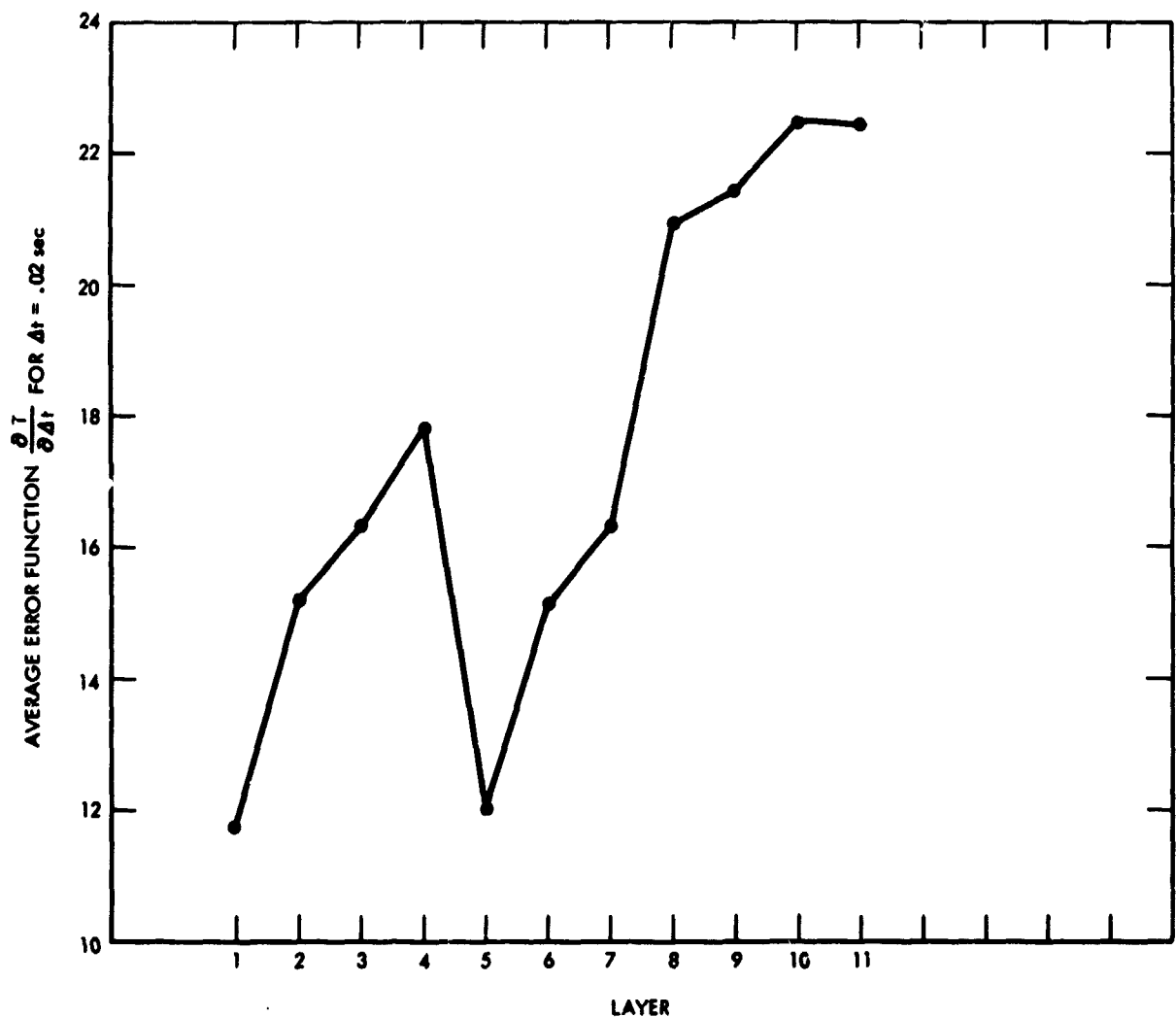


FIGURE 40.—Graph of $\frac{\partial W}{\partial \Delta t}$ vs. layer where $\Delta t = .02$ sec. (average of 16 firings).

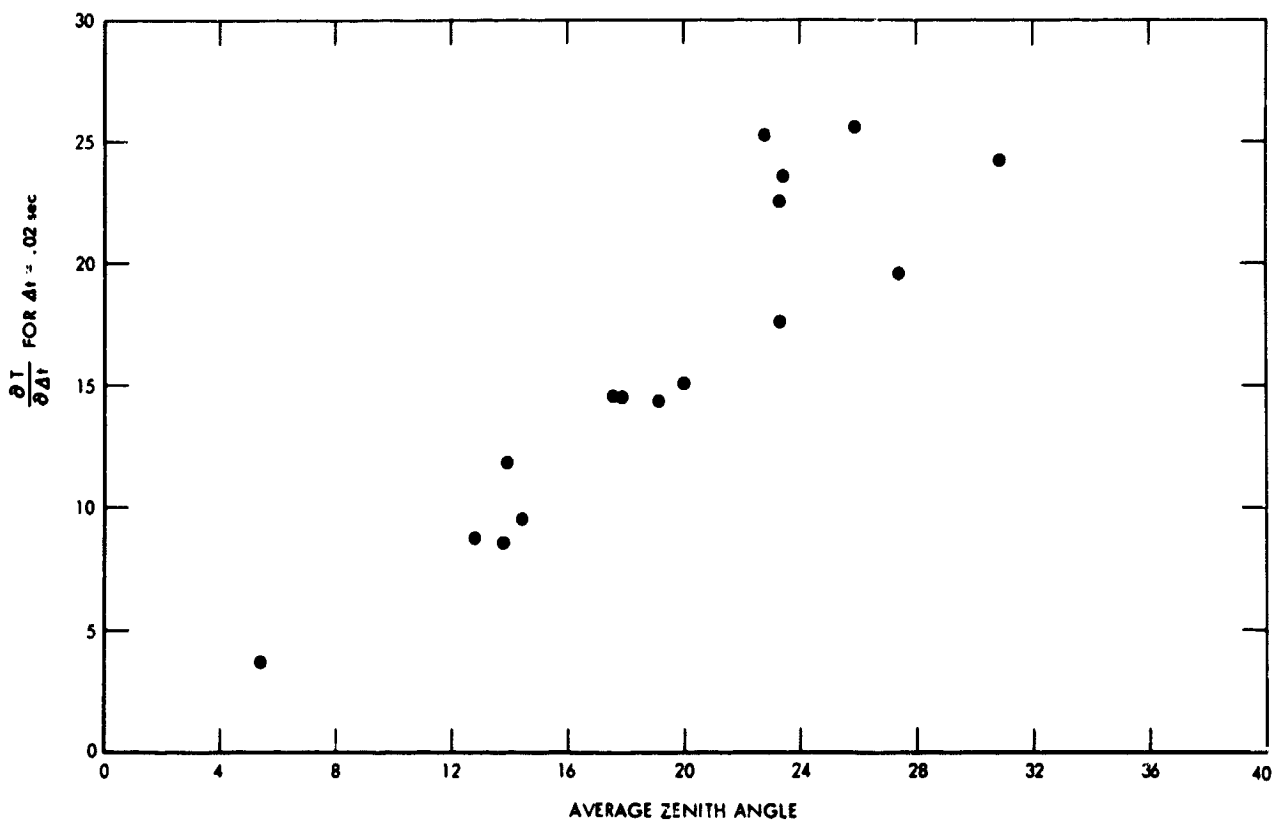


FIGURE 41.—Dependence of $\frac{\partial T}{\partial \Delta t}$ upon zenith angle, where $\Delta t = .02$ sec. for the 16 firings 1960–1963.

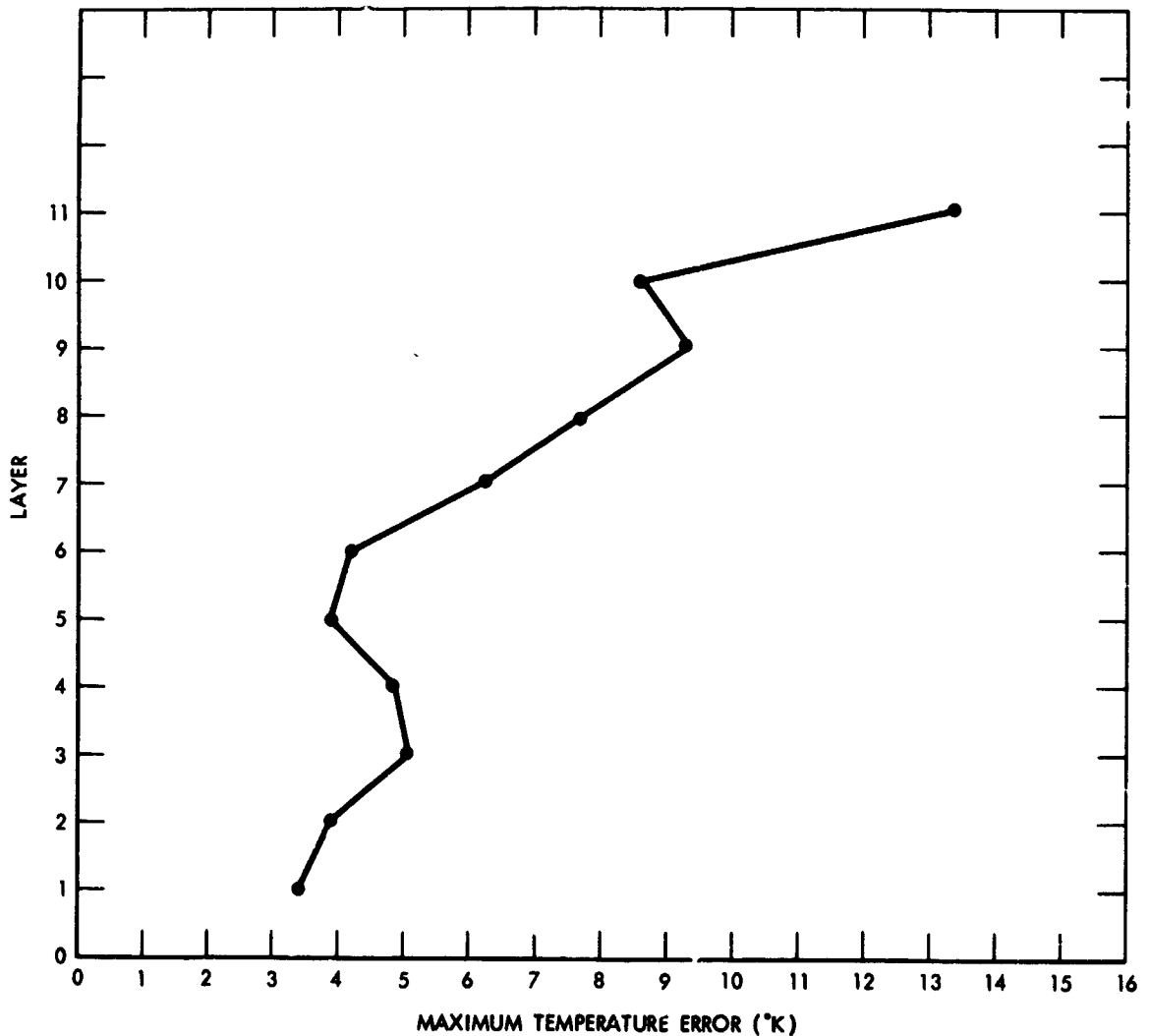


FIGURE 42.—Maximum temperature errors for the 16 firings 1960-1963.

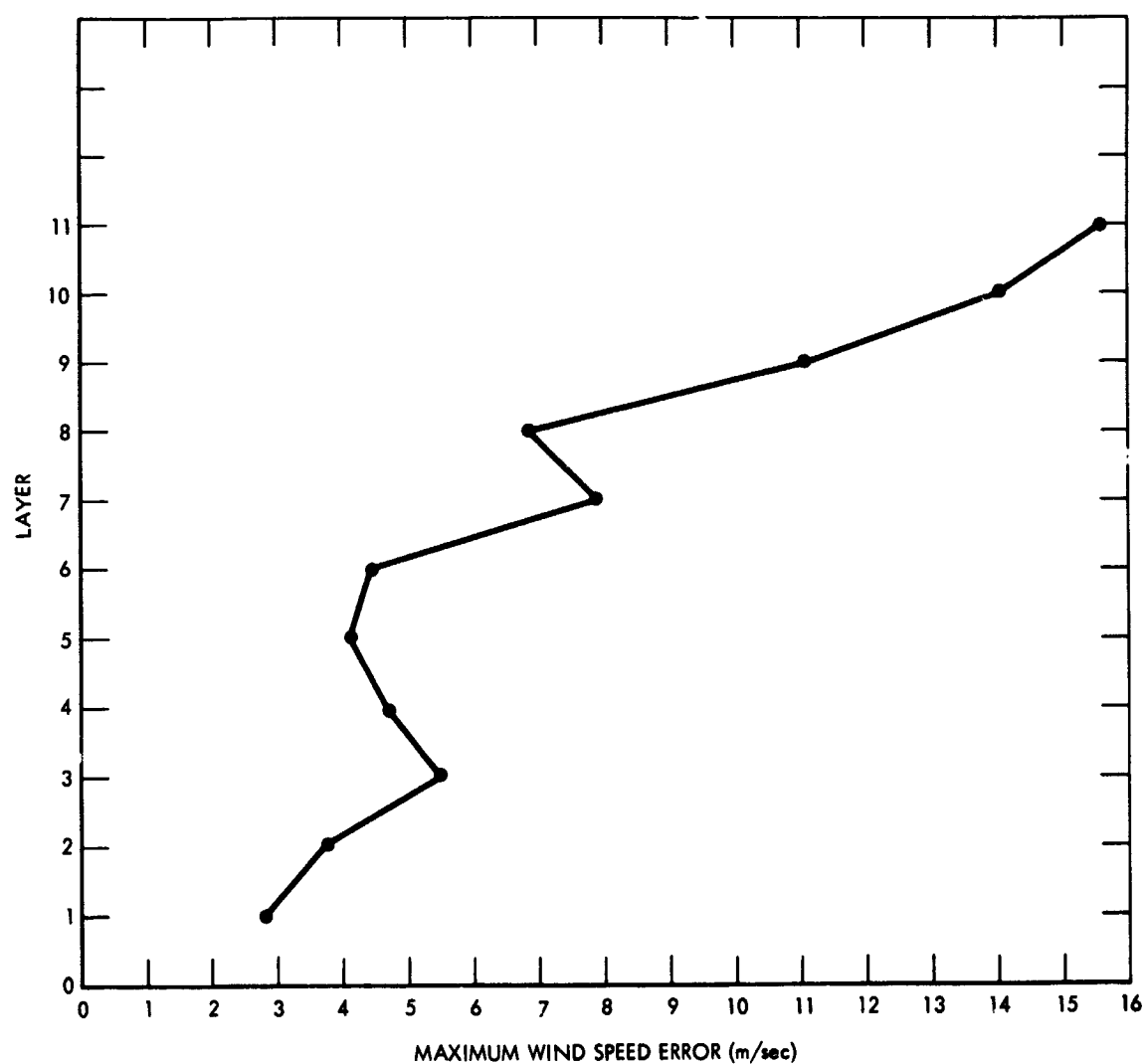


FIGURE 43.—Maximum wind errors for the 16 firings 1960–1963.

May 10 1968

NEW KNOWLEDGE OF THE EARTH'S ATMOSPHERE FROM THE AERONOMY SATELLITE (EXPLORER XVII)*

N. W. SPENCER, G. P. NEWTON, C. A. REBER, L. H. BRACE AND R. HOROWITZ

The Explorer XVII satellite performed direct, very localized measurements of the total neutral particle density, the concentration of neutral particle masses 4, 14, 16, 28, and 32 and the temperature and concentration of thermal electrons, between the altitudes of 258 km and 920 km over those regions of the earth where the satellite was accessible to the Minitrack network, and in particular between $\pm 58^\circ$ latitude. Pressure gages on the satellite showed that the total density at 280 km was about 50 percent lower than is given by the appropriate atmospheric models based on satellite drag measurements. Daily variations in total density are more strongly dependent on a_p (the magnetic index) than had been believed previously. Neutral mass spectrometers showed that He is the predominant neutral constituent above 600 km, O is predominant between 250 km and 600 km, and N_2 is predominant below 250 km. The scale heights of the various constituents agree in general with the corresponding model atmospheric scale heights. Langmuir probe results confirmed the global extent of thermal non-equilibrium ($T_e > T_g$) and provided high resolution of the diurnal variation of electron temperature and density at several stations. For example, the electron temperatures near the F_2 maximum over Blossom Point show a nighttime value of about 1100° K, followed by a mid-morning maximum of 2800° K and an afternoon plateau of 2200° K. A consistent and strong latitude effect, evident particularly at Blossom Point, caused a significant positive gradient in electron temperature (the order of 25° K/degree of latitude) and an inverse gradient in electron density in a manner approximately in accord with recent theories of Hanson and Dalgarno.

INTRODUCTION

The Explorer XVII satellite, Figure 1, was designed to provide direct measurements of aeronomical parameters as a basis for new studies of the physics of the Earth's upper atmosphere. Thus, instruments were selected for the satellite which would provide both total and relative concentration of the neutral particles, and high-resolution measurements of the electron temperature and density; all of considerable significance in studies of the physical processes controlling the upper atmosphere. These data would help also to (a) clarify and define the structural properties of the atmosphere, previously established primarily through inferences from satellite drag measurements, and (b) investigate the variability and dependence of the atmosphere on solar conditions.

The technological advance of measurement techniques was also an objective of the project, as

part of a continuing effort to improve experimental capability. The application of laboratory-developed techniques required engineering as well as measurement technique refinement and adaptation to new environments. The atmospheric data to be obtained, if it were to be of maximum benefit consistent with its timeliness, required computer usage for processing the large quantity of data (the order of 2×10^9 bits of information).

EXPERIMENTS

The choice of experiments to obtain the desired data was based mainly upon laboratory vacuum technique experience; thus both thermionic and cold-cathode pressure gages, derived from proven laboratory sensors, were selected for the measurements of the total neutral particle density. Double-focusing magnetic mass spectrometers were chosen for the measurements of neutral particle concentrations. Two Langmuir probe experiments were employed for measurements of the electron temperature and ion density.

*Published as Goddard Space Flight Center Document X-651-64-114, May 1964.



FIGURE 1.—Artist's conception of Explorer XVII in orbit.

It is of special significance from the point of view of determining local values of the ambient concentrations of constituents that proven laboratory vacuum system techniques were employed in construction of the satellite. For example, to minimize potential sources of contaminating gases, nearly all external surfaces were constructed of stainless steel, and all satellite joints were either welded or utilized copper shear gaskets for vacuum sealing. A significant effort was thus devoted to making the satellite-sensor system a true inside-out ultra-high vacuum system so that the experimenter could be confident that the atmospheric samples measured were not contaminated by materials carried aloft by the satellite.

Pressure Gage Experiments

The density measurements made by the Explorer XVII ionization gages extended to satellite usage the technique employed in rocket manometer experiments (Schultz, Spencer, Reifman, 1948) (Horowitz, Kleitman, 1953) to measure the total atmospheric density. The description of the instrumentation, the calibration technique, and the flight response of the Explorer XVII sensors have been reported (Newton, Pelz, Miller, Horowitz, 1963).

Four independent pressure gage experiments were employed: two Bayard-Alpert type (thermionic cathode) ionization gages and two Redhead type (cold-cathode, magnetic) gages. Each sensor was equipped with a special vacuum-sealed orifice that could be opened after the satellite was in orbit. Thus it was possible for the sensor to be properly cleaned, calibrated, sealed under vacuum, and opened on command to the space environment. This procedure, whose validity was previously established through rocket experience, assured the necessary high degree of vacuum cleanliness for the sensors.

The use of both cold and thermionic cathode gages was considered essential because of uncertainties in (a) the response of a hot-cathode gage in a sometimes predominately atomic oxygen environment (not subject to adequate laboratory calibration) and, (b) the general applicability of ionization gages to the high-velocity satellite environment. At the same time, a desirable redundancy was accomplished and valuable studies of the usefulness of the two fundamentally differ-

ent sensors were made possible. Each pressure gage was provided with an appropriate electrometer amplifier and other electronic support devices which enabled conversion of the sensor output current to a voltage suitable for telemetry. The electronic systems also included provision for in-orbit current calibration of the amplifiers once during each operation of the gages.

Neutral Particle Mass Spectrometers

Two identical double focusing magnetic mass spectrometers were employed for the determination of the local concentrations of atmospheric helium (mass 4), atomic nitrogen (mass 14), atomic oxygen (mass 16), molecular nitrogen (mass 28) and molecular oxygen (mass 32). Although detailed descriptions of the spectrometers are provided elsewhere (Meadows, 1960) (Hall, Howden, Iwasaki, 1960), (Spencer, Reber, 1962), (Reber, Hall, in prep.), the significant features are summarized here. The external ion source, designed to reduce the interactions of the sampled particles with the sensor, was followed by an electrostatic ion lens which focused the relatively high energy ions on the entrance slit of the analyzer. In this way, it was possible for the instrument to accept particles from a 2π steradian solid angle, and up to 12 ev kinetic energy. In the magnetic analyzer the beam of ions was separated according to mass, a given mass falling on the appropriate collector electrode in spectrograph fashion.

Each of the spectrometers was provided with a sensitive electrometer and logarithmic amplifier for conversion of the collected ion current to the proper telemetry voltages. Electronic logic circuitry accomplished the required changes in sensitivity and mass-number selection. As with the pressure gages, a vacuum-seal arrangement was adopted which permitted exposure of the spectrometer ion source to the atmosphere after orbit was attained.

The primary data analysis task was to determine the relationship of the measured ion currents to the ambient neutral particle densities. Particles could enter the region of ionization in one of three ways: (1) directly with no collisions; (2) after suffering one or more collisions with surfaces in the source region; (3) by entering the spectrometer analyzer, becoming thermalized, and

subsequently being re-emitted. The relationships between the measured ion currents and the ambient atmosphere were computed on the basis of these three mechanisms and the laboratory gas calibrations. The validity of these calculations is demonstrated by the fact that the total mass-density measured by the spectrometer is in satisfactory agreement with that obtained independently by the companion pressure gage experiments described above.

Langmuir Probes

Two independent Langmuir probe systems, based on established techniques and previous rocket usage (Spencer, Brace, Carignan, 1962), (Brace, Spencer, Carignan, 1963), (Nagy, Brace, Carignan, Kanal, 1963) were employed to provide measurements of the ion concentration (N_i), and the electron temperature (T_e) of the ionosphere. Each probe system used a cylindrical electrode (projecting into the plasma) whose potential was varied with respect to the satellite shell. The resulting current to the probe was converted to a voltage suitable for telemetry.

Using the following equation, the temperature was derived from the electron current to the probe as it was swept from the satellite potential to the plasma potential:

$$\frac{d \log_e i_e}{dV} = \frac{e}{kT_e} \quad (1)$$

To localize the T_e measurement, the electron temperature probe was swept at a rate of 10 sweeps per second; and to maximize the resolution, the voltage was swept in two ranges, 0 to $\frac{3}{4}$ V and 0 to $1\frac{1}{2}$ V, respectively. As a result, each temperature measurement was completed in less than 400 meters of the satellite path, and to that extent represents a point measurement. The telemetry sampling rate was sufficiently high to permit determination of temperature values as low as 400°K (although the lowest temperatures actually recorded were about 900°K).

The ion density probe was swept from -3 to +2 volts in a 2-second period, which was long compared with the satellite spin period of 0.7 seconds. N_i was derived from the ion current maxima which occurred each time the probe axis was perpendicular to the velocity vector.

Sensor Location

As noted above, the capability to provide measurements of the constituents of the space environment required close adherence to established laboratory vacuum techniques. Thus, in addition to providing a sealed housing which would not itself contaminate the local atmosphere, the eight sensors were located so as to provide maximum separation from each other.

Consideration of sensor orientation with respect to the direction of motion required that the mass spectrometers be located at the two ends of the spin axis to minimize changes in orientation during each mass-sampling sequence. The four pressure gages were distributed uniformly about the spherical satellite to insure that at least one gage would always experience pressure variations due to satellite spin, regardless of the spin axis orientation. One of each type of pressure gage was located on the satellite equator to enable a comparison of the gage responses under identical conditions. The two Langmuir probes were also located on the equator at points nearly diametrically opposite each other.

SUPPORTING SYSTEM

Interpretation of the data from the various sensors required detailed knowledge of the instantaneous angle between any sensor and the direction of motion of the satellite. This information was provided through the use of a multiple optical sensor arrangement, which enabled sensing the direction of the sun and/or moon and the instants of passage, during spin, of the Earth's horizons.

Direct measurement sensors like those employed in Explorer XVII provide time rates-of-change of data requiring high telemetry sampling rates. For example, the spectrometers and pressure gages required 60 samples per second and the "high speed" Langmuir probe required 180 samples per second. To meet these needs a pulse code modulation (PCM) telemetry system capable of 1000 samples per second was selected. This system had the additional advantage of providing a digital format which facilitated computer data processing.

The satellite was powered exclusively by silver-zinc cells, since solar cells presented the possibility of local contamination of the atmosphere. The

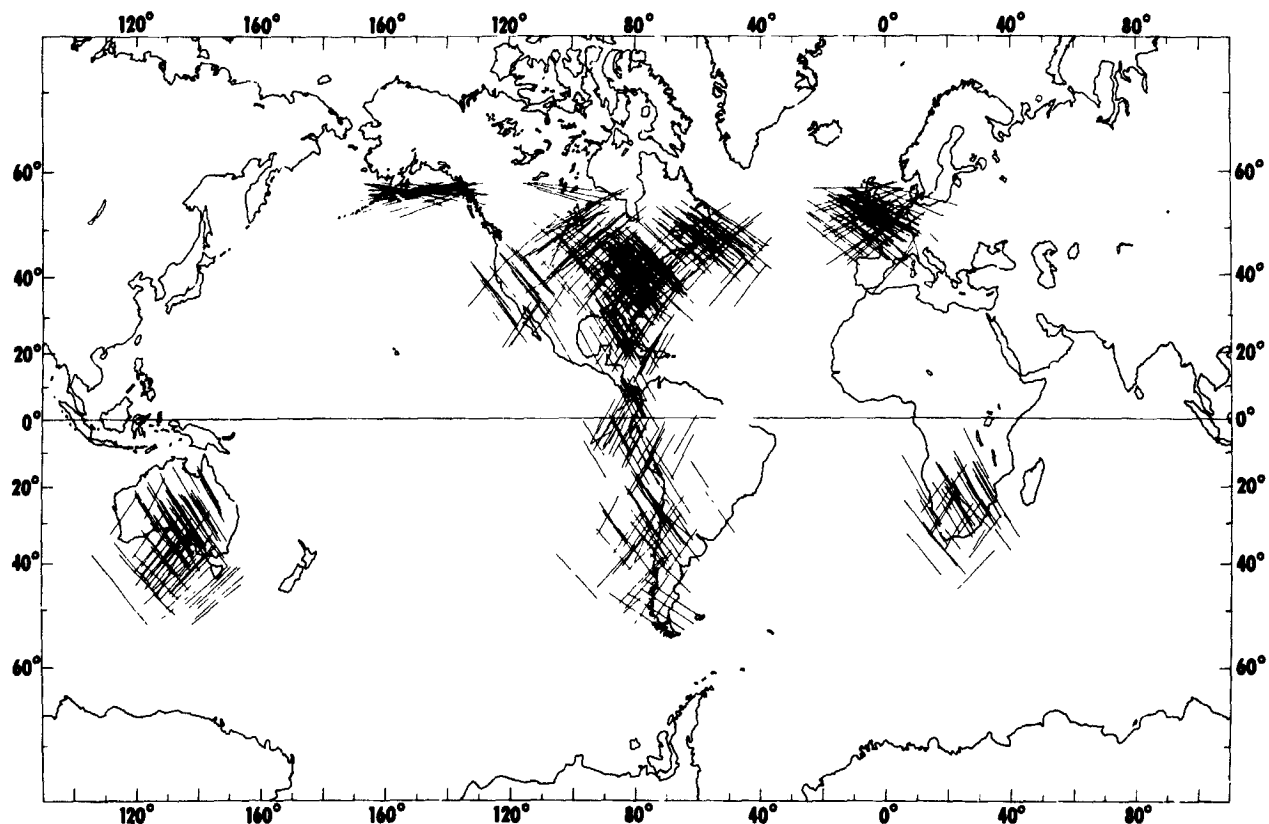


FIGURE 2.—Explorer XVII geographic coverage.

150 pounds of cells which were employed provided adequate energy to operate the entire satellite system for a total of 75 hours. A command-control system permitted the experiments to be turned on for four-minute periods, each of which was terminated by an internal programmer. Because a tape recorder was not employed, responses were confined to geographic regions of approximately 4000 kilometers diameter about each minitrack command station. Figure 2 illustrates the geographic coverage attained by showing the path of the satellite during each data-producing response. Table I summarizes some of the pertinent statistics of the satellite, and other information.

EXPERIMENTAL RESULTS

Pressure Gage Results

As noted above, four independent gage systems were employed on the satellite, and all gages operated in orbit. Three of the gages gave useful and meaningful data during the active lifetime of the satellite. The fourth gage, however, experienced an apparent decrease in sensitivity after

TABLE I.—*Explorer XVII Statistics*

Launch Date.....	April 3, 1963
Inclination.....	58°
Perigee.....	258 km
Apogee Range.....	920-870 km
Useful lifetime.....	100 days
Perigee motion.....	+39° to +58° to -18°
Data responses.....	650 on command
Telemetry.....	PCM—8640 bits/sec
Spin rate.....	90 RPM
Power supply.....	Chemical
Size and shape.....	1 meter sphere
Weight.....	410 pounds

opening in orbit and no atmospheric structure data is available at present from this gage. Some of the results from the other three gages for five northern mid-latitude stations, representing approximately 25 percent of the total available data are presented here.

Figure 3 shows the measured atmospheric density over Grand Forks, Minnesota, during a pass at 2000 hours local time and demonstrates typical resolution of the density gage data. It may be

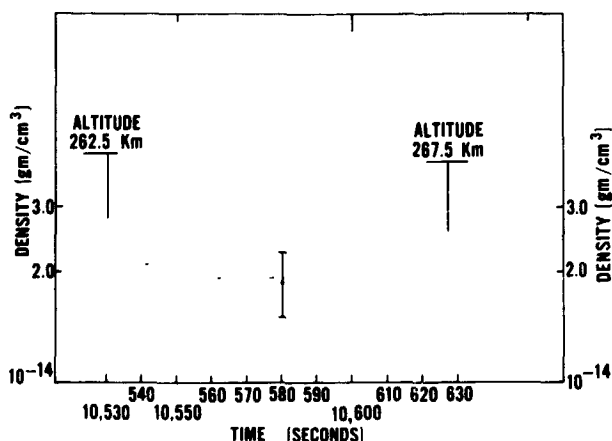


FIGURE 3.—Density data derived from a single pass over Grand Forks, Minn., demonstrating the resolution of the pressure gauge data.

seen that the total altitude change was only 5 km for this pass, and at the average altitude of 265 km, the atmospheric density was 2×10^{-14} gm/cm³. Each point shown is the average of the three independent density measurements. The resolution of the density data from each gage is such that the density was measured every 700 milliseconds or once every six kilometers along the satellite orbit. The observed small scatter of the density data makes quantitative density scale-height determination possible for passes possessing significant altitude changes. The magnitude of the error in the absolute value of the density is ± 25 percent for this pass and can be attributed primarily to uncertainty in the absolute calibration of the sensors in the laboratory. At an altitude of 600 km, the error in the absolute value of the measured density is ± 55 percent for some passes. Generally, the precision of the density measurements is better than ± 20 percent.

Figure 4 (Newton, Horowitz, Priester, 1964) provides a comparison of the atmospheric densities directly measured by the gages in the altitude range 258 to 300 kilometers, to the density obtained from drag observations of Explorer XVII (Bryant, 1964) and Injun 3 (Jacchia, Slowey, 1964). All data are normalized to a height of 280 kilometers for comparison purposes, by using density gradients obtained from the Harris and Priester model with $S = 90$.

The Injun 3 data, indicated by squares, were selected for quiet geomagnetic conditions ($A_p = 2$), for the time interval of 18 February through

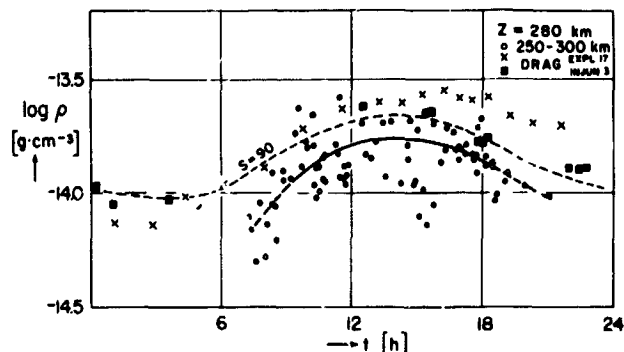


FIGURE 4.—Comparison of directly-measured and drag-derived atmospheric densities.

30 June 1963. During this period, the latitude of the satellite perigee varied between -40° and $+60^\circ$. The drag data from Explorer XVII, indicated by crosses, correspond to the time interval from 3 April to 6 July 1963, when the latitude of the satellite perigee was between $+58^\circ$ and -20° . All Explorer XVII data in the figure have been reduced to quiet conditions ($A_p = 0$) by using the preliminary linear reduction relation:

$$\log \rho = 0.006 A_p$$

Further analysis of the gate data indicates, however, that the correlation between density and geomagnetic activity should be a steeper, non-linear relation with the steepest portion applicable for low A_p (Newton, Horowitz, Priester, 1964). Application of the modified relation is expected to (a) remove some of the scatter from the gage data (which reflects real atmospheric variations), and (b) lower the average value of the directly measured densities by a small amount.

It is observed that the densities determined from drag are systematically 40 percent to 50 percent greater than the normalized densities measured by the gages, and that this separation is just outside the combined, stated uncertainties of the two sets of data. This difference is significant but at this time is not considered serious, since it could be accounted for by modest changes in the altitude to which the drag data are assigned, the drag coefficient, or the gage calibration constants.

Figure 5 shows measured atmospheric density-versus-altitude for the altitude range 258 to 600 km. These data result from approximately 60 passes for an A_p between 0 and 10, $F_{10.7}$ between

70 and 100, and most local times. It is seen that considerable variation in the atmospheric density occurs, resulting primarily from the differences in local time, a factor of 5 diurnal variation at 360 km being observed. The Harris and Priester model densities ($S=90$) for 0400 and 1400 hours are shown for comparison purposes.

Continued analysis of the Explorer XVII data is currently underway to further define:

- (1) The quiet atmosphere and its variation with local time.
- (2) The variations from the quiet atmosphere resulting from solar and geomagnetic disturbances.
- (3) Other effects not now apparent.

Mass Spectrometer Experiment Data

Concentrations as a function of altitude are shown in Figure 6 (Reber and Nicolet, 1964) where Nicolet's model (private communication) is included for reference. The data points shown are measured values, converted to ambient number densities. Measurements of each mass taken on the same satellite interrogation are made approximately one minute apart and are shown in the figure joined by straight lines. The numbers refer to orbit numbers. Table II lists pertinent information for the passes shown in the figure.

Of particular interest are the helium concentration vs. altitude, and the altitude regions where helium, atomic oxygen and molecular nitrogen are predominant. It is seen that helium is the major constituent above 600 km, molecular nitrogen is predominant below 250 km, and atomic

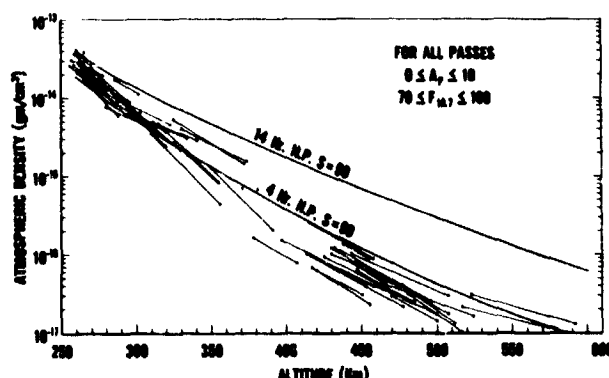


FIGURE 5.—Atmospheric density versus altitude measured by the pressure gauge experiment.

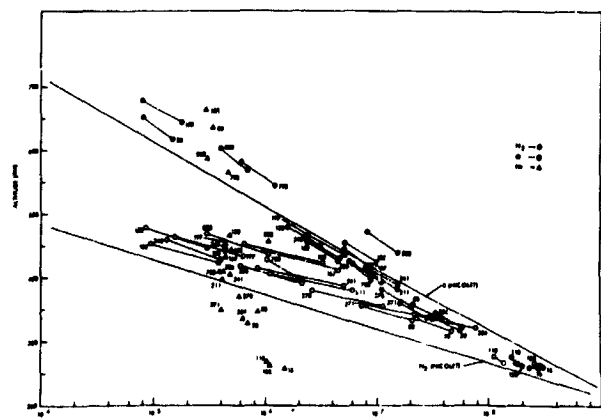


FIGURE 6.—Average daytime and nighttime concentrations of He, O, and N₂ from Explorer XVII mass spectrometer experiment.

oxygen is predominant between these levels. It should be noted that the scale heights of the constituents at higher altitudes correspond to temperatures of about 700° at night.

A possible deviation of the nighttime N₂ distribution from a diffusive equilibrium condition at altitudes less than 400 km is also suggested by this figure. One possible explanation is that the diffusion time in this altitude region is the same order of magnitude as the diurnal variation period. It should also be kept in mind, however, that these data represent a variety of times and geographic locations and thus do not accurately present an instantaneous vertical profile.

Figure 7 shows the variation of mean mass with altitude. The mean mass was computed using the major constituents, N₂, O and He. Hydrogen, which the instrument was not designed to measure, could significantly reduce the value of the mean mass at higher altitudes.

The variation of concentration ratios of helium-to-oxygen and atomic oxygen-to-molecular nitrogen with altitude is shown in Figure 8. The solid lines drawn through the points are averages; as in all the data presented, the points are measured values and are not averaged, nor do they reflect any smoothing. It can be seen here again that helium is the dominant component above 600 km and that molecular nitrogen is predominant below about 250 km.

Langmuir Probe Experiment Results

Figure 9 shows the detailed variation of T_e and

TABLE II.—*Tabulated Mass Spectrometer Data*

<i>Pass & Station</i>	<i>Date</i>	<i>Local Time</i>	α	<i>Geo. Lat.</i>	<i>Geo. Long.</i>
# 15 BP	4/4/63	21.15 hrs.	6°	38.5°	-75.0°
# 50 COL	4/6/63	0.65	16°	57.0°	-149.0°
# 80 COL	4/8/63	0.99	9°	55.0°	-147.0°
# 80 FTM	4/8/63	4.89	63°	18.0°	-92.0°
#118 BP	4/10/63	18.81	70°	37.0°	-72.0°
#120 GF	4/11/63	20.32	51°	51.0°	-98.5°
#138 BP	4/12/63	2.51	12°	37.0°	-84.0°
#152 BP	4/13/63	2.01	14°	39.5°	-68.5°
#167 BP	4/14/63	1.65	20°	39.5°	-75.0°
#182 BP	4/15/63	1.54	25°	37.0°	-78.0°
#183 QUI	4/15/63	3.26	23°	4.5°	-79.0°
#197 BP	4/16/63	1.43	27°	34.0°	-81.5°
#211 BP	4/17/63	0.53	45°	41.5°	-71.5°
#226 BP	4/18/63	0.48	53°	38.5°	-74.0°
#241 BP	4/19/63	24.19	62°	38.0°	-79.5°
#242 MOJ	4/19/63	0.64	54°	31.0°	-121.5°
#254 NFL	4/20/63	22.75	82°	49.0°	-53.0°
#270 BP	4/21/63	23.30	80°	41.5°	-71.5°
#271 GF	4/21/63	22.88	85°	45.0°	-101.0°
#708 NFL	5/20/63	7.18	39°	49.5°	-49.5°
#795 OOM	5/26/63	15.81	63°	-34.0°	137.5°
#800 JOB	5/26/63	15.90	65°	-37.5°	19.0°
#888 JOB	6/1/63	13.24	33°	-27.0°	25.0°

The local sun time, angle of attack (α), geographic latitude and longitude are averaged over the four minute pass. The stations involved are: BP—Blossom Point, Md.; COL—College, Alaska; FTM—Fort Myers, Fla.; GF—Grand Forks, Minn.; QUI—Quito, Ecuador; MOJ—Mojave, Calif.; NFL—Newfoundland; OOM—Woomera, Australia; JOB—Johannesburg, South Africa.

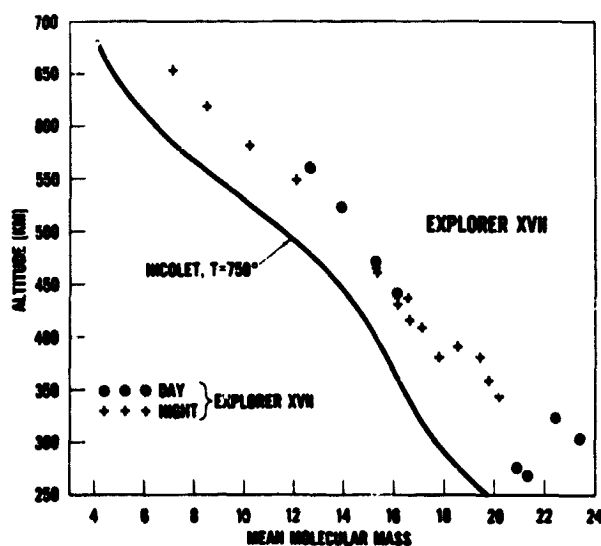


FIGURE 7.—Mean molecular mass versus altitude from mass spectrometer.

N_t , measured during a series of near perigee passes near the F_2 maximum over Blossom Point, Maryland. These data were obtained over the three

month satellite lifetime during which the rotation of the orbit plane caused a complete diurnal variation to occur. The data are shown as points or pairs of points, the latter corresponding to the measured values at the beginning and at the end of individual satellite passes.

At first glance one is struck by the lack of correlation between the gross diurnal variations (smoothed curves) and the changes during the individual passes, especially in the afternoon. Since perigee passes such as these can exhibit very little altitude change, this in-pass variation must be largely latitude dependent (10° change in latitude within average pass). The average in-pass change in T_e implies a latitude gradient near Blossom Point of approximately 25° K per degree of latitude, corresponding to about a 10 percent change in T_e within a pass. With few exceptions the changes in T_e within a pass are accompanied by an inverse change in N_t which is even greater than 10 percent.

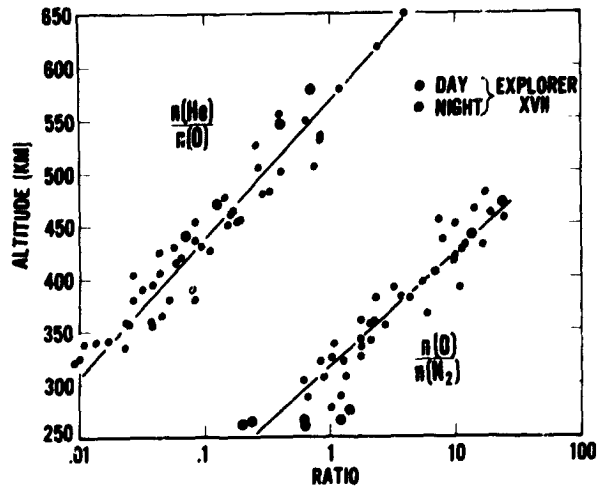


FIGURE 8.—Ratios of $n(\text{He})/n(\text{O})n(\text{N}_2)$ versus altitude from mass spectrometer experiment.

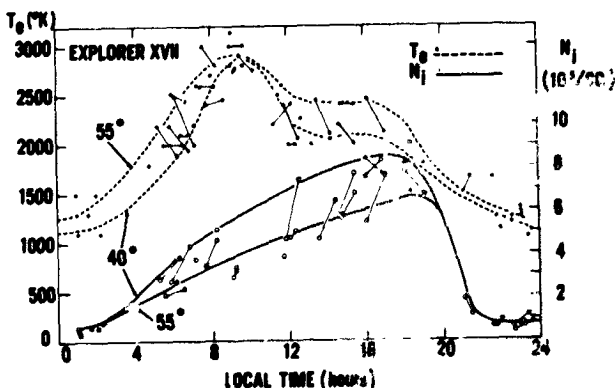


FIGURE 9.—Diurnal variation of T_e and N_i for magnetic latitudes $40\text{--}50^\circ\text{N}$ and altitudes 208 to 350 km, from the Langmuir probes.

Plots similar to Figure 9 have been prepared from T_e and N_i measurements at two other latitudes (10°N at Quito, 60°N at College), and the resulting gross diurnal variation curves at all three latitudes are shown in Figure 10. These data also correspond to the region of the F_1 maximum (below 400 km).

The T_e variation at the F_1 maximum at all latitudes shown is characterized by a steep morning rise, a midmorning maximum, and afternoon plateau, and a gradual decrease near sunset. The nighttime values of T_e are somewhat variable but are always significantly above the neutral particle temperature (Harris and Priester, 1962), particularly at College, Alaska where the summer night at F_1 altitudes is short or non-existent.

The values of N_i rose gradually throughout the

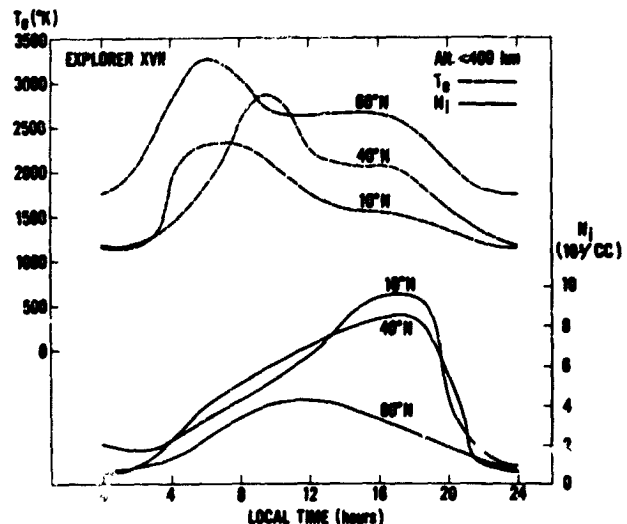


FIGURE 10.—Averaged T_e and N_i showing the diurnal variation above three selected stations; Quito (10°N), Blossom Point (40°N) and College (60°N).

day, reaching a maximum density in the late afternoon, except at College where the maximum occurred in the early afternoon.

It should be noted that the curves in Figure 10 represent direct "in situ" measurements above specific geographic locations during the late spring and summer of 1963, and therefore should not be considered models of the diurnal variation at other altitudes, longitudes, and seasons. However, the analysis of higher altitude data from these sites, as well as data from other sites is now in progress, and it is hoped that these data will help provide a better understanding of the global structure of the ionosphere.

In conclusion, it is clear from the simultaneous measurements that T_e and N_i are related in a generally inverse manner which agrees reasonably well with the inverse square relationship predicted by Hanson (1962) and Dalgarno, et al (1963). The elevated nighttime values of T_e show that there is a heat source for the electrons at night, although its energy content is only a few percent of that required to cause the electron temperatures observed in the daytime (Brace, Spencer, Dalgarno, 1964).

ACKNOWLEDGMENTS

The success of a satellite laboratory such as discussed above results, clearly, from the efforts of many individuals. The authors gratefully and

sincerely wish to acknowledge these efforts and specifically mention the major contributing group leaders: James S. Albus—aspect system, Joseph P. Corrigan—tracking and data systems, James L. Cooley—coordinator, Paul C. Donnelly—batteries, Donald F. Fitzpatrick—mechanical design, William D. Hoggard—environmental testing, Robert E. Kidwell—thermal systems, John N. Libby—electronic control, Chris C. Stephanides—spacecraft system and integration engineer, Virginia Zanner—computer data analysis.

REFERENCES

- BRACE, L. H., N. W. SPENCER, G. R. CARIGNAN, Ionosphere electron temperature measurements and their implications, *J. Geophys. Res.*, **68**, 5397-5412, 1963.
- BRACE, L. H., N. W. SPENCER, A. DALGARNO, Explorer XVII electrostatic probe data and interpretation (Explorer XVII) American Geophysical Union, 45th Annual meeting, Washington, D.C., April 1964.
- BRYANT, R., Densities obtained from drag on the Explorer XVII satellite, *J. Geophys. Res.*, **69**, 1423-1425, 1964.
- DALGARNO, A., M. B. McELROY and R. J. MOFFETT, Electron temperatures in the ionosphere, *Planet. Space Sci.*, **11**, 463-484.
- HALL, L. G., P. F. HOWDEN and T. F. IWASAKI, Design of a mass spectrometer for use in a satellite, presented at the 8th Annual Meeting of the ASTM Committee E-14 on Mass Spectroscopy.
- HANSON, W. B., Electron temperatures in the upper atmosphere, *Space Research*, Proc. Intern. Space Sci. Symp. 3rd, Washington 1962, edited by W. Priester, pp. 282-302, North Holland Publishing Co., Amsterdam.
- HARRIS, I. and W. PRIESTER, Theoretical models for the solar cycle variation of the upper atmosphere, *J. Geophys. Res.*, **67**, 45-4591, 1962.
- HOROWITZ, R. and D. KLEITMAN, Upper atmosphere research report No. XVIII, N.R.L. Report 4246, Naval Research Lab., Washington, D.C., Oct. 1953.
- JACCHIA, L. G. and J. SLOWEY, Atmospheric heating of the auroral zones: A preliminary analysis of atmospheric drag of the Injun 3 satellite. SAO Special Report 136, Sept. 1963, *J. Geophys. Res.*, **69**, 905-910, 1964.
- MEADOWS, E. B., Design requirements of a mass spectrometer for satellite use, presented at 8th Annual Meeting of ASTM Committee E-14 on Mass Spectroscopy Atlantic City, N. J., June 1960.
- NAGY, A. F., L. H. BRACE, G. R. CARIGNAN, M. KANAL, Direct measurement bearing on the extent of thermal non-equilibrium in the ionosphere, *J. Geophys. Res.*, **68**, 6401-6412, 1963.
- NEWTON, G. P., D. J. PELZ, G. E. MILLER, and R. HOROWITZ, Response of modified Redhead magnetron and Rayar-Alpert vacuum gages aboard Explorer XVII, Transactions of the Tenth National Vacuum Symposium, edited by George H. Bancroft, pp. 208-212, The Macmillan Company, New York, 1963.
- NEWTON, G. P., R. HOROWITZ, W. PRIESTER, Pressure gage experimental data and interpretation; AGU Presentation of Aeronomy Results from the Explorer XVII satellite, 45th Annual Meeting, Washington, D.C., April 23, 1964.
- REBER, C. A., Preliminary results regarding neutral atmospheric composition from the Explorer XVII satellite, presented at the Third Western National Meeting, American Geophysical Union, Boulder, Colorado, Dec. 1963.
- REBER, C. A. and M. NICOLET, Explorer XVII mass spectrometer data and interpretation, AGU Presentation of Aeronomy Results from the Explorer XVII satellite, 45th Annual Meeting, Washington, D.C., April 23, 1964.
- REBER, C. A., and L. G. HALL, The Explorer XVII mass spectrometer, (in preparation).
- SCHULTZ, F. V., N. W. SPENCER, and A. Reigman, Upper Air Research Program, Progress Report No. 2, Contract W-33-038 ac-14050. Engineering Research Institute, University of Michigan, pp. 129-137, July 1, 1948.
- SPENCER, N. W., and C. A. REBER, A mass spectrometer for an Aeronomy satellite, Proceedings of the Third International Space Science Symposium, Washington, D.C., May 1962.
- SPENCER, N. W., L. H. BRACE, G. R. CARIGNAN, Electron temperature evidence for non-thermal equilibrium in the ionosphere, *J. Geophys. Res.*, **67**, 157-175, 1962.